ELECTRICAL AND OPTICAL PROPERTIES OF THE AMORPHOUS Si-As-Te SEMICONDUCTOR SYSTEM

by

Masahiro NUNOSHITA

January, 1975

Central Research Laboratory
Mitsubishi Electric Corporation
Amagasaki, Hyogo

ELECTRICAL AND OPTICAL PROPERTIES OF THE AMORPHOUS Si-As-Te SEMICONDUCTOR SYSTEM

Masahiro NUNOSHITA

Central Research Laboratory
Mitsubishi Electric Corporation
Amagasaki, Hyogo

January, 1975

ABSTRACT

Systematic experimental investigations are carried out on electrical and optical properties of amorphous semiconductors in the Si-As-Te glass system. Temperature dependence of the dc conductivity σ_T follows fairly well the formula of $\sigma_T=\sigma_o \cdot \exp\{-E_{g(el)}/2kT\}$, and the pre-exponential term σ_o is estimated to be $(2.1\pm0.6)\times10^4$ $(\Omega\cdot cm)^{-1}$ for all Si-As-Te amorphous system. A quite wide range of the dc conductivity of $10^{-4}\sim10^{-11}$ $(\Omega\cdot cm)^{-1}$ at room temperature is obtained by controlling the glass compositions. A systematic relationship between the compositional changes in the electrical gap $E_{g(el)}$ and the optical gap $E_{g(op)}$ has been found. The energy-band gaps increase linearly with increasing the Si content but decreasing the Te content, and are almost insensitive to the As content. The relation between $E_{g(el)}$ and $E_{g(op)}$ is expressed by $E_{g(el)}=1.60\ E_{g(op)} - 0.15$ in eV. On the other hand, the optical absorption coefficient $\alpha(\omega)$ near the fundamental edge follows the empirical formula, $\alpha(\omega)=\alpha_o \cdot \exp(\hbar\omega/E_s)$. The experimentally determined factor E_s increases linearly with the gap $E_{g(op)}$ and is closely related to the energy difference between the two gaps. A tentative energy-band model to explain these experimental results is proposed by taking account of

the effect of potential fluctuations in such disordered materials.

Several steps of stabilization are realized from a rapidly quenched state to the well annealed state by heat treatment at a temperature below the glass transition temperature T_g. The weight density, thermal expansion, heat capacity, dc conductivity, electrical and optical gaps and the band-tailing factor E_s change consistently with logarithm of the annealing time, and saturate finally at certain values at a given annealing temperature. It is considered that variations of the physical properties are yielded from two separate sources; one is an increase of the packing density in the disordered structure which is regarded as rather an atomic fashion, and the other is a decrease in the local strain and deformation fields corresponding to the electronic effects.

Since the Si-As-Te-(Ge) glass has a relatively high softening temperature with a wide glass-forming region, suitable material properties for practical applications would be expected. In this viewpoint, some attempts to make electronic and opto-electronic devices have been made. Particularly, threshold switching phenomena of the chalcogenide glasses are presented in the thesis work. To find the proper synthetic conditions for the stable switching operation, the breakdown regime is systematically examined for the material properties and device geometries. A thin-film switching device with the composition $Si_6As_{26}Te_{55}Ge_{13}$ has been fabricated in the form of a multi-film sandwitch-type structure. Some basic technical data for practical operation are also presented.

CONTENTS

CONTENTS(Continued)

Chapter-I

INTRODUCTION

1-1. Historical Background of Amorphous Semiconductor Investigations

Since the age of ancient Egypt, vitreous materials, mainly oxide glasses, have been used as an important substance for favorite necessaries or ornaments in human life. In the 1920's the mass production techniques of common oxide glasses had already developed to a considerably high level. Recent rapid advance of the glass technologies is still more bringing new materials and their practical applications such as crystallized glass, optical glass, optical fiber, glass laser, photochromic glass. However, even an analysis of the glass structures was not started until 1936.[1] A major class of non-crystalline solids —common oxide glasses— have been extensively studied mainly from the point of view of their thermodynamical and structural properties, not for their electronic properties.

In 1968, Ovshinsky reported on a reversible electrical threshold switch of non-crystalline materials.[2] This new kind of vitreous materials, so-called semiconducting glasses containing S, Se, or Te elements, was given attention as electronic and optical materials exhibiting many interesting properties. Since then, the electronic processes in amorphous semiconductors, particularly chalcogenide glasses, have been intensively investigated in a field of basic solid-state physics as well as on practical applications to electronic and opto-electronic devices. The effort has been concentrated on the purely scientific interest and on the search for possibility of new active devices. However many important ambiguities have still remained

in the problems concerned with the structural stabilization and electronic behavior, which play an important role in various interesting phenomena in the amorphous semiconductors.

A great success of the solid-state physics consisting of analysis of crystal structures and quantum mechanics has been seen in studies of almost perfect crystals such as metals, semiconductors and magnetic materials.[3] In the last decade, solid-state physicists have started an attempt to explore non-crystalline substances and disordered systems.[4,5] Some theoretical approaches like the coherent-potential method and the simple tight-binding method have been made on the basis of highly simplified model Hamiltonians for one electron in *ideal* disordered systems.[6,7] However, no accurate comprehensive theory for the electronic properties of *real* amorphous substances has been yet established because of the lack of long-range order and symmetry in their structures. By taking account of experimental results on electronic properties of semiconducting chalcogenide glasses, Davis, Mott and Cohen *et al.*[8] have recently proposed a concept of the *mobility gap*, so-called the Mott-CFO model. Strictly speaking, this conceptive model is available only to explain their temperature-dependent dc conductivity. Thus, the complexity in these disordered systems keeps the most part of this field on the level of an empirical science. On the other hand, experimentalists are plagued not only with the vaguely defined concepts and generalities of the present theories but also with difficulties of mastering the reproducible preparations of materials. Besides, the inherent metastability of the amorphous state compared to the crystalline state is also responsible for many confusions and discrepancies in the experimental results.

1-2. Purpose and Significance of The Present Work

In view of the present status of the basic physics and the practical applications in this field, the most necessary thing is to interpret sufficiently correlations between the electronic processes and configurational stability in *real* non-crystalline semiconductors. To do this, one has to accumulate firstly systematic experimental data on the electronic properties in connection with the structural and compositional changes in individual amorphous materials.

The subject matter of this thesis work is to carry out some systematic investigations on compositional dependences and stabilization process of electrical, optical and thermodynamic properties of typical semiconducting chalcogenide glasses in a Si-As-Te ternary system.[9-12] Characteristic parameters of the electronic properties like dc and ac conductivities, electrical and optical energy-band gaps, band-tailing factor are examined, and an electronic structure and transport mechanisms in the Si-As-Te amorphous semiconductors are discussed from the viewpoint of the network structures.[13] Another considerable effort is made to develop a useful and reliable amorphous active device of electrical threshold switch, and to elucidate the physics underlying the switching operation to a practical interest. A series of engineering researches are carried out for a thin-film crossover switching device of the Si-As-Te-(Ge) amorphous system, which exhibits the electrical threshold switching action attributed to the electronic breakdown process.[14]

In Chapter-II, the author discusses about concise descriptions of classification and general features of amorphous semiconductors,

especially chalcogenide glasses, and makes clear the principal reasons for using the Si-As-Te ternary glass system in this thesis work. Then, a peculiar fabrication procedure by RF heating and preparation techniques of the samples are presented.[10,11] By measuring the basic thermodynamic properties and the X-ray diffractions of the synthesized chalcogenide alloys of different compositions, their vitrification is confirmed, and consequently the glass-forming composition region determined in this Si-As-Te ternary system is demonstrated.[9]

Chapter-III first indicates the experimental results on electrical and optical properties of the Si-As-Te vitreous semiconductors and manifests that the electronic parameters such as electrical and optical band gaps play an important role in the semiconducting properties.[9] It is verified that the basic factors for the electronic properties in these disordered materials can be analogous to those for band-conduction processes in the *intrinsic* region of covalent single-crystal semiconductors like silicon and germanium.[11] In order to explain the electronic semiconducting properties in the chalcogenide glasses, a tentative energy-band model is postulated and transport mechanisms are discussed.[13]

In Chapter-IV, the author describes about a systematic investigation on the compositional dependences of the electrical, optical and other structural properties within the glass-forming region of the Si-As-Te system.[9-11] In looking through the experimental results, the basic molecular structures of this vitreous material can be proposed in the form of three-dimensionally cross-linked and covalent-bonded networks to explain the data of compositional

dependences. Moreover, the static electronic state is discussed on the basis of electronic configurations of chemical bonds almost preserved as a short-range order even in such a disordered system.

In Chapter-V, an experimental approach to explore an electronic character of long-range disorders is given by studying on stabilization effects during heat treatment upon the electrical, optical and thermodynamic properties of the Si-As-Te amorphous semiconductors.[12] In the stabilization process due to relaxation of internal deformation energy stored in as-quenched glasses, consistent changes of various electronic and configurational factors such as the band gap, the band-tailing factor, ac conductivity, weight density and specific heat are observed as a function of the annealing time at a temperature slightly below the glass transition temperature T_g. More detailed discussions are given about the correlation between the configurational relaxation kinetics of the internal deformations and the electronic effect of the long-range disorders like localized tail states.[13]

Chapter-VI deals exclusively with reversible threshold switching devices made of bulk alloys and thin films in the Si-As-Te-(Ge) glass system.[14] The author has concentrated primarily on the critical experiments which separate the switching mechanism due to electronic breakdown process from that due to thermal runaway, and systematic experiments on the electric pre-breakdown regime are made for practical application under various conditions of the material parameters and device geometries of the amorphous switching devices. Consequently the thin-film crossover switching device with a considerably high reliability and reproducibility has been

developed in practice.

In the final chapter, conclusions obtained in this thesis work are summarized, and finally the author expresses his gratitude for persons concerned with this work.

REFERENCES-I

1) B. E. Warren, J. Appl. Phys. 8, 645 (1937).

2) S. R. Ovshinsky, Phys. Rev. Letters 21, 1450 (1968).

3) See, e.g., C. Kittel, *Introduction to Solid State Physics*, 3rd ed. (Wiley, New York, 1966).

4) A. I. Gubanov, *Quantum Electron Theory of Amorphous Conductors* (Consultants Bureau, New York, 1963).

5) N. F. Mott, Phil. Mag. 19, 835 (1969).

6) R. E. Borland, Proc. Phys. Soc. 78, 926 (1961).

7) D. Weaire and M. F. Thorpe, Phys. Rev. B 4, 2508 (1971).

8) E. A. Davis and N. F. Mott, Phil. Mag. 22, 903 (1970).

M. H. Cohen, H. Fritzsche and S. R. Ovshinsky, Phys. Rev. Letters 22, 1065 (1969).

9) M. Nunoshita, H. Arai, T. Taneki and Y. Hamakawa, J. Non-Cryst. Solids 12, 339 (1973).

10) M. Nunoshita and H. Arai, Solid State Commun. 11, 213 (1972).

11) M. Nunoshita and H. Arai, *ibid.* 11, 337 (1972).

12) M. Nunoshita, H. Arai, Y. Hamakawa and T. Fujimoto, in *Proceedings of the 5th International Conference on Amorphous and Liquid Semiconductors, Garmisch-Partenkirchen,* (Taylor & Francis LTD, London, 1974) Vol.2, p.753.

13) M. Nunoshita, H. Arai, Y. Hamakawa and T. Fujimoto, in *Proceedings of the 10th International Congress on Glass, Kyoto,* (The Ceramic Soc. of Japan, Kyoto, 1974) 7, p.37.

14) M. Nunoshita, T. Suzuki, M. Hirano and H. Arai, Mitsubishi Denki Gihoh 47, 1303 (1973).

Chapter-II

GLASS-FORMATION METHOD AND BASIC PROPERTIES OF CHALCOGENIDE GLASSES IN THE Si-As-Te SYSTEM

2-1. Introduction

Non-oxide chalcogenide glasses have various useful and attractive characteristics as one of electronic and opto-electronic materials.[1] By controlling their compositions or mixtures, it would be possible to achieve new and extensively desirable material properties. In addition, the unique properties are expected not to change by means of thin-film deposition processes, which do not limit their size and pile. However, even at present, poor understanding of the amorphous or glassy states as well as the absence of reproducible technologies of the glass fabrication and amorphous thin-film processes impedes practical applications of these materials.[2]

In this chapter, an attempt is first made to classify many non-crystalline semiconductors, particularly the chalcogenide glasses, into some categories mainly according to the structural features. Next, the author gives some principal reasons for the use of a Si-As-Te ternary glass system in this work. The peculiar RF heating method which was adopted to fabricate these glasses and the sample preparation processes are presented in detail. Vitrification of the chalcogenide alloys obtained is confirmed by means of X-ray diffraction and basic thermal analyses, and consequently the glass-forming region in this Si-As-Te system is determined.

2-2. Definitions and Classification of Non-Crystalline Semiconductors

The author gives exact definitions of a glassy (vitreous) material and an amorphous semiconductor used frequently in this thesis. An *amorphous* material is defined crystallographically as a substance which does not have such three-dimensionally periodic and symmetric arrangements of atoms or molecules as a crystal. Virtually it is characterized by the X-ray diffraction pattern, consisting not of sharp Bragg reflections but of a few broad halos. However, the X-ray diffraction cannot distinguish evidently between a random arrangement of atoms and a microcrystalline material containing approximately two hundred atoms.[3] *Amorphous* and *non-crystalline* are synonymous in present termenology. A distinctive class of amorphous solids are glasses. From the chemical point of view, a *glass* (or a *vitreous* material) is defined as an inorganic product solidified from the fusion without crystallizing. Such a glass always undergoes what is called a glass transition. These materials all can be classified as a *disordered* system. Most of non-crystalline and vitreous solids are characterized as good insulators, but some kinds of them are included in a category of semiconductors, as shown as follows.[4]

The amorphous semiconductors may be grouped into three major categories as classified in Table-1.[5] The first main group in the table contains the oxide glasses including transition metal ions. The conduction proceeds via a charge exchange among the mixed valence transition metal ions.[6] The dielectric films listed secondly in Table-1 are sensitive to disorder, and their electronic conduction relies on deviations from stoichiometry and on the presence of defect centers which act as donors and acceptors.[7] The third group contains the covalently

Table-1. Classification and Examples of Non-Crystalline Semiconductors. (after Fritzsche[5])

1. *Semiconducting Oxide Glasses*

$V_2O_5-P_2O_5$	$MnO-Al_2O_3-SiO_2$
$V_2O_5-P_2O_5-BaO$	$CoO-Al_2O_3-SiO_2$
$V_2O_5-GeO_2-BaO$	$FeO-Al_2O_3-SiO_2$
$V_2O_5-PbO-Fe_2O_3$	$TiO_2-B_2O_3-BaO$
.....	.....

2. *Dielectric Films*

SiO_x, Al_2O_3, ZrO_2, Ta_2O_3, Si_3N_4, BN, ...

3. *Covalent Non-Crystalline Solids*

A. *Tetrahedral Amorphous Films*

Si, Ge, SiC, InSb, GaAs, GaSb.....

B. *Tetrahedral Glasses,* $A^{II}B^{IV}C_2^V$

$CdGe_xAs_2$, $CdSi_xP_2$, $ZnSi_xP_2$, $CdSn_xAs_2$ .....

C. *Lone Pair Semiconductors*

(i) *elements and compounds*

Se, S, Te, As_2Se_3, As_2S_3 .....

(ii) *cross-linked networks*

Ge-Sb-Se	Si-Ge-As-Te
Ge-As-Se	As_2Se_3-As_2Te
As-Se-Te	Tl_2Se-As_2Te_3
.....	.....

D. *Others*

B, As, $(Cu_{1-x}Au_x)Te_2$ .....

Table-2. Chalcogenide Glass Systems.

Elementary System	VI	Amorphous S, Amorphous Se
Binary System	VI-VI	S-Se, S-Te, Se-Te
	V -VI	As-S, As-Se, As-Te
	IV-VI	Ge-S, Ge-Se, Ge-Te, Si-Te
Ternary System	VI-VI-VI	S-Se-Te
	V -VI-VI	As-S-Se, As-S-Te, As-Se-Te
	V -V -VI	As-Sb-S, As-Sb-Se, As-Bi-S, As-Bi-Se
	III-V-VI	Tl-As-S, Tl-As-Se, Tl-As-Te, Ga-As-Te
	I -V -VI	Ag-As-S
	V-VI-VII	As-S-I, As-S-Br, As-S-Cl, As-Se-I, As-Te-I
	IV-V-VI	Si-As-Te, Si-P-Te, Si-Sb-S, Si-Sb-Se, Ge-P-S, Ge-P-Se, Ge-P-Te, Ge-As-S, Ge-As-Se, Ge-As-Te, Ge-Sb-Se, Pb-As-S
Quaternary System		Ge-Si-As-Te, Ge-Sb-S-Te, Ga-Ge-As-Te, Tl-As-Se-Te, Ge-As-S-Te, Ge-As-Se-Te, K-Ca-Ge-S, Ba-Ca-Ga-S, etc.

bonded amorphous semiconductors: (A) the tetrahedral semiconductors, which can only be prepared by thin-film deposition, (B) the tetrahedral glasses and (C) the lone-pair semiconductors. The lone-pair semiconductors imply a large variety of non-oxide chalcogenide glasses and thin-films, characterized by containing the Group-VI chalcogen elements, i.e. S, Se, or Te. From the structural point of view, they are distinguished (i) the elements and compounds with chain-like molecular complexes of larger size as regarded as inorganic polymers, and (ii) the three-dimensionally cross-linked network structures which approximate more closely the ideal of structural disorder.

As shown in Table-2, these chalcogenide glasses can be classified according to the compositions from elementary systems to ternary or more multicomponent mixtures. Through a great number of recent investigations on these chalcogenide glasses, various useful and interesting properties shown in Table-3 have been found out. These characteristics can be controlled desirably over very wide ranges by changing the com-

Table-3. General Features of Chalcogenide Glasses

1. Electrical Properties
Semiconductive Materials[8]
Memory & Threshold Switches[9]
Photo-Conductive & Photo-Voltaic Effects[8]
Thermo-Electric Power[8]
2. Optical Properties
Infrared Transmission[10]
Large Refractive Index[10]
Large Acousto-Optic Effect[11]
Photo-Induced Index Change[12]
3. Thermal & Mechanical Properties[13]
Large Expansion Coefficient
Low Softening Temperature
Low Hardness
Small Young's Modulus

positions and constituents within inherent glass-forming composition regions of individual glass systems. The glass-forming regions give an important factor for glass formation and stability. In comparison of the size of these regions especially of IV-V-VI ternary systems, it has been qualitatively shown that the glass-forming tendency decreases with increasing atomic mass of the constituent elements in order Si>Ge >Sn, As>P>Sb, S>Se>Te in respective groups.[13] This tendency is also found in dependences of the physical properties like softening point on individual elements of these glasses, except for the reversal of P and As.

In this thesis work, the author has conducted systematic investigations on electrical and optical properties of the Si-As-Te glass system chosen especially from among ternary chalcogenide systems of IV-V-VI elements. Though few investigations on the electronic semiconducting properties have been made so far, this Si-As-Te glass system has considerably high softening temperatures, a very wide glass-forming region and a wide controllable dc conductivity range($10^{-4}\sim10^{-11}$ $\Omega^{-1}\cdot cm^{-1}$) compared with other ternary systems. Therefore, this glass system would be very relevant not only to studying on the compositional dependences of the semiconducting properties, but also to some practical applications to electronic devices.

2-3. Sample Preparations

Vitreous materials are produced by being rapidly cooled from their melts. Since many chalcogenide glass systems include volatile components, e.g. arsenic, sulfur, tellurium, and much care must be taken to exclude atmospheric oxygen, the sample fabrications are usually carried

out by heating the mixtures in evacuated sealed fused-silica ampoules. In order to ensure good mixing and reaction of various components, a rotating or rocking electric furnace is often employed. Reactions are continued at a high temperature for many hours (8∿24 hours) enough to obtain a homogeneous low viscosity melt.[14)]

In this work, a new fabrication procedure by convenient RF heating has been developed to obtain large ingots of the semiconducting Si-As-Te glasses with a good homogeneity in a relatively short melting time. Figure 2-1. shows a schematic diagram of the peculiar induction furnace with a heater of a SiC ceramic tube employed in this thesis work. By the method, these Si-As-Te glasses were synthesized in the following way.[15)] Each of the three raw materials of purity better than 99.999% was ground to 100 mesh powder, weighed with an accuracy of 0.1 mg to

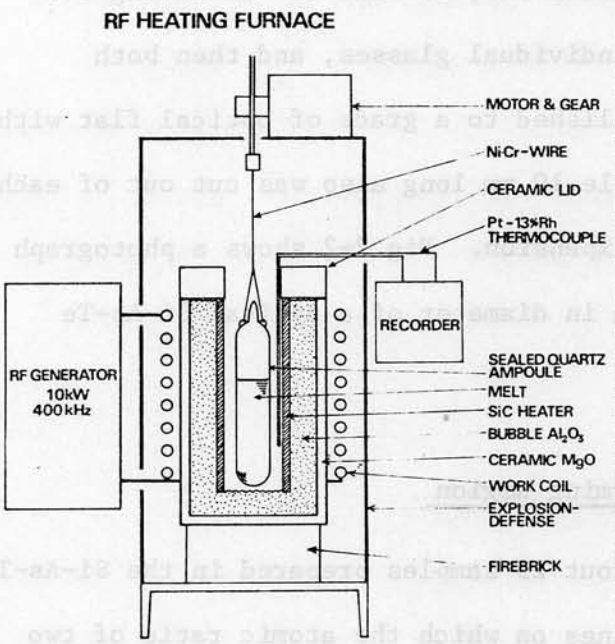

Fig.2-1. A schematic diagram of the induction furnace used for fabrications of Si-As-Te chalcogenide glasses.

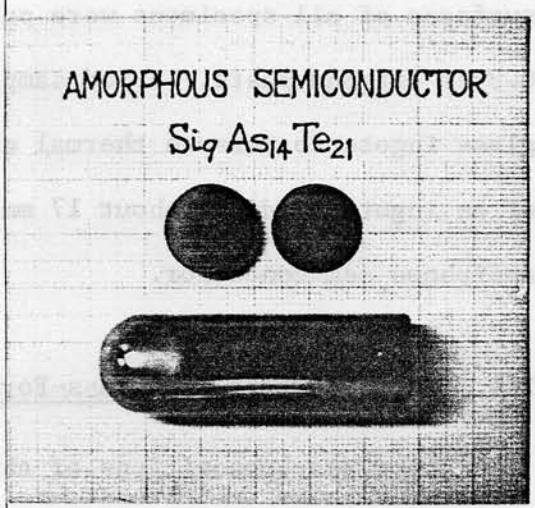

Fig.2-2. An ingot and disks of $Si_9As_{14}Te_{21}$ amorphous semiconductor fabricated by the RF heating method.

the total amount of about 50 g and at once sealed up into a fused-silica ampoule at a pressure below 10^{-5} Torr. The mixture sealed in the ampoule was heated at 1100∿1200 °C continuously for 6 hours by the RF heating method. Self-agitating effect on the melt by the electromagnetic force has enabled the good reaction of mixtures in such a relatively short time. After that, air-quenching was accomplished by removing quickly the ampoule from the furnace. The glasses fabricated have a similar look of the silicon single crystal. Some disks about 1 mm thick were sliced from each ingot of the glasses stabilized sufficiently by heat treatment. The disk samples were polished with 0.3 μm Al_2O_3 powder and washed well in alcohol. The 1 mm thick samples were provided with evaporated Au film electrodes of 1 cm^2 area on both faces for electrical conductivity measurements. For optical measurements, three types of specimens of thickness 100, 200 and 350 μm having 5×5 mm^2 area were prepared from the individual glasses, and then both surfaces of all specimens were polished to a grade of optical flat with 0.3 μm diamond paste. A rod sample 10 mm long also was cut out of each glass ingots to measure thermal expansion. Fig.2-2 shows a photograph of an ingot and disks about 17 mm in diameter of a typical Si-As-Te amorphous semiconductor.

2-4. Vitreous State and Glass-Forming Region

The glass-compositions of about 25 samples prepared in the Si-As-Te system were selected along the lines on which the atomic ratio of two elements is kept constant, as shown in Fig.2-3. The real compositions were confirmed to be in good agreement with the values weighed at the start within about 2% on the inspection by the atomic absorption analy-

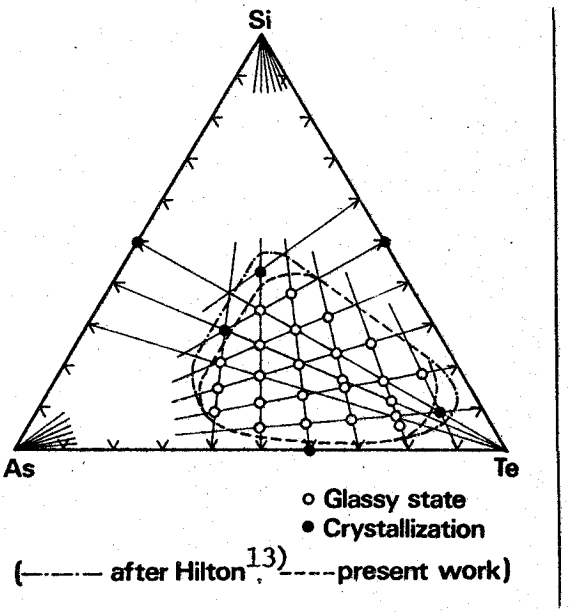

Fig.2-3. Compositions of synthesized glasses and glass-forming region in the Si-As-Te system.

sis (Nippon Jarrell-ASH, Jaco AA-1E).

Vitrification of the as-fabricated alloys was examined by using the following methods: (i) the X-ray or electron diffraction (Shimadzu VD-1 or Electron Microscope JEM-7A), (ii) the thermal expansion (Leitz Dilatometer model-UBD or Perkin Elmer TMS-1), (iii) the thermal analysis of DSC traces (Perkin Elmer DSC-1), and (iv) the electrical dc conductivity and the optical transmission (Shimadzu 2-beam Spectrometer), etc. As previously mentioned, the vitreous (or glassy) materials are considered to be a kind of amorphous solids frozen in with disordered atomic arrangements in their fused state. Such vitreous materials can be structurally distinguished from crystalline ones by the X-ray or electron diffraction. Therefore, as shown in Figs.2-4 and 2-5(a) and (b), the sample solidified to a glass does not exhibit sharp reflections associated with various crystallized materials, but represents a few broad halos in the X-ray and electron diffraction patterns from some

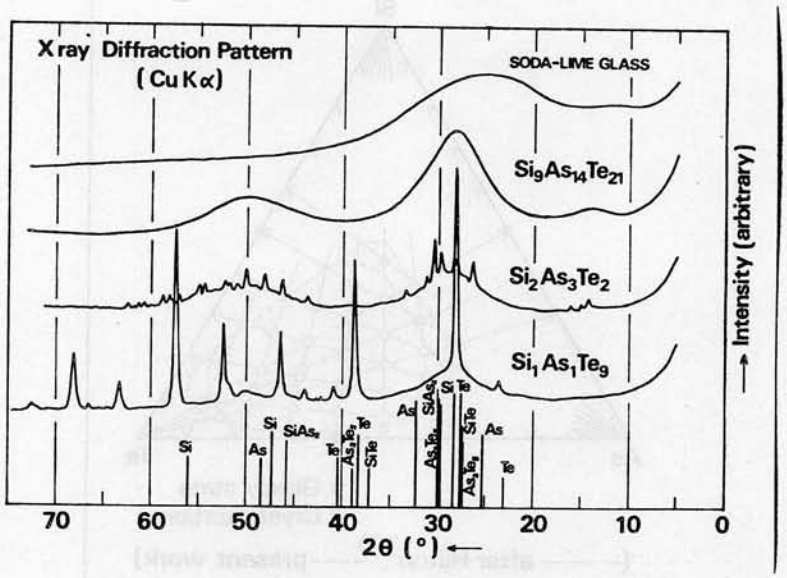

Fig.2-4. X-ray diffraction patterns of some Si-As-Te chalcogenide alloys and a soda-lime glass (Cu-Kα; 40kV, 20mA).

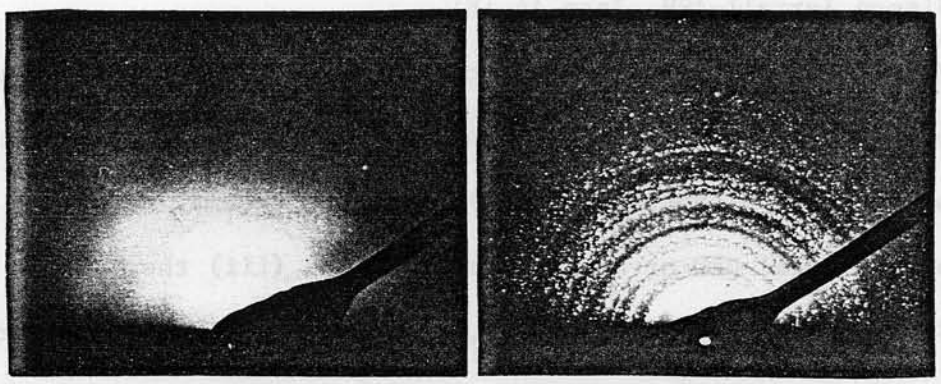

(a) *amorphous* (b) *crystalline*

Fig.2-5. Reflected electron diffraction patterns from two Si-As-Te alloy samples (100 kV, beam ∿1 μmϕ).

Si-As-Te glasses as well as a soda-lime glass. The crystallized materials can be identified mainly as Te polycrystals. On the other hand, Fig.2-6 illustrates the linear thermal expansion curve and the differential scanning calorimetric (DSC) trace for a typical chalcogenide glass, $Si_1As_6Te_9$, togather with those for a Sn metal at the same heating rate of 20 °C/min. From these measurements, a vitreous state was

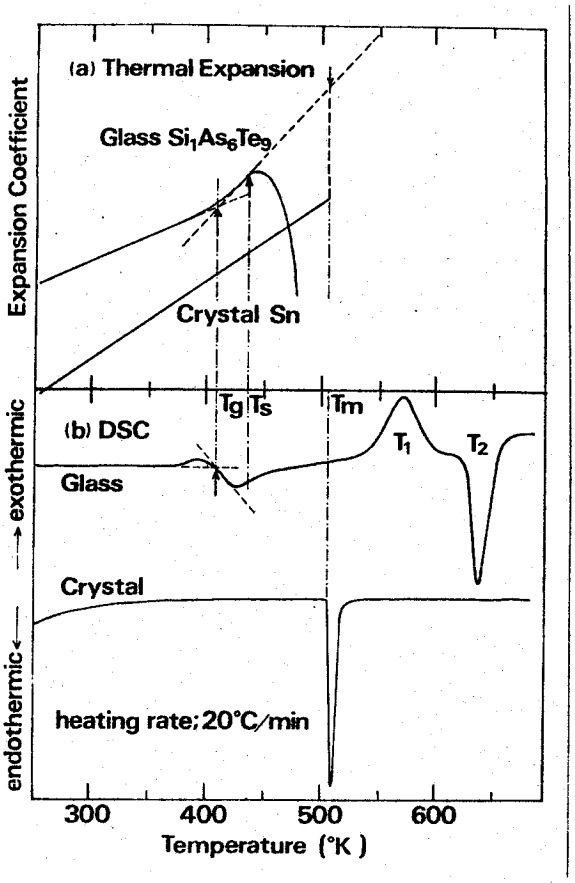

Fig.2-6. Linear thermal expansion and differential scanning calorimetric (DSC) curves as a function of temperature for a typical chalcogenide glass, $Si_1As_6Te_9$, and a Sn metal at the same heating rate of 20 °C/min.

confirmed by the occurence of a glass transition: remarkable increases of thermal expansion coefficient and of heat capacity in the vicinity of the glass transition temperature T_g. On the DSC traces for the glasses containing silicon less than 10 atomic %, an exothermic peak T_1 due to divitrification and an endothermic peak T_2 due to the eutectic melting appear above the T_g. At the same time, softening effect of the sample is observed at the softening temperature T_s on the expansion curve. From such thermal measurements made at the heating rate of 20 °C/min, the glass transition temperature T_g, the softening temperature T_s and the thermal expansion coefficient β below the T_g were determined

for all the Si-As-Te glasses. Likewise, extreme differences between a vitreous phase and a crystallized one have been found in the electrical and optical properties; that is, the vitreous phase material is much more infrared transparent and has very much lower electrical conductivity than the crystallized alloy.

As a result of the above examinations, a glass-forming region of the Si-As-Te ternary system has been determined and is depicted as an island enclosed by a dotted line in the Gibbs' composition triangle of Fig.2-3. As seen in Fig.2-3, the glass-forming region obtained in this thesis work coincides almost with the result of Hilton *et al.*[13], and is localized below 40 atomic % for the Si content and above 30 atomic % for the Te content in the Gibbs' triangle. Strictly speaking, this region becomes the wider, the greater the cooling rate and the smaller the sample volume. Crystalline materials such as small crystallites of elementary tellurium and stoichiometric binary compounds are apt to precipitate from the glass of compositions along the boundaries of the region. Therefore, the Si-As-Te system having such a large glass-forming region enables one to get stable glasses, and the glass in the center of the region is of course more stable than one near the border.

2-5. Summary

In this chapter, the general features and the classifications of various chalcogenide glasses and amorphous semiconductors have been reviewed. From among a large variety of chalcogenide glasses, the Si-As-Te ternary system having a very wide glass-forming region and a wide controllable dc conductivity range has been chosen for the use of this thesis work. In order to fabricate a series of the Si-As-Te amorphous

semiconductors of a large size with a good homogeneity in a relatively short melting time, a peculiar RF heating method has been developed. The confirmation of the vitrification has been made for the individual Si-As-Te alloys by means of the X-ray diffraction, the thermal expansion, the scanning calorimetric trace, and the glass-forming region in the Si-As-Te ternary system has been determined.

REFERENCES-II

1) S. R. Ovshinsky and H. Fritzsche, IEEE Tran. Electron Devices ED-20, 91 (1973).

2) R. G. Neale, J. Non-Cryst. Solids 2, 558 (1970).

3) B. G. Bagley, *Amorphous and Liquid Semiconductors*, ed. by J. Tauc (Plenum Press, London and New York, 1974) p.1.

4) G. W. Morey, *The Properties of Glass*, 2nd ed. (Reinhold Publ., New York, 1954).

5) H. Fritzsche, *Bussei* 13, 59 ((1972).

6) N. F. Mott, J. Non-Cryst. Solids 1, 1 (1968).

7) A. K. Jonscher, Thin Solid Films 1, 213 (1967).

8) B. T. Kolomiets, Phys. Stat. Sol. 7, 713 (1964).

9) A. M. Andriesh and B. T. Kolomiets, Sov. Phys. Solid State 6, 2652 (1965).

9) S. R. Ovshinsky, Phys. Rev. Letters 21, 1450 (1968).

10) A. R. Hilton, Appl. Optics 5, 1877 (1966).

11) D. A. Pinnow *et al.*, Appl. Phys. Letters 15, 83 (1969).

12) T. Igo and Y. Toyoshima, J. Non-Cryst. Solids 11, 304 (1973).

13) A. R. Hilton, C. E. Jones and M. Brau, Phys. Chem. Glasses 7, 105 (1966).

14) A. D. Pearson, J. Non-Cryst. Solids 2, 1 (1970).

15) M. Nunoshita and H. Arai, Solid State Commun. 11, 213, 337 (1972).

Chapter-III

ELECTRICAL AND OPTICAL PROPERTIES OF Si-As-Te AMORPHOUS SEMICONDUCTORS

3-1. Introduction

Recent intensive investigations on amorphous semiconductors have revealed that there exists an energy-band gap in the electronic density of states and it plays an important role in the electrical and optical properties.[1] The band gap in semiconducting chalcogenide glasses is usually determined from the activation energy of dc conductivity or the optical absorption edge. Other experimental evidences for the presence of the gap have been provided by means of fundamental optical absorption,[2] photo-emission spectrum,[3] tunneling spectroscopy,[4] etc. in amorphous Ge and Si films. In order to explain electronic processes in such an amorphous semiconductor, Mott *et al.*[5] and Cohen *et al.*[6] have proposed a concept of the *mobility edge*, what is sometimes called Mott-CFO model. The essential features of this model are (i) the existence of an energy pseudo-gap in the electronic structure, and (ii) the electronic localized states in the pseudo-gap up to critical energies defining a mobility gap. However, this model has not yet been experimentally confirmed in detail, and there is even some disagreement in the energy profile of electronic states between the concepts of Mott *et al.* and Cohen *et al.* These problems have not so far been studied systematically because of the complicated features of localized states inside the mobility gap.[7]

This chapter deals with electrical and optical properties of the

Si-As-Te amorphous semiconductors. From measurements of the temperature-dependent conductivity and optical absorption spectrum, some electronic parameters such as electrical and optical energy gaps are determined. The author verifies that these parameters play an important role in the semiconducting properties.[8] On the basis of the experimental results on the electronic properties, a tentative energy-band model in the Si-As-Te amorphous semiconductors is postulated in consideration of the extended and localized electronic states, and then discussions are given as compared with the intrinsic band-conduction of covalent crystalline semiconductors such as germanium and silicon.

3-2. Optical Absorption and Optical Energy Gap

It is well known that most of non-oxide chalcogenide glasses are good transparent in a very wide infrared region.[9] A typical infrared transmission spectrum obtained in the $Si_9As_{14}Te_{21}$ glass is shown in Fig.3-1. This spectrum was measured for the sample 350 μm thick by

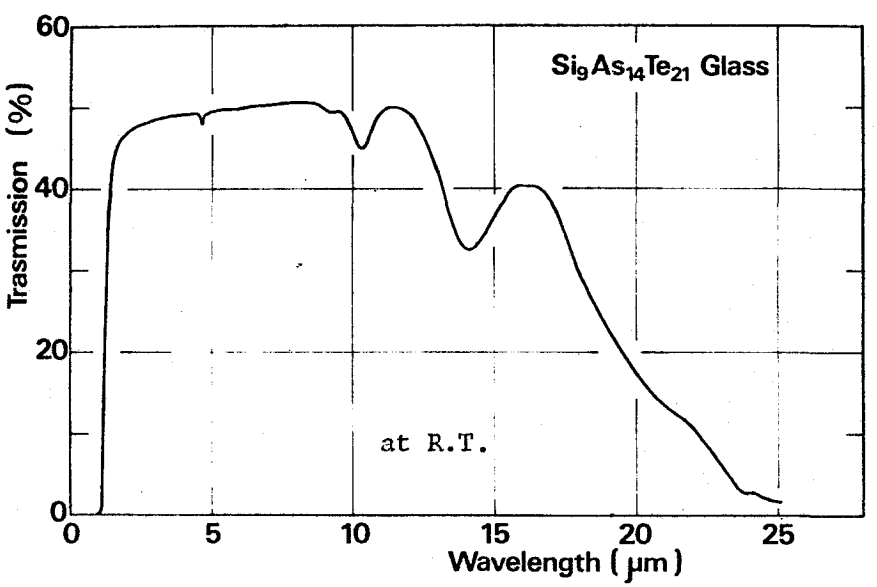

Fig.3-1. Infrared transmission spectrum of $Si_9As_{14}Te_{21}$ glass.

using Shimadzu 2-beam Spectrometer (0.6∿2.5 μm) and Shimadzu Recording Infrared Spectrophotometer (2.5∿25 μm) at room temperature. As seen in this spectrum, an excellent and wide transparent region is found between two values. In this transmission range, the low transmission of about 40∿50 % is not due to the absorption but caused by the large reflection; therefore the magnitude of absorption coefficients in this region has been found to be less than 0.1 cm^{-1} for some chalcogenide glasses. The appearance of such a wide transparent region suggests that the Si-As-Te amorphous semiconductor has a forbidden gap in the electronic density of states similar to that in a conventional crystalline semiconductor. Fundamental absorptions at the short wavelength edge of the transparent range in Fig.3-1 are caused by electronic interband transitions between the valence and conduction bands. The absorption edge is corresponding roughly to the width of a forbidden gap between both bands. In contrast, the long wavelength cut-off may be determined by the infrared absorption of the constituent atoms or molecules. Fig.3-2 represents the transmis-

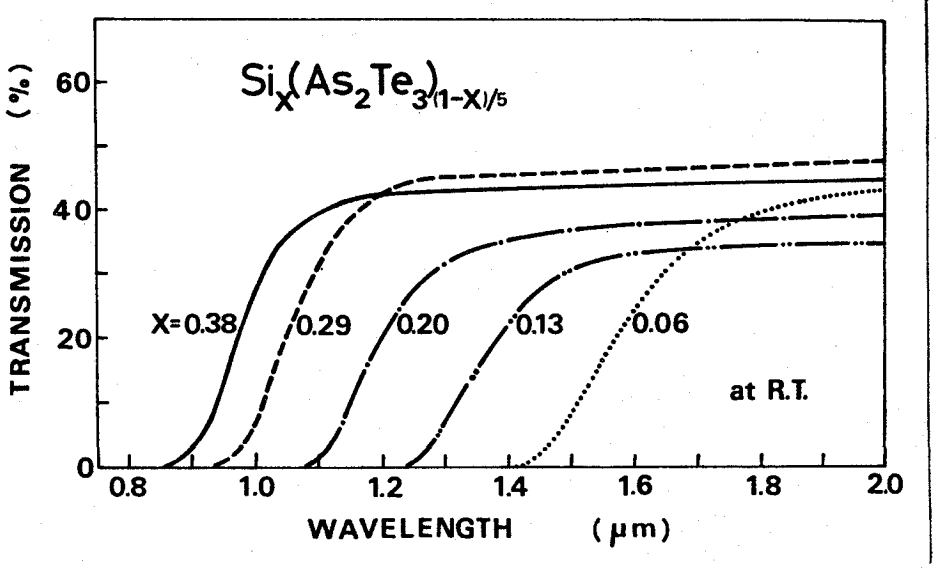

Fig.3-2. Optical transmission spectra in the vicinity of fundamental absorption edge of several Si-As-Te glasses 350 μm thick at room temperature.

sion spectra in the vicinity of the fundamental edges of some Si-As-Te amorphous solids 350 μm thick at room temperature. As can be seen in the figure, the optical absorption edge is rather soft as compared with those of single-crystal semiconductors. General features in the obtained spectra and compositional changes agree fairly well with the result of Minami *et al.*[10)]

Optical absorption coefficients $\alpha(\omega)$ can be easily calculated from the transmission spectrum near the fundamental absorption edge by using

$$t = (1-r)^2 \cdot \exp[-\alpha(\omega) \cdot d] \quad , \qquad \ldots\ldots \qquad (3\text{-}1)$$

where t is the transmission, r the reflectivity and d the thickness in cm of the glass specimen. Even without knowledge of r, $\alpha(\omega)$ can be estimated from the transmission spectra measured for two specimens of different thickness, 100 and 200 μm, cut away from the same glass ingot. The transmission spectra were measured by using SPEX No.1700-III or the Shimadzu 2-beam Spectrometer. The absorption $\alpha(\omega)$ estimated by using Eq.(3-1) is plotted as shown in Fig.3-3 for various Si contents of the Si-As-Te glasses. A spectral change in the optical absorption near the fundamental edge is characterized by $\alpha(\omega)$ which increases exponentially the incident photon energy $\hbar\omega$ in the range $10<\alpha(\omega)<10^3$ cm^{-1}, obeying an empirical relationship of the form:

$$\alpha(\omega) = \alpha_o \cdot \exp(\hbar\omega/E_s) \quad , \qquad \ldots\ldots \qquad (3\text{-}2)$$

where α_o is a constant and E_s a constant, so called band-tailing factor. Such an exponential absorption edge is frequently called Urbach tail in heavily doped covalent semiconductors[11)]. Here, the optical energy-band gap $E_{g(op)}$ of the amorphous semiconductor is expediently defined as the photon energy $\hbar\omega$ corresponding to $\alpha(\omega)=10cm^{-1}$. This value of $\alpha(\omega)$ gives the upper limit of about 2.5×10^{17} states/cm^3 for the density of gap

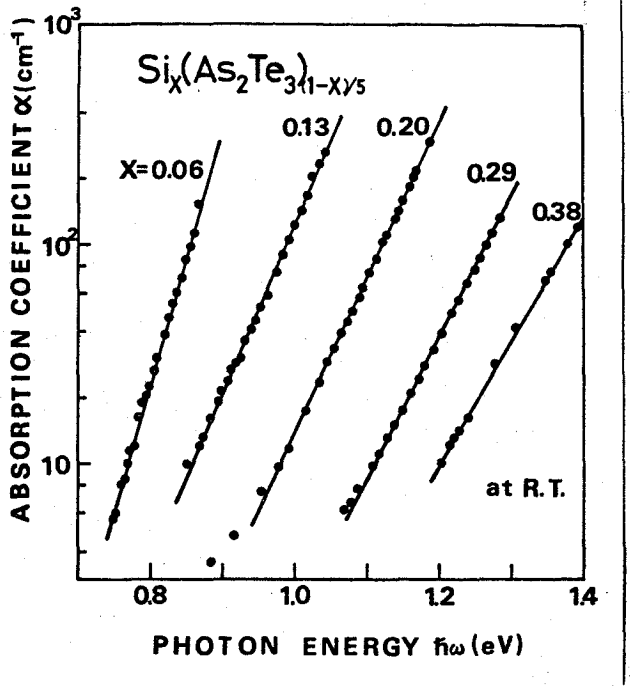

Fig.3-3. Optical absorption edges of several Si-As-Te vitreous solids at room temperature.

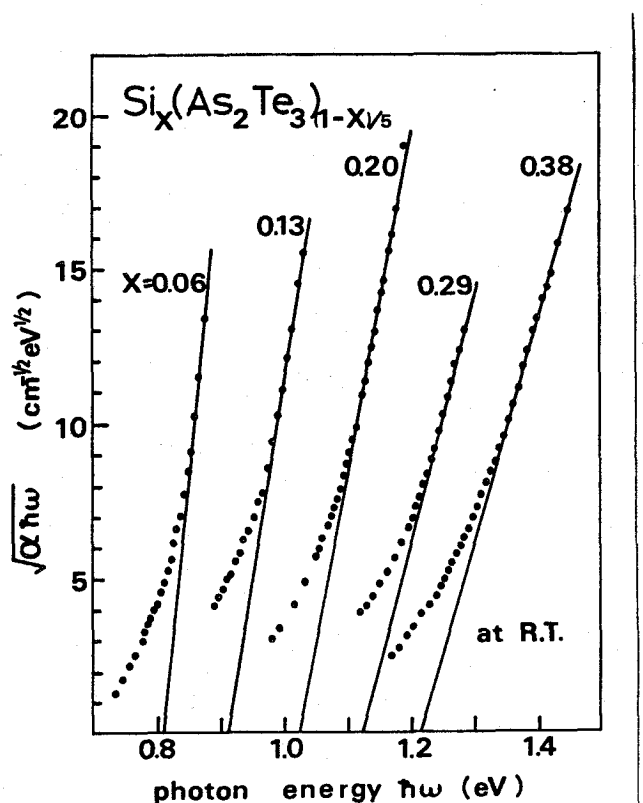

Fig.3-4. Functional dependence of optical absorption edges on photon energy $\hbar\omega$ in several Si-As-Te glasses in the form of $(\alpha\hbar\omega)^{1/2}$ versus $\hbar\omega$.

states in amorphous Ge films.[3]

In amorphous semiconductors, the transitions between localized and extended states as well as the interband transitions have to be considered; however, when both initial and final states are localized, the lack of spacial overlap between the eigenstates may cut down the transition probability to small values. According to Fritzsche[1] and Davis *et al.*[5], the absorption coefficient $\alpha(\omega)$ is expressed as follows:

$$\alpha(\omega) = A\frac{|M|^2}{\hbar\omega}\int g_v(E)\cdot g_c(\hbar\omega+E)\cdot dE \ , \qquad \ldots\ldots \qquad (3\text{-}3)$$

where A is a constant, M the optical matrix element and $g_v(E)$, $g_c(E)$ are the densities of the initial and final states. The above integration is over all pairs of states in the valence and conduction bands separated by an energy $\hbar\omega$. Without knowledge of the form of g(E) at the band edges it is speculative to take the calculation further. If either the initial or the final eigenstate is localized, the $\vec{k}$-vector is not conserved for the transition between the states, what is called *non-direct* transition having constant matrix elements and a relaxed $\vec{k}$-conservation rule found in most amorphous semiconductors unlike in crystalline semiconductors. Then the absorption edge for the *non-direct* transitions can be expressed by the following simple form:

$$\alpha(\omega) = \frac{\alpha_o}{\hbar\omega}[\ \hbar\omega - E^*_{g(op)}\ ]^n \ , \qquad \ldots\ldots \qquad (3\text{-}4)$$

where α_o is a constant, n is an exponent and $E^*_{g(op)}$ can be defined as another optical gap. Here Eq.(3-4) can be deduced on the assumption that $g_c(E)=g_v(-E)$ and g(E) obeys some power of E near the band edges.

It has been often observed in many semiconducting glasses, i.e., As_2S_3, As_2Se_3, As_2Te_3, [5,12] whose absorption has perfectly fitted the

formula with a value of n=2 in Eq.(3-4) at enough high absorption levels of $\alpha(\omega) \geq 10^4$ cm^{-1} above the exponential tail. The author also attempts to re-plot $[\alpha(\omega)\hbar\omega]^{1/2}$ against $\hbar\omega$ in Eq.(3-4) from the experimental results in Fig.3-3 for some Si-As-Te glassy semiconductors. As shown in Fig.3-4, the plots fit the linear relation of $[\alpha(\omega)\hbar\omega]^{1/2}$ versus $\hbar\omega$ only in the range of $[\alpha(\omega)\hbar\omega]^{1/2} > 10$ $(eV/cm)^{1/2}$. It is expected that the Eq.(3-4) might be more profitable in the high absorption range with $\alpha(\omega) \geq 10^3$ cm^{-1}. Unfortunately it is very difficult to obtain such high values of $\alpha(\omega)$, because of the technical difficulty of making thin films less than 50 μm thick for the multicomponent Si-As-Te glasses. As a result of the above discussion, the optical gap $E^*_{g(op)}$ is determined from an extrapolation of the plots of $[\alpha(\omega)\hbar\omega]^{1/2}$ versus $\hbar\omega$ in the high absorption region. In comparison of the $E_{g(op)}$ with $E^*_{g(op)}$ for the same sample, the small difference between both gap energies can justify the above-mentioned expedient definition of the optical gap $E_{g(op)}$ corresponding to $\alpha(\omega)=10$ cm^{-1}. Therefore, the value of $E_{g(op)}$ is adopted as the optical gap of the Si-As-Te amorphous semiconductor in this work and shown in Table-4 together with the values of $E^*_{g(op)}$ and E_s.

Fig.3-5 shows temperature dependence of the optical absorption $\alpha(\omega)$ of the $Si_3As_3Te_7$ glass. The exponential tails of $\alpha(\omega)$ shift almost in parallel to the lower energies with increasing temperature. Fig.3-6 exhibits typical curves of the temperature dependence of $E_{g(op)}$, that is, the shift of the photon energy $\hbar\omega$ at $\alpha(\omega)=10$ cm^{-1} with temperature. As seen in Fig.3-6, the gap $E_{g(op)}$ decreases almost linearly with the increase of T near room temperature and can be approximated as follows:

$$E_{g(op)} \simeq E'_g(0) - \gamma T \quad , \qquad \cdots\cdots \qquad (3\text{-}5)$$

where γ is the temperature coefficient of $E_{g(op)}$ near room temperature

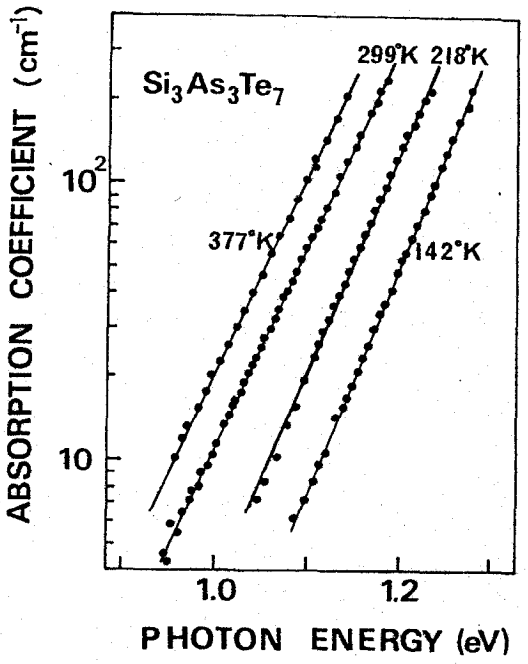

Fig.3-5. Temperature dependence of optical absorption edge in $Si_3As_3Te_7$ glass.

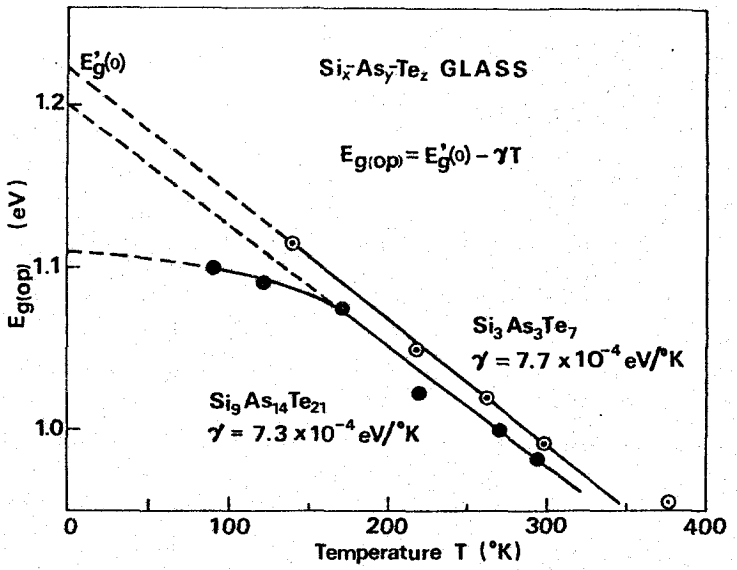

Fig.3-6. Temperature dependence of optical gap $E_{g(op)}$ in $Si_3As_3Te_7$ and $Si_9As_{14}Te_{21}$ glasses.

and $E'_g(0)$ is a constant zero-gap but not the real optical gap at T=0°K because the curves are expected to approach T=0°K with zero slope.

From the slope of the linear portion in Fig.3-6, the γ-values of 7.7×10^{-4} and 7.3×10^{-4} eV/deg are estimated for the $Si_3As_3Te_7$ and $Si_9As_{14}Te_{21}$ glasses, respectively. According to Kolomiets[13] and Fagen *et al.*[14], the γ-value in amorphous materials can be given by the following thermodynamic relationship:

$$-\gamma = \left(\frac{\partial E_g}{\partial T}\right)_P = \left(\frac{\partial E_g}{\partial T}\right)_V - \frac{3\beta}{K_s}\left(\frac{\partial E_g}{\partial P}\right)_T , \qquad \text{.....} \qquad (3\text{-}6)$$

in which β is the linear thermal expansion coefficient and K_s the bulk compressibility. On the right side of Eq.(3-6), the first term arises from the interaction of electrons with phonons, and is at least an order of magnitude larger than the second term due to lattice dilation of the substance. Mott has suggested that the γ-value is generally greater in

amorphous semiconductors than that in crystalline ones because of large thermal disordering of the network structures based on their spiral chains or layer-like lattices.[15] Indeed, the γ-values obtained here are relatively larger than those of crystalline semiconductors, and besides are almost equal to $\gamma=7\sim8\times10^{-4}$ eV/deg in most chalcogenide glasses[16] other than a few such as amorphous Se[17] and GeTe[18].

3-3. DC Conductivity and Electrical Energy Gap

Temperature dependence of the dc conductivity σ_T was measured by using a dc microvolt ammeter (TOA, PM-18C) and a high impedance electrometer (Takeda, TR-8651) for the 1 mm thick disk of each Si-As-Te glassy

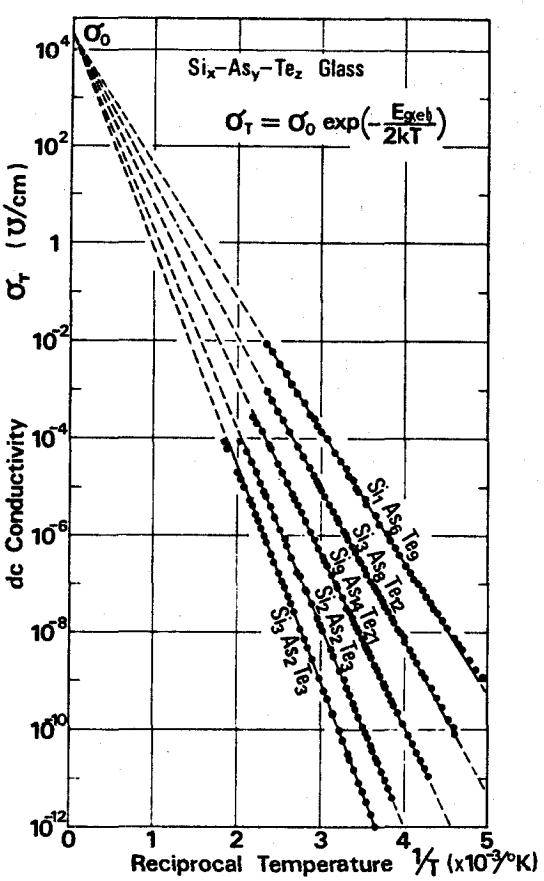

Fig.3-7. Temperature dependence of dc conductivity σ_T of several Si-As-Te amorphous semiconductors.

semiconductor held in a metal vessel at a pressure below 10^{-3} Torr. The temperature was raised very slowly from about -100 °C to the glass transition temperature T_g of each of the glass samples. This upper limit of the temperature range was determined with a view to avoid non-electronic influences like ionic conduction, crystallization, devitrification, deformation. The values of σ_T were estimated from the dc conductances in the low-field Ohmic region (below 10^4 V/cm at room temperature) of the dc voltage-current characteristics. Fig.3-7 shows typical data of the conductivity σ_T plotted semilogarithmically against the reciprocals of absolute temperature T for some Si-As-Te amorphous semiconductors. These plots give precisely straight lines as illustrated in the figure. Over the considerably wide temperature range, the dc conductivity σ_T is fitted into a familiar formula as

$$\sigma_T = \sigma_o \cdot \exp(-\Delta E/kT) = \sigma_o \cdot \exp[-E_{g(el)}/2kT] \quad \ldots\ldots \quad (3\text{-}7)$$

Here σ_o is a constant pre-exponential term, ΔE the thermal activation energy and k Boltzmann's constant. In general, the electrical energy-band gap $E_{g(el)}$ of amorphous semiconductors is defined as twice the activation energy ΔE in Eq.(3-7) by analogy with the intrinsic band-conduction process in crystalline semiconductors. The values of $E_{g(el)}$ and σ_o determined for all the samples in the Si-As-Te system are summarized in Table-4. A remarkable point in the figure and table is that the values of σ_o for all the Si-As-Te glasses prepared in this thesis work are included within the following range:

$$\sigma_o = (2.1 \pm 0.6) \times 10^4 \ (\Omega \cdot cm)^{-1}. \quad \ldots\ldots \quad (3\text{-}8)$$

Therefore the dc conductivity σ_T at a certain temperature, e.g. σ_{25} at 25 °C shown in Table-4, can be directly related to the electrical gap $E_{g(el)}$, as represented in Fig.3-8. Similar values of σ_o have often been

Table-4. Electrical and Optical Properties of Si-As-Te Glasses

COMPOSITIONS (Atomic Ratio)	σ_{25} $(ohm\cdot cm)^{-1}$	σ_o $[\times 10^4$ $(ohm\cdot cm)^{-1}]$	$E_{g(el)}$ (eV)	$E_{g(op)}$ (eV) for $=10cm^{-1}$	$E'_{g(op)}$ (eV) by $\sqrt{\alpha\hbar\omega}$	E_s (eV)	F_b (kV/cm) 1ms pulse 10% duty
$Si_9 As_4 Te_{36}$	1.01×10^{-6}	2.12	1.21				10.6
$Si_1 As_3 Te_{12}$	7.15×10^{-5}	2.03	0.99				2.8
$Si_4 As_9 Te_{36}$	3.05×10^{-5}	2.07	1.03				5.0
$Si_2 As_3 Te_{12}$	8.69×10^{-6}	2.19	1.10				6.4
$Si_1 As_1 Te_4$	9.65×10^{-7}	2.23	1.22	0.86		0.057	13.4
$Si_{12}As_7 Te_{28}$	7.11×10^{-9}	1.97	1.46				
$Si_7 As_{27}Te_{63}$	2.23×10^{-5}	1.63	1.04	0.76	0.79	0.042	4.5
$Si_7 As_{12}Te_{28}$	8.15×10^{-7}	1.70	1.22	0.85		0.057	13.4
$Si_2 As_3 Te_7$	3.10×10^{-7}	2.65	1.29	0.89	0.93	0.059	23.4
$Si_3 As_3 Te_7$	1.60×10^{-8}	2.10	1.44	0.99	1.03	0.067	
$Si_{14}As_9 Te_{21}$	1.45×10^{-10}	1.98	1.66	1.13		0.073	
$Si_1 As_6 Te_9$	1.46×10^{-5}	2.01	1.07	0.77	0.81	0.038	4.6
$Si_3 As_8 Te_{12}$	6.39×10^{-7}	2.08	1.24	0.86	0.91	0.056	16.0
$Si_9 As_{14}Te_{21}$	2.05×10^{-8}	1.97	1.42	0.98	1.02	0.059	69.0
$Si_2 As_2 Te_3$	4.52×10^{-10}	2.05	1.61	1.11	1.13	0.067	
$Si_3 As_2 Te_3$	1.29×10^{-11}	2.06	1.78	1.20	1.22	0.075	
$Si_1 As_9 Te_9$	1.04×10^{-5}	2.19	1.10	0.77		0.045	6.0
$Si_1 As_4 Te_4$	5.81×10^{-7}	1.94	1.24	0.87		0.048	17.3
$Si_3 As_7 Te_7$	2.96×10^{-8}	2.56	1.41	0.98		0.051	45.0
$Si_2 As_3 Te_3$	9.94×10^{-10}	1.85	1.56	1.08		0.064	
$Si_1 As_1 Te_1$	7.76×10^{-11}	2.19	1.71	1.15		0.070	
$Si_1 As_6 Te_4$	3.44×10^{-7}	1.58	1.27				23.9
$Si_6 As_{21}Te_{14}$	2.17×10^{-8}	1.60	1.39	0.99		0.054	51.6
$Si_4 As_9 Te_6$	9.10×10^{-9}	1.59	1.57				
$Si_{12}Ge_{10}As_{30}Te_{48}$ (Ovonic glass)	4.05×10^{-8}	1.92	1.37				44.0

observed not only for most of semiconducting chalcogenide glasses but also for the intrinsic conduction in the single-crystal silicon, germanium, or other covalent semiconductors,[19] as inscribed with black circlets in Fig.3-8. This pre-exponential term σ_o for the intrinsic crystalline semiconductors is essentially expressed by a product of the effective density of states and the microscopic mobility at the band edges. The σ_o-value for the intrinsic band-conduction in purely covalent semiconduc-

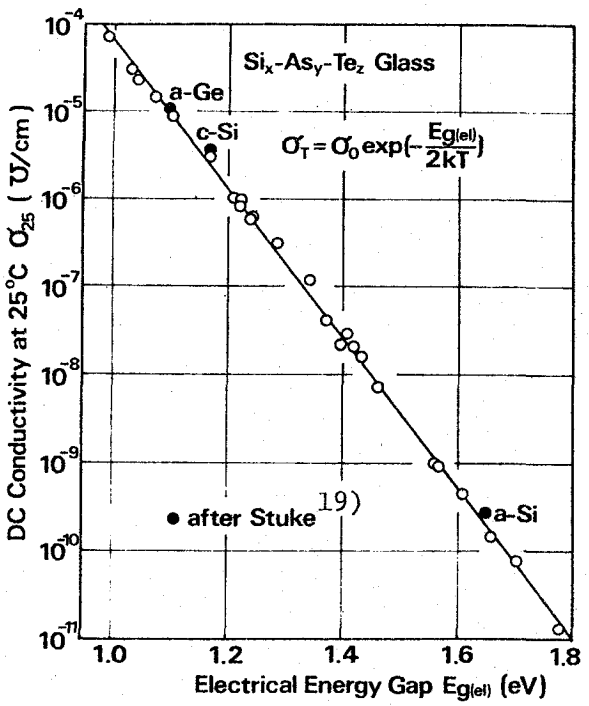

Fig.3-8. Relation between dc conductivity σ_{25} at 25°C and electrical gap $E_{g(el)}$ for all Si-As-Te amorphous semiconductors, and for intrinsic crystalline or amorphous Si and Ge.

tors is generally larger than that for hopping or ionic conductions in various semiconductors and semi-insulators. These facts imply that the basic factors for electronic conduction in these amorphous semiconductors can be analogous to those for the intrinsic band-conduction in the covalent crystalline semiconductors.

On the basis of the standard semiconductor theory, the σ_o term of the temperature-dependent intrinsic conduction can be derived in Appendix-B as follows:

$$\sigma_o = 2e \cdot g(E_{c,v}) \cdot \mu_o \cdot \exp(\gamma/2k) \ , \qquad \ldots\ldots \qquad (3\text{-}9)$$

where $g(E_{c,v})$ is the effective density of states at the band edges, μ_o the microscopic band-conduction mobilities of electrons and holes, and γ the temperature-dependent coefficient of the band gap near room temperature as assumed in Eq.(3-5). If g(E) and μ(E) do not vary too

rapidly with T above E_c and below E_v into the bands, one can use their average values, $g(E_{c,v})$ and μ_o. The value of $g(E_{c,v})$ can be estimated to be about 2.5×10^{19} cm^{-3}. If extended states at the band edges are not strongly affected by disorderness, μ_o might describe the motion of nearly free electrons or holes with occasional scattering. In most amorphous semiconductors it appears likely that $\mu_o \simeq 50 \sim 100$ $cm^2/V \cdot sec$, which corresponds to a mean free path less than average de Broglie wavelength of free electrons in solids ($\sim$100 Å).[20] By substituting these values and $\gamma = 7.3 \times 10^{-4}$ eV/deg, the value of σ_o can be approximately estimated to lie within $2 \sim 6 \times 10^4$ $(\Omega \cdot cm)^{-1}$, which agrees very closely with the experimental result of Eq.(3-8) obtained for the Si-As-Te system.

In studies of the optical absorption and of the electical conduction, their infrared transparency and thermal activation energy of dc conductivity have evidently taught that there exists an energy-band gap between the valence and conduction bands and nearly intrinsic electronic band-conduction is predominant in the Si-As-Te amorphous semiconductors, in a similar way to intrinsic semiconductors such as silicon and germanium. Recently, many experimental investigations on the presence of band gap and band-broadening mainly in amorphous Ge and Si films have been made by means of the ε_2 spectra (imaginary part of dielectric constants) from optical absorptions above the fundamental edge,[2] the photo-emission spectra,[3] the tunneling conductance spectroscopies,[4] etc. These results have manifested that even in the amorphous Ge and Si films a pseudo-gap is preserved between the valence and conduction bands, at the edges of which band-broadening takes place. Likewise, the electron tunneling spectroscopy has provided strong evidence for a Fermi level

that, at the film surface least, is positioned close to the center of the band gap. Unfortunately, these experimental methods have not been yet applied to multicomponent chalcogenide systems like the Si-As-Te amorphous semiconductors, but the above-obtained results on the optical and electrical properties make one feel confident that similar electronic processes proceed in the Si-As-Te amorphous materials.

3-4. Photo-Conductivity, AC Conductivity and Localized States

As shown in Table-4, one can find out considerably large difference of the electrical gap $E_{g(el)}$ to the optical gap $E_{g(op)}$ determined in the Si-As-Te amorphous system. A linear relation between both gaps is plotted in Fig.3-9. As seen from the figure, the energy difference,

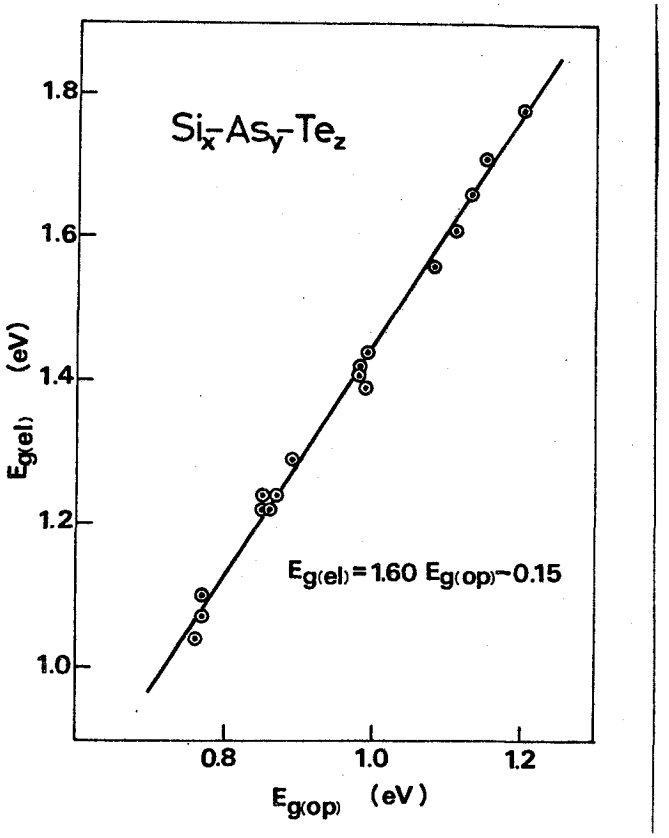

Fig.3-9. Empirical relation between $E_{g(el)}$ and $E_{g(op)}$ in Si-As-Te amorphous semiconductors.

$E_{g(el)}-E_{g(op)}$, varies linearly with the width of the band gap as follows:

$$E_{g(el)} - E_{g(op)} = 0.60\ E_{g(op)} - 0.15 \quad \text{in eV.} \quad \ldots\ldots \quad (3\text{-}10)$$

As discussed in detail in Appendix-B, this value can be derived in the following form:

$$E_{g(el)} - E_{g(op)} = 2 \cdot E_t + \gamma \cdot T \mp \hat{\varepsilon}\ . \quad \ldots\ldots \quad (3\text{-}11)$$

The above equation (3-11) indicates that the large difference between the two gap energies should originate from the activation energy E_t of the effective trap-limited drift mobility, the temperature coefficient γ of the band gap, and an error $\hat{\varepsilon}$ from the procedure used to determine the optical gap. Therefore, the measured difference must offer an experimental evidence for the presence of localized tail states near the band edges. Since all Si-As-Te amorphous semiconductors used in this work are considered to have an almost constant γ-value of about $7\sim8 \times 10^{-4}$ eV/deg regardless of the compositions, the term of γT is assumed about equal to 0.21 eV at room temperature. The error $\hat{\varepsilon}$ in Eq.(3-11) will be negligible. As a result, the E_t-values are estimated to be 0.04 to 0.19 eV in the Si-As-Te system, and thus the term of $2E_t$ is likely related to the compositional-dependent term in the empirical equation (3-10). Therefore, the simple correlation between E_t and $E_{g(op)}$ implies that in the Si-As-Te amorphous system the distribution depth of the localized tail states into the pseudo-gap increases as the optical gap $E_{g(op)}$ increases.

By Nagels *et al.*[21], the activation energy of thermo-electric power curve has been recently found to be less than the corresponding slope of the dc conductivity in the Si-As-Te amorphous semiconductors. In account for the difference in the activation energies of $0.1\sim0.2$ eV and the positive sign of thermo-power, Mott suggested[15] that the range of

localized tail states at the conduction band edge is wider than at the valence band edge, so that conduction by holes slightly predominates, and one-carrier conduction in the localized states, involving an activation energy for hopping, also is taken part in. Such an outline of electronic processes is supported by the experimental fact that the drift mobility of holes is larger and has a higher activation energy than that of electrons in amorphous selenium.[22] Further, energy values in the range of 0.1∿0.3 eV obtained as the E_t-value have often been observed for trap-limited drift mobility, photo-conductivity, Hall mobility, etc. in various amorphous semiconductors.[23,24]

On the other hand, the reciprocal of the slope of exponential absorption tail, i.e. the E_s in Eq.(3-2), at room temperature has been shown in Table-4. The values of E_s are called the *band-tailing factor* and are of the same order of 0.05 eV as that of Urbach tail observed in ionic or covalent solids.[11] Fig.3-10 shows the E_s factor as a function of the gap $E_{g(op)}$ for the Si-As-Te glass system. The linear relation-

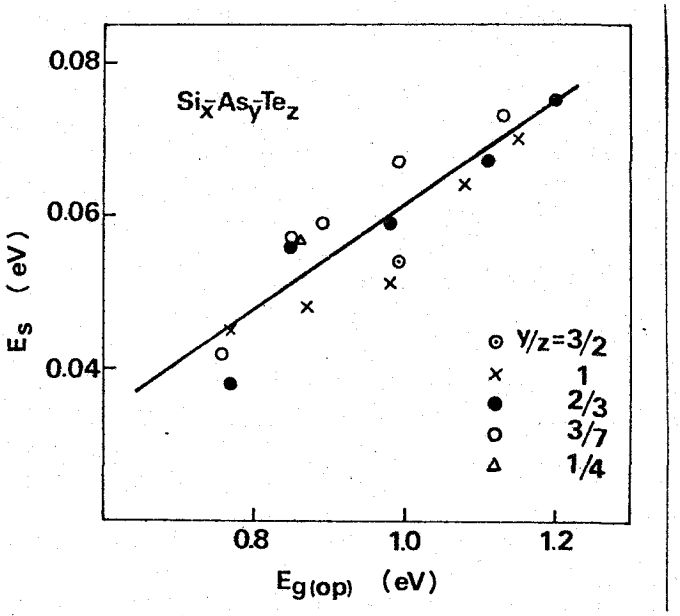

Fig.3-10. Peciprocal of slope of exponential absorption edge, E_s factor, as a function of optical gap $E_{g(op)}$ in Si-As-Te glasses.

ship is empirically obtained by the method of least squares as shown in Fig.3-10:

$$E_s = 0.068\ [\ E_{g(op)} - 0.10\ ]\ \text{in eV.} \quad \ldots\ldots \quad (3\text{-}12)$$

As shown in Fig.3-10, the value of E_s factor changes linearly with the optical gap $E_{g(op)}$, and particularly it is likely to increase conspicuously with the Si content in the Si-As-Te system. Two plausible explanations have been offered for the existence of an exponential absorption tail; (i) It would be corresponding to optical transitions involving the localized tail states, which are exponentially distributed from the band edges into the band gap.[25] (ii) It is due to an effect of internal electric microfields and potential fluctuations, which may be associated with various kinds of disorders.[26] Though it has recently been reported by Olley *et al.*[27] that the ion bombardments on amorphous Se and As_2Se_3 films cause increases of the optical absorption $\alpha(\omega)$ and E_s-value, there is no conclusive evidence yet at the present stage of experiments on amorphous materials. Whichever is true, it should be obvious that the existence of the exponential tails and the E_s factor are closely related to the potential fluctuations at the valence and conduction band edges. Because the value of E_s is expected to be in proportion to the average magnitude of microfields,[26] the linear relation in Fig.3-10 indicates that the microfields due to the fluctuations increase with increasing the gap energy. From a theory and measurements of the Franz-Keldish effect, the internal fields have been estimated to be about $10^5 \sim 10^6$ V/cm in magnitude.[28] Thus, it is obvious that the microfields and potential fluctuations give rise to localization of the electronic eigenstates and to the smearing or tailing of the band edges, and they break the k-conservation selection rule for some optical tran-

sitions to result in the exponential absorption edge.

Two other experiments have been made in order to study about the localized states: photo-conductivity and ac conductivity. Figs.3-11 and 3-12 show spectral and temperature dependences of photo-conductivity responses measured for the Si-As-Te amorphous semiconductors with an interdigital surface electrode of a gap 0.5 mm wide and 5-pair fingers. As shown in Fig.3-11, the spectral response has a relatively sharp rising and a peak at a photon energy above the electrical gap $E_{g(el)}$. The photo-current consists of the product of quantum efficiency, recombination rate, drift mobility and incident light intensity. The observed peak is caused by spectral changes of the quantum efficiency and the incident light. The rising point E_o is in good agreement with the mobility gap at room temperature, i.e. $E_{g(el)}-\gamma T$, and a tail is observed

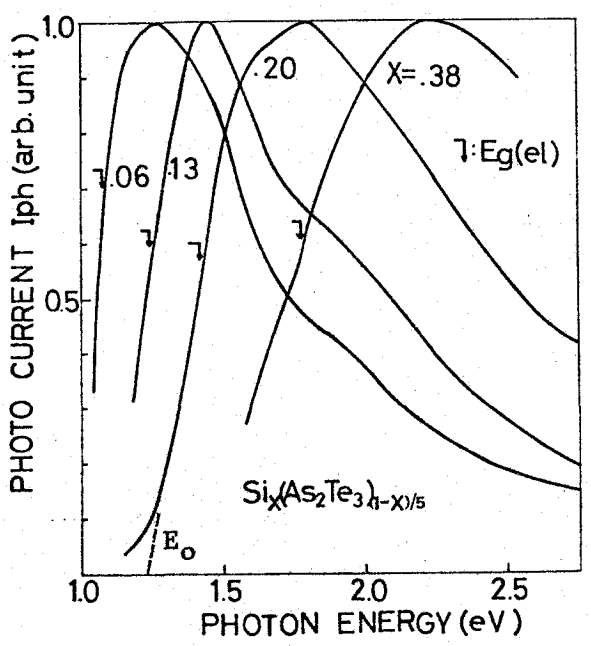

Fig.3-11. Spectral dependence of photo-current for some Si-As-Te amorphous semiconductors at room temperature.

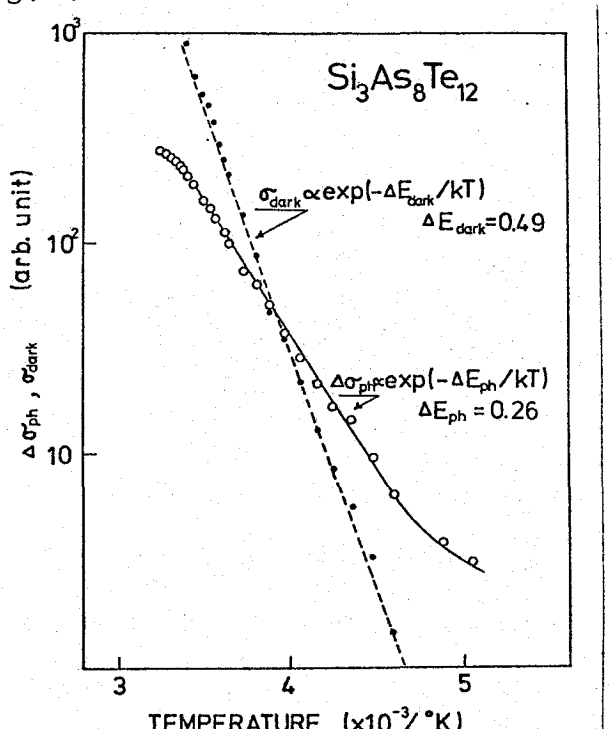

Fig.3-12. Temperature dependence of photo-conductivity $\Delta\sigma_{ph}$ and dark dc conductivity σ_T for $Si_3As_8Te_{12}$ glassy semiconductor.

below the E_o in Fig.3-11. These facts suggest that the recombination process may be governed mainly by the transitions related to the localized tail states near the valence and conduction band edges, but provide no explicit evidence that the midgap states at the Fermi level participate in the process. From the temperature dependence of photo-conductivity response shown in Fig.3-12, the thermal activation energy can be estimated to be about 0.26 eV for the $Si_3As_8Te_{12}$ glass, and the value obtained is much smaller than that of the dark dc conductivity. This activation energy is doubtlessly associated with a distribution depth of the localized tail states through those for the carrier lifetimes by recombination and the trap-limited drift mobilities.[29] Minami *et al.*[30] have pointed out that superlinearity observed in the weaker light range of the light-intensity dependence of photo-current for the Si-As-Te system is related to trapping and recombination centers of different cross-sections lying at various levels. In principle, thus, such photo-conductivity measurements have offered much information on the trapping and recombination centers at the band edges, but details of the mechanism have been unclear so far.

The other experimental evidence about the localized states can be gained from ac conductivity measurements for the Si-As-Te system. The temperature dependence of the ac conductivity $\sigma(\omega)$ was measured in a range from 180 to 350 °K with a transformer bridge (Ando-Denki, TR-10C), and the results obtained for the $Si_6As_{21}Te_{14}$ vitreous semiconductor are shown in Fig.3-13 as a parameter of frequency. To one's surprise, both magnitude of $\sigma(\omega)$ and its frequency- and temperature-dependences are almost similar to those of a large number of non-crystalline semiconductors and insulators.[31] As seen in the figure, the ac conductivity $\sigma(\omega)$

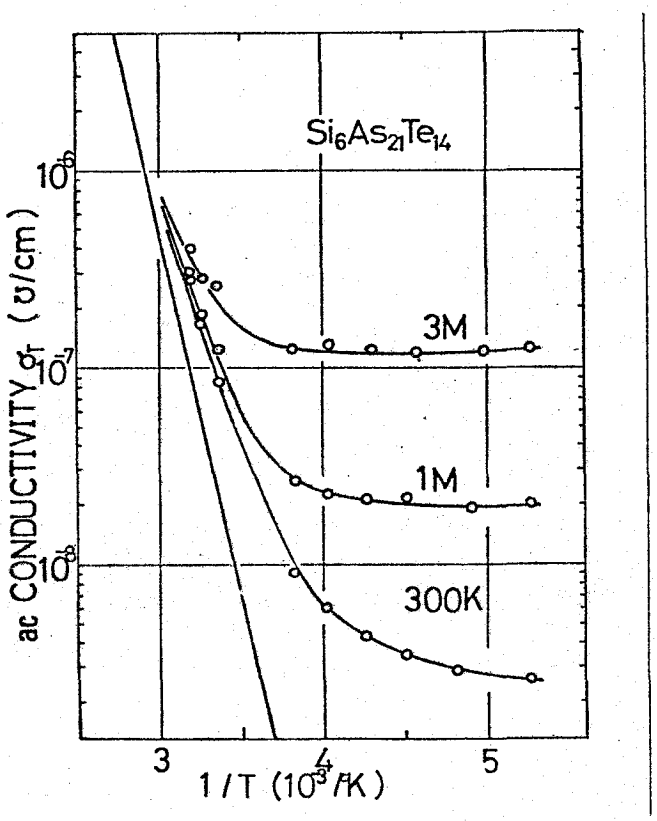

Fig.3-13. Temperature dependence of ac conductivity $\sigma(\omega)$ as a parameter of frequency for $Si_6As_{21}Te_{14}$ amorphous semiconductor.

in the lower temperature region becomes larger by several orders of magnitude than dc conductivity with increasing the frequency, and is little temperature-dependent. As the temperature is increased, $\sigma(\omega)$ approaches asymtotically the dc one at all frequencies. The frequency dependence of $\sigma(\omega)$ is expressed by $\sigma(\omega) \propto \omega^{1.7}$ at 250 °K. According to a theory of $\sigma(\omega)$ developed by Pollak,[32] Austin and Mott,[33] and Rockstad,[34] carriers can move only by phonon-assisted hopping (tunneling) between pairs of the localized gap states within an energy pseudogap in amorphous semiconductors. When $\sigma(\omega) \propto \omega^2$, the ac hopping takes place between identical sites of localized states rather than between random distributed states. Using the theory and the obtained values of $\sigma(\omega)$ the density of localized gap states participating in this process

is roughly estimated to be $10^{18}\sim10^{20}$ $eV^{-1}cm^{-3}$, while the distribution can not yet be described adequately by any of the existing theoretical treatments of amorphous materials. Austin and Mott have assumed[33] the presence of the high density of localized midgap states at Fermi level, and on the other hand Rockstad has suggested[34] on the basis of his observations that regular tail states localized near the band edges participate in the ac hopping process. At the present time, few experimental evidences have been obtained to manifest the existence of high dense midgap states at Fermi level, at least in this work about the Si-As-Te amorphous system.

3-5. Energy-Band Model and Electronic Transport Mechanism

The amorphous covalent alloys in the Si-As-Te system can be characterized as a low-mobility intrinsic semiconductor with a proper energy

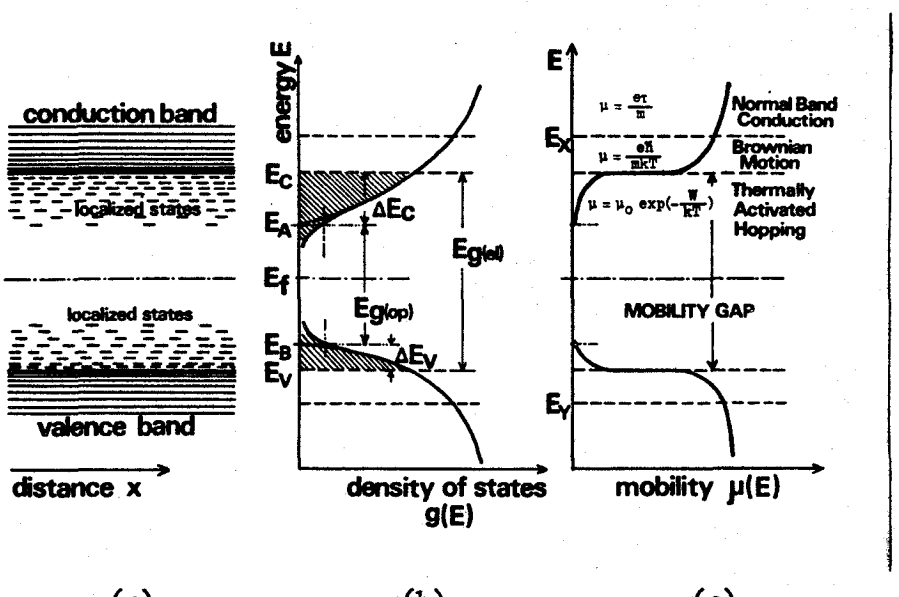

(a) (b) (c)

Fig.3-14. A sketch of energy-band model for the Si-As-Te amorphous semiconductors. (a) Energy-band diagram. (b) Energy distribution of density of electronic states. (c) mobility μ(E) as a function energy (T>0 °K). The critical energies E_c and E_v define a mobility gap or the electrical gap $E_{g(el)}$. Electronic states in the valence and conduction band-tails within the gap are localized.

band gap. On the basis of the experimental results on the electrical and optical properties described in the previous sections, a tentative energy-band model for the electronic states of the Si-As-Te vitreous semiconductor can be postulated and demonstrated in Fig.3-14(a) and (b). Essential features of this model are qualitatively (i) the existence of a composition-dependent pseudo-gap between conduction- and valence-band states and (ii) the high dense localized states tailing into the gap from critical energies, E_c and E_v. The valence-band states are filled almost perfectly by valence or lone-pair electrons and the conduction-band states are almost empty, like in conventional single-crystal semiconductors. The distribution of states in each band is assumed as $g(E) \propto E^{1/2}$. The character of the wavefunctions changes at the energies E_c and E_v which separate the extended and the localized states. The width of $(E_c - E_v)$, defined as a mobility gap by Mott and Cohen *et al.*[5,6], may correspond to the electrical gap $E_{g(el)}$, while the optical gap $E_{g(op)}$ is defined as an energy region which does not contain gap-states more than the density of about 10^{17} $eV^{-1}cm^{-3}$. The energies E_c and E_v, defined as *mobility edges* in Fig.3-14(c), can be discernible optically, and the concept is meaningful and useful only if one tries to explain the temperature-dependent dc conductivity. Both band-tails of ΔE_c below E_c and ΔE_v above E_v contain the high density of localized states more than 10^{19} cm^{-3} estimated roughly from the ac conductivity $\sigma(\omega)$. The depthes of tails, maybe $\Delta E_c > \Delta E_v$, are of less than 0.2 eV, and related linearly to the width of band gap. The Fermi level may be situated near the middle of the gap. This model does not have essential conflicts with the conceptive Mott-CFO model and the expectations of other theoretical studies, except the distribu-

tion of the density of localized states. No experimental result to prove the presence of the high dense midgap states at Fermi level or the overlapping of both band-tails has been obtained for the Si-As-Te vitreous system.

Great efforts of theorists have been concentrated on establishing a plausible model for electronic structures in amorphous materials.[35] In order to gain the electronic states from the one-electron Schrödinger equation in such a disordered system, recently, successive approximations for a configuration average of the Green function have been formulated. One theoretical approach is made by using the quasi-free one-electron Hamiltonian; $H(\vec{r})=-\frac{\hbar^2}{2m}\nabla^2 + V(\vec{r})$, where the perturbation term, $V(\vec{r})=\sum_i v(\vec{r}-\vec{r}_i)$, is randomly distributed potential in one- or three-dimensional atomic chains.[36] In another method, the electronic states are discussed on the basis of a simple tight-binding Hamiltonian; $H = \sum_i E_i a_i^* a_i + \sum_{i,j} V_{ij} a_i^* a_j$, where E_i is the intra-atomic interaction on the site i, V_{ij} the overlap integral between the sites i and j, and a_i and a_i^* are annihilation and creation operators for an electron on the site i, respectively.[37] In a similar way, Weaire and Thorpe have recently derived rigorous bounds for the density of states of tetrahedrally bonded amorphous solids, silicon and germanium, by taking account only of interactions between nearest neighbors of perfect 4-fold coordination.[38] In the most recent chemical-bond approach, the electronic states of amorphous Se, As_2S_3 and As_2Se_3 have been successfully interpreted by the extended Huckel's (molecular-orbital) theory.[39] The interactions between the nearest-neighboring bonds, or lone-pair hybrid orbitals, are presented by using a *molecular orbital* obtained as a linear combination of atomic orbitals. In this case,

the effect of disorder is treated by imposing a Gaussian distribution *a priori* on each energy level calculated by assuming the short-range order. The resulting lone-pair and antibonding orbital states form principally the valence and conduction bands, respectively, in the chalcogenide glasses.

From the above-mentioned theoretical approaches to amorphous materials, universal features of the electronic structure have been obtained as follows:

(i) allowed energy levels, forming continuous or quasicontinuous bands,

(ii) a pseudo-gap in the electronic energy spectrum, containing localized gap states,

(iii) the electron behavior is described by certain waves propagated in the disordered substance, at least in the first approximation; i.e., electrons are quasi-free.

This theoretical conclusion so far obtained is essentially consistent with the experimental results characterized in the band model of Fig.3-14 for the electronic energy spectrum of the Si-As-Te amorphous semiconductors.

The conductivity σ_T for any semiconductor can be given from the Kubo-Greenwood formula:

$$\sigma_T = e \int g(E) \cdot \mu(E) \cdot f(E) \cdot \{1-f(E)\} \cdot dE \ . \quad \ldots\ldots \quad (3\text{-}13)$$

Here g(E) is the density of states, $\mu(E)$ the average mobility for all carriers at energy E and f(E) is the Fermi-Dirac distribution function. In an amorphous semiconductor with the energy-band profile as shown in Fig.3-14, the electronic transport is strongly affected by the energy-dependent mobility $\mu(E)$, which can be principally distinguished in three

energy ranges in Fig.3-14(c).[40] Sufficiently deep into the band beyond E_X and E_Y, band-conduction similar to that in crystalline semiconductors will occur with normal mobility $\mu=\frac{e}{m}\langle\tau\rangle$, where $\langle\tau\rangle$ is a carrier mean free time. The mobility in this range can be estimated about 50∿100 $cm^2/V\cdot sec$ by using a mean free path equal to the de Broglie wavelength of an electron. In the next region immediately beyond E_c and E_v where the states remain still delocalized but the mean free path is expected to be of the order of an interatomic distance a; therefore the mobility in the Brownian motion regime is expressed by $\mu=\frac{ea^2}{kT}\nu_e=\frac{e\hbar}{mkT}$, where ν_e is an electronic frequency. The upper limit of mobility is 5∿40 $cm^2/V\cdot sec$. In the electrical gap $E_{g(el)}$ between E_c and E_v where the states are localized, the electron motion can take place only by a thermally activated tunneling process similar to impurity conduction in a heavily doped semiconductor. The mobility is given by $\mu=\mu_o\cdot\exp(-W/kT)$, where W is a measure of the average activation energy required for the phonon-assisted hopping, and is estimated to be less than 0.1 cm^2/V sec at finite temperatures. The mobility in this range goes to zero at T=0°K. Thus, the electron and hole mobilities drop sharply at the critical energies E_c and E_v, and these so-called mobility edges define a mobility gap which contains only localized states, as shown in Fig.3-14.

To explain the near-intrinsic conduction in an amorphous covalent semiconductor, Mott, Davis and Cohen *et al.*[5,6] have speculated that individual constituent atoms can satisfy their coordination and valency requirements and high density of overlapping or midgap centers pins the Fermi level at the middle of pseudo-gap. However, it is unlikely that such high dense localized states lie at the midgap in most amorphous semiconductors. According to Roosbroeck *et al.*[41], dynamic electronic

behavior in most amorphous semiconductors may be macroscopically characterized as the *relaxation-case* regime, in which *dielectric relaxation time* $\tau_d=\varepsilon\varepsilon_o/\sigma_T$ is greater than *recombination time* or *diffusion-length lifetime* τ_o. The Si-As-Te amorphous system having the time τ_d larger than 10^{-7} sec and the lifetime τ_o about 10^{-12} sec estimated from a mean free path of the order of the electron wavelength may be regarded as a typical relaxation case material. As shown in Appendix-A, in these materials with the relation $\tau_d>>\tau_o$, the product $n\cdot p$ of the electron and hole concentrations in extended states retains locally its thermal-equilibrium value n_i through the electron-hole recombination rather than the dielectric relaxation; $n\cdot p=n_i^2$. When carriers are injected, thus, these materials no longer obey a neutrality-condition; therefore the steady-state carrier transport in such an amorphous semiconductor may be strongly affected by a region of minority-carrier space-charge. In the region of injected space-charge, where electron and hole currents are equal through change of sign of the space-charge, the conductivity is fixed nearly to its minimum value for the given intrinsic carrier concentration n_i:

$$\sigma_T = \sigma_{min} = 2e\cdot n_i\sqrt{\mu_n\cdot\mu_p} = 2e\cdot n_i\cdot\mu_{eff} , \qquad \text{.....} \qquad (3\text{-}14)$$

where μ_n and μ_p are electron and hole mobilities. Accordingly the temperature dependence of dc conductivity σ_T should show always near-intrinsic behavior because $n_i = g(E_{c,v})\cdot\exp[-E_g(T)/2kT]$ for the real energy-band gap $E_g(T)$. Thus, the amorphous semiconductors are expected to have the Fermi level pinned at the position for the minimum and near-intrinsic conductivity simply through the recombination statistics and not necessarily by large concentration of the midgap centers.

On the simple and unified electronic basis, Roosbroeck[42] has

accounted for many other aspects of macroscopic carrier-transport observed in amorphous semiconductors. Photoconductivity is, as one consequence, due mainly to majority carriers. Non-linear high-field dc conduction and threshold switching in semiconducting chalcogenide glasses are dominated by the characteristic injected space-charge effects of minority carriers. In these materials, the drift mobility μ_d is usually not equal to the microscopic band-conduction mobility μ_o, and observed as the trap-limited drift mobility approximated by $\mu_d = \mu_o \cdot \exp(-E_t/kT)$, where E_t is an activation energy associated with depth and distribution of trapping centers near the band-tails. In addition, under ac current of frequencies larger than the reciprocal time-constant of establishing the steady state, the measured ac conductivity $\sigma(\omega)$ corresponds rather to the bulk conductivity much larger than σ_{min}. Other aspects treated include the small negative Hall coefficient, positive thermoelectric power, preswitching delay time and the field effect, which are closely related to the recombination and trapping processes and space-charge effects in amorphous semiconductors.

Recently Seager *et al.*[43] have employed a new conduction model to explain consistently various transport coefficients obtained from temperature dependences of Hall mobility, Seebeck coefficient and dc conductivity of As-Te based glasses. In this model, the prevalent charge carriers are hole-like small-polarons between sites associated with a common As-Te structural entity.

However, no unified theory of the electronic process and transport mechanism in amorphous materials has been established so far. In the present theoretical arguments based on the energy-band model and carrier mobilities in amorphous semiconductors, many problems in microscopic

carrier kinetic studies especially associated with the recombination and trapping processes still remain almost outstanding.

3-6. Summary

In this chapter, some basic electrical and optical properties measured for the Si-As-Te amorphous semiconductors have been represented. The temperature-dependent dc conductivity σ_T obeys the formula of $\sigma_T = \sigma_o \cdot \exp[-E_{g(el)}/2kT]$, and the σ_o-term has been estimated to be about $(2.1\pm0.6)\times10^4$ $(\Omega\cdot cm)^{-1}$ for all Si-As-Te glasses. The optical absorption spectrum near the fundamental edge has an exponential tail; $\alpha(\omega) = \alpha_o \times \exp(\hbar\omega/E_s)$, where the band-tailing factor E_s is of the order of 0.05 eV and increases linearly with increasing the band gap. The electrical and optical gaps, $E_{g(el)}$ and $E_{g(op)}$, have been determined for various Si-As-Te glasses. An empirical relationship between both gaps is expressed as $E_{g(el)}=1.60E_{g(op)}-0.15$ in eV. From these experimental results and the evaluation of σ_o-value, it has been cleared that the basic electronic properties in these semiconducting glasses are essentially analogous to those in intrinsic crystalline semiconductors.

Theoretical backgrounds for the E_s factor and the relation between both gaps have been discussed on the basis of the localized tail states. The presence of the tail states has been confirmed by measurements of the photo-conductivity and the ac conductivity for the Si-As-Te system.

A tentative energy-band model of the Si-As-Te amorphous semiconductors has been postulated by taking account of a pseudo-gap and localized tail states to explain the whole electronic semiconducting properties. Discussions have been given on the theoretical approaches to the electronic band model and transport mechanisms.

Appendix-A

Current density $\vec{I}$ generated in a solid by electric field $\vec{F}$ can be determined from the following equation:

$$\vec{I} = \frac{e}{4\pi^3} \int \vec{v}(\vec{k}) \cdot f \cdot d\vec{k} \ , \qquad \text{.....} \qquad \text{(A-1)}$$

where f is a distribution function dependent on the energy (i.e., $\vec{k}$) of electron, temperature and the field $\vec{F}$, and $\vec{v}(\vec{k})$ is a group velocity of electrons in the state $\vec{k}$:

$$\vec{v}(\vec{k}) = \frac{1}{\hbar} \mathrm{grad}_{\vec{k}} E(\vec{k}) \ . \qquad \text{.....} \qquad \text{(A-2)}$$

The current density $\vec{I}$ will equal zero if the distribution $f=f(\vec{k})$ is equal to the Fermi distribution function corresponding to the equilibrium state; $f_o = \{1 + \exp[(E-E_f)/kT]\}^{-1}$. The new distribution f induced by the field $\vec{F}$ is calculable from the condition of stationary state, termed the Boltzmann-Bloch's transport equation:

$$\frac{df}{dt} = -\frac{e\vec{F}}{\hbar} \frac{\partial f}{\partial \vec{k}} + \frac{f - f_o}{\tau(\vec{k})} = 0 \ . \qquad \text{.....} \qquad \text{(A-3)}$$

In Eq.(A-3), the collision term $(\partial f/\partial t)_{\mathrm{coll}}$ is assumed, as a first approximation, to be proportional to a very small change $(f-f_o)$, and the relaxation time $\tau(\vec{k})$ is introduced. Here the following mean values are defined:

$$\langle \tau \rangle = \int |\vec{v}|^2 \cdot \tau(\vec{k}) \cdot \frac{\partial f_o}{\partial E} \cdot d\vec{k} \ / \ \int |\vec{v}|^2 \cdot \frac{\partial f_o}{\partial E} \cdot d\vec{k} \ ,$$

$$n = \frac{1}{4\pi^3} \int f_o \cdot d\vec{k} \ . \qquad \text{.....} \qquad \text{(A-4)}$$

By using Eq.(A-2), Eq.(A-4) and the function f calculated from Eq.(A-3), integration of Eq.(A-1) can be carried out separately for the conduction and the valence bands, and it holds in general that

$$\vec{I} = \vec{I}_n + \vec{I}_p \ . \qquad \text{.....} \qquad \text{(A-5)}$$

For the carrier concentrations of electrons and holes, n and p, the electron and hole current densities $\vec{I}_n$ and $\vec{I}_p$ are given by

$$\vec{I}_n = e \cdot n \cdot \mu_n \cdot \vec{F} \ ,$$
$$\vec{I}_p = e \cdot p \cdot \mu_p \cdot \vec{F} \ , \qquad \text{.....} \qquad \text{(A-6)}$$

where the electron and hole mobilities, μ_n and μ_p, are expressed by using effective masses, m_n and m_p, of electrons and holes as follows:

$$\mu_n = \frac{e}{m_n}\langle\tau_n\rangle \ , \ \mu_p = \frac{e}{m_p}\langle\tau_p\rangle \ . \qquad \text{.....} \qquad \text{(A-7)}$$

Therefore, the conductivity σ_T of the semiconductor with two-type carriers can be expressed as

$$\sigma_T = \frac{\vec{I}}{\vec{F}} = e(n \cdot \mu_n + p \cdot \mu_p) \ . \qquad \text{.....} \qquad \text{(A-8)}$$

To derive an expression of the conductivity in amorphous semiconductors, the mean value of relaxation time $\langle\tau\rangle$ in Eq.(A-4) must be calculated by taking account of the *relaxation-case* regime,[41] i.e., recombination and trapping processes rather than carrier scattering. From the Boltzmann-Bloch's equation, continuity equations can be written as follows:

$$\frac{\partial n}{\partial t} = \text{div } \vec{I}_n/e - R + \Delta g$$
$$\frac{\partial p}{\partial t} = -\text{div } \vec{I}_p/e - R + \Delta g \qquad \text{.....} \qquad \text{(A-9)}$$

where R and Δg are net non-equilibrium interband recombination and volume generation rate of electron-hole pairs. Poisson's equation in its general form includes changes $\Delta\hat{p}$ and $\Delta\hat{n}$ in concentrations of fixed charges:

$$\text{div } \vec{F} = \frac{e}{\varepsilon\varepsilon_o}(p-n+\hat{p}-\hat{n}) = \frac{e}{\varepsilon\varepsilon_o}(\Delta p+\Delta\hat{p}-\Delta n-\Delta\hat{n}) \ , \qquad \text{.....} \qquad \text{(A-10)}$$

where $\hat{p}$ and $\hat{n}$ are concentrations of fixed positive and negative charges. If trapping is present, $\hat{p}$ or $\hat{n}$ is not constant and departs from its thermal equilibrium.

In the simple case of acceptor-type traps in which recombination occurs at a single energy level, the recombination rate in steady state is derived in the following form:

$$R = [\, C_i + \frac{C_n \cdot C_p \cdot N_t}{C_n(n+n_1)+C_p(p+p_1)} \,](\, n \cdot p - n_i^2) \ , \quad \ldots\ldots \qquad (A\text{-}11)$$

in which N_t is density of the traps, C_i the direct electron-hole recombination coefficient, C_n and C_p the recombination coefficients for electrons and for holes through the traps, and n_1 and p_1 the electron and hole concentrations if the Fermi level were at the energy level of the traps. The relaxation-case material, in which dielectric relaxation time τ_d exceeds diffusion-length lifetime τ_o, will no longer obey a charge-neutrality-condition. Injected excess carriers recombine before their charges can be neutralized through dielectric relaxation. therefore, the net local recombination rate in Eq.(A-11) is approximately zero after an initial rapid recombination; i.e., R=0. From Eq.(A-11),

$$n \cdot p = n_i^2 \ . \qquad \ldots\ldots \qquad (A\text{-}12)$$

Eq.(A-12) can be interpreted by saying that local equilibrium is always enforced by traps and recombination processes in steady state. When one type carriers are injected, the other type mobile carriers are depleted locally through recombination, space charge will occur and the conductivity no longer increases after injection. On the application of the external field $\vec{F}$ to such a material, there will always be one point where the conduction or the space-charge changes from n-type to p-type. This implies equation of the hole and electron currents at the conversion point; i.e., the current is always fixed at this point, then,

$$\mu_n \cdot n = \mu_p \cdot p \ . \qquad \ldots\ldots \qquad (A\text{-}13)$$

By substituting the above Eq.(A-13) into Eq.(A-8), the conductivity has locally a near-intrinsic minimum:

$$\sigma_T = \sigma_{min} = 2e \cdot n_i \sqrt{\mu_n \cdot \mu_p} \ . \qquad \ldots\ldots \qquad (A\text{-}14)$$

A similar discussion can be made for traps of more than one kind, and R still has $(\, n \cdot p - n_i^2)$ as factor.

Appendix-B

As can be seen from Eq.(A-14), the temperature dependence of dc conductivity of amorphous semiconductors would always show a near-*intrinsic* behavior because n_i is given by

$$n_i = g(E_{c,v}) \cdot \exp[-E_g(T)/2kT] \ , \qquad \text{.....} \qquad \text{(B-1)}$$

where $E_g(T)$ is a band gap in the density of electronic states, and $g(E_{c,v})$ is an inherent constant associated with the effective density of states at reduced band edges. As shown in Fig.3-14, the distribution of states in both bands except tail-states is approximated[18] as

$$g_c(E)\,dE = 4\pi\left(\frac{2m_n}{h^2}\right)^{3/2}(E-E_A)^{1/2}dE \ ,$$

$$g_v(E)\,dE = 4\pi\left(\frac{2m_p}{h^2}\right)^{3/2}(E_B-E)^{1/2}dE \ . \qquad \text{.....} \qquad \text{(B-2)}$$

Accordingly the gap $E_g(T)$ is corresponding to (E_A-E_B). Near room temperature, the gap $E_g(T)$ can be assumed to have approximately the same temperature coefficient as $E_{g(op)}$ in Eq.(3-5):

$$E_g(T) = E_g(0) - \gamma T \ , \qquad \text{.....} \qquad \text{(B-3)}$$

where $E_g(0)$ is a constant not corresponding to the real gap at T = 0°K.

Carrier mobilities, μ_n and μ_p in Eq.(A-14), are obtained by calculations of mean free times $\langle\tau_n\rangle$ and $\langle\tau_p\rangle$ for an electron and a hole in Eqs.(A-4) and (A-7). In amorphous materials, the recombination and trapping processes dominate their carrier transport rather than the carrier scattering. From Eq.(A-11) on the assumption of $C_i \ll 1$ and $N_t > n_o, p_o$, the equilibrium lifetimes are derived as follows:[44]

$$\langle\tau_n\rangle = \frac{C_n(n_o+n_1) + C_p(\hat{n}_o+p_o+p_1)}{C_n \cdot C_p(p_o+n_o)N_t \cdot N_t} \ ,$$

$$\langle\tau_p\rangle = \frac{C_p(p_o+p_1) + C_n(N_t-\hat{n}_o+n_o+n_1)}{C_n \cdot C_p(p_o+n_o)N_t \cdot N_t} , \qquad \text{.....} \qquad \text{(B-4)}$$

for the simple case of acceptor type traps. Here N_t is introduced as

the trapping factor, and can be approximated with Boltzmann statistics:

$$N_t = 1 + \frac{\hat{n}_t}{p_o + n_o} = 1 + \exp\left(\frac{\hat{E}_t}{kT}\right) >> 1 \qquad \text{.....} \qquad \text{(B-5)}$$

in which $\hat{n}_t$ is the concentration of traps that have become filled by the minority carriers and $\hat{E}_t$ the depth of trap level from the edge of conduction band. For various kinds of traps near the band edges, also, the mean free times include the trapping factors related to the depth of traps. This factor insures the predominant drift, and then the mobilities are rather the trap-limited drift mobility μ/N_t than the microscopic majority-carrier mobility or the minority-carrier mobility. Therefore, in such a trap-dominated relaxation-case semiconductor, the effective mobility $\mu_{eff} = \sqrt{\mu_n \cdot \mu_p}$ in Eq.(3-14) may have approximately the following temperature-dependent form:

$$\mu_{eff} = \sqrt{\mu_n \cdot \mu_p} = \mu_o \cdot \exp(-E_t/kT) \ , \qquad \text{.....} \qquad \text{(B-6)}$$

where μ_o is the effective band-conduction mobility and E_t the activation energy of the effective trap-limited mobility associated with the distribution of the localized gap states.[22)]

Inserting Eqs.(B-1), (B-3) and (B-6) into Eq.(3-14), one deduces

$$\sigma_T = \sigma_o \cdot \exp\{-[E_g(0)+2E_t]/2kT\} \ , \qquad \text{.....} \qquad \text{(B-7)}$$

where $$\sigma_o = 2e \cdot g(E_{c,v}) \cdot \mu_o \cdot \exp(\gamma/2k) \ . \qquad \text{.....} \qquad \text{(B-8)}$$

Comparing Eq.(B-7) with Eq.(3-7) yields

$$E_{g(el)} = E_g(0) + 2E_t \ . \qquad \text{.....} \qquad \text{(B-9)}$$

On the other hand, the optical gap $E_{g(op)}$ is assumed to be different by $\pm\hat{\varepsilon}$ eV from the real gap $E_g(T)$ at room temperature. Hence

$$E_{g(op)} = E_g(T) \pm \hat{\varepsilon} = E_g(0) \pm \hat{\varepsilon} - \gamma T \ . \qquad \text{.....} \qquad \text{(B-10)}$$

Then the energy difference between $E_{g(el)}$ and $E_{g(op)}$ is derived from Eqs.(B-9) and (B-10) as follows:

$$E_{g(el)} - E_{g(op)} = 2E_t + \gamma T \mp \hat{\varepsilon} \ . \qquad \text{.....} \qquad \text{(B-11)}$$

REFERENCES-III

1) H. Fritzsche, J. Non-Cryst. Solids 6, 49 (1971).

2) J. Tauc and A. Abrahám, Czech. J. Phys. B19, 1246 (1969).

3) W. E. Spicer and T. M. Donovan, J. Non-Cryst. Solids 2, 66 (1970).

4) J. W. Osmun and H. Fritzsche, Appl. Phys. Letters 16, 87 (1970).

5) E. A. Davis and N. F. Mott, Phil. Mag. 22, 903 (1970).

6) M. H. Cohen, H. Fritzsche and S. R. Ovshinsky, Phys. Rev. Letters 22, 1065 (1969).

7) H. Fritzsche, J. Non-Cryst. Solids 8-10, 1025 (1972).

8) M. Nunoshita, H. Arai, T. Taneki and Y. Hamakawa, J. Non-Cryst. Solids 12, 339 (1973).

9) A. R. Hilton and C. E. Jones, Phys. Chem. Glasses 7, 112 (1966).

10) T. Minami and M. Tanaka, Bull. Univ. Osaka Pref. A18, 165 (1969).

11) D. Redfield and M. A. Afromowitz, Appl. Phys. Letters 11, 138 (1967).

12) See, e.g., K. Weiser and M. H. Brodsky, Phys. Rev. B1, 791 (1970).
F. Kosek and J. Tauc, Czech. J. Phys. B20, 94 (1970).

13) B. T. Kolomiets and E. M. Raspopava, Soviet Phys. Semi. 4, 124 (1970).

14) E. Q. Fagen, S. H. Holmberg, R. W. Seguin and J. C. Thompson, in *Proceedings of the 10th International Conference on the Physics of Semiconductors, Cambridge, Mass,* (1971) p.672.

15) N. F. Mott, Phil. Mag. 24, 1 (1971).

16) J. T. Edmond, Brit. J. Appl. Phys. 17, 979 (1966).
N. S. Platakis *et al.*, J. Electrochem. Soc. 116, 1436 (1969).

17) K. J. Siemsen *et al.*, Phys. Rev. 161, 632 (1967).

18) R. Tsu, W. E. Howard and L. Esaki, J. Non-Cryst. Solids 4, 322 (1970).

19) J. Stuke, J. Non-Cryst. Solids 4, 1 (1970).

20) K. W. Böer, Phys. Status Solidi 34, 721 (1969).

21) P. Nagels, R. Callaerts and M. Denayer, in *Proceedings of the 5th International Conference on Amorphous and Liquid Semiconductors, Garmisch,* (Taylor & Francis, London, 1974) Vol.2, p.753.

22) J. M. Marshall *et al.*, J. Non-Cryst. Solids 8-10, 760 (1972)
J. L. Hartke, Phys. Rev. 125, 1177 (1962).

23) C. Main and A. E. Owen, in *Proc. 5th Intl. Conf. on Amor. and Liquid Semi., Garmisch,* (Taylor & Francis, London, 1974) Vol.2, p.781.

24) M. Roilos and E. Mytilineou, *ibid.* (1974) Vol.1, p.319.

25) J. Tauc, A. Menth and D. L. Wood, Phys. Rev. Letters 25, 749 (1970).

26) J. D. Dow and D. Redfield, Phys. Rev. B5, 594 (1972).

27) J. A. Olley and A. D. Yoffe, J. Non-Cryst. Solids 8-10, 850 (1972).

28) B. T. Kolomiets *et al.*, Soviet Phys. Semi. 5, 2004 (1972).

29) K. Weiser, J. Non-Cryst. Solids 8-10, 922 (1972).

30) T. Minami and M. Tanaka, *Ōyo-Butsuri* 39, 541 (1970).

31) A. I. Lakatos and M. Abkowitz, Phys. Rev. B3, 1791 (1971).

32) M. Pollak and T. H. Geballe, Phys. Rev. 122, 1742 (1961).

33) I. G. Austin and N. F. Mott, Adv. in Phys. 18, 41 (1969).

34) H. K. Rockstad, J. Non-Cryst. Solids 8-10, 621 (1972).

35) A. I. Gubanov, *Quantum Electron Theory of Amorphous Conductors* (Consultants Bureau, New York, 1963).

36) S. F. Edwards and J. M. Loveluck, J. Phys. C, S261 (1970).

37) P. Soven, Phys. Rev. 178, 1136 (1969).

38) D. Weaire and M. F. Thorpe, Phys. Rev. B4, 2508 (1971).

39) I. Chen, Phys. Rev. B7, 3672 (1973), *ibid.* B8, 1440 (1973).

40) E. A. Davis and R. F. Shaw, J. Non-Cryst. Solids 2, 406 (1970).

41) W. van Roosbroeck and H. C. Casey, Jr., Phys. Rev. B5, 2154 (1972).

42) W. van Roosbroeck, J. Non-Cryst. Solids 12, 232 (1973).

43) C. H. Seager, D. Emin and R. K. Quinn, Phys. Rev. B8, 4746 (1973).

44) W. van Roosbroeck, Phys. Rev. 119, 636 (1960).

Chapter-IV

COMPOSITIONAL DEPENDENCES OF BASIC PROPERTIES IN THE Si-As-Te SYSTEM

4-1. Introduction

It has been well known that electronic structure of single crystals can be derived from the consequence of long-range order and perfect periodicity of their atomic arrangements. Recently great interest has been focused on electronic band structures in non-crystalline semiconductors having no long-range order. Ioffe and Regel[1)] first pointed out that basic electronic properties of a solid are governed by short-range order rather than by long-range order like periodicity and symmetry; that is, even in amorphous materials their energy bands and band gap depend primarily upon characters of chemical bonds such as coordination numbers, interatomic distances and bond energies between the nearest-neighboring atoms. Therefore, the knowledge of their molecular structures, particularly of the short-range order is necessary to make theoretical treatments for the electronic spectrum in amorphous semiconductors. However, it has been very difficult to find available experimental techniques which can determine directly a three-dimensional picture of the short-range order in amorphous chalcogenides. So far, even diffraction experiments with X-rays, electrons and neutrons have been quite powerless for the structural analysis of ternary or multi-component amorphous alloys.

In this chapter, in order to obtain useful informations about the structure and short-range order of amorphous semiconductors in the Si-

As-Te system, compositional dependences of their electrical, optical and other basic properties have been systematically measured. It is found out in this glass system that the electronic properties like the energy-band gap, dc conductivity and breakdown field have the same compositional dependence as their structural parameters. From these experimental results, a structural model of the Si-As-Te glasses can be constructed in the form of three-dimensionally cross-linked and covalent-bonded networks. On the basis of this model and the theory of chemical bonds, a discussion is given about the close correlation between the static electronic states and the electronic configuration of covalent bonds preserved almost as the short-range order in such a disordered material.[2-4)]

4-2. X-ray Diffraction Pattern and Infrared Absorption Spectrum

Informations about the periodic and symmetric lattices of crystals are obtained mainly from the structural analysis by X-ray and electron diffraction. As described in Section 2-4, amorphous materials do not exhibit such sharp reflections as observed for crystalline solids, but exhibit a few broad halos. In Fig.4-1, the X-ray diffraction patterns for three Si-As-Te glasses with different Si content are presented. As seen from this figure, they exhibit three haloed peaks of the scattering X-ray intensity in the measured angle range, and the angles of the peaks shift slightly with the change of the glass compositions. These peaks for amorphous materials do not always reflect exact interatomic separation between the nearest neighboring atoms, but result from an interference effect of the X-rays scattered from several pairs of atoms with certain interatomic distances.[5)] The angle 2θ of the

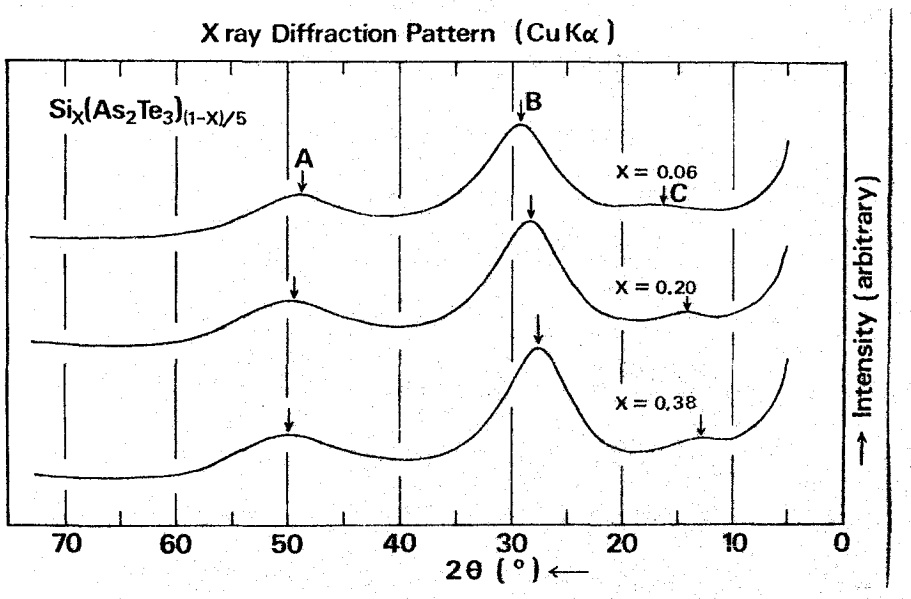

Fig.4-1. X-ray diffraction paterns of Si-As-Te glasses having different Si content.

maximum peak corresponds to the average interatomic distance estimated roughly from the weight density. These aspects suggest the existence of some three-dimensionally configurational short-range order in the glass network. However, it is impossible to deduce the three-dimensional short-range order of the amorphous solids from these diffraction patterns. By a standard Fourier integration method, only a one-dimensional description of this order is given in the form of a radial distribution function, which yields the electron or atom density as a function of the distance from an arbitrarily chosen atom. The position and area of peaks in the radial distribution function indicate respectively the average interatomic distances to neighbored atoms round the chosen atom and the number of atoms at the distance. However, for multicomponent glasses there is not exactly a one-to-one correspondence between the short-range order and the peaks of the radial distribution function, so that it is difficult to identify the configurational order by these peaks.

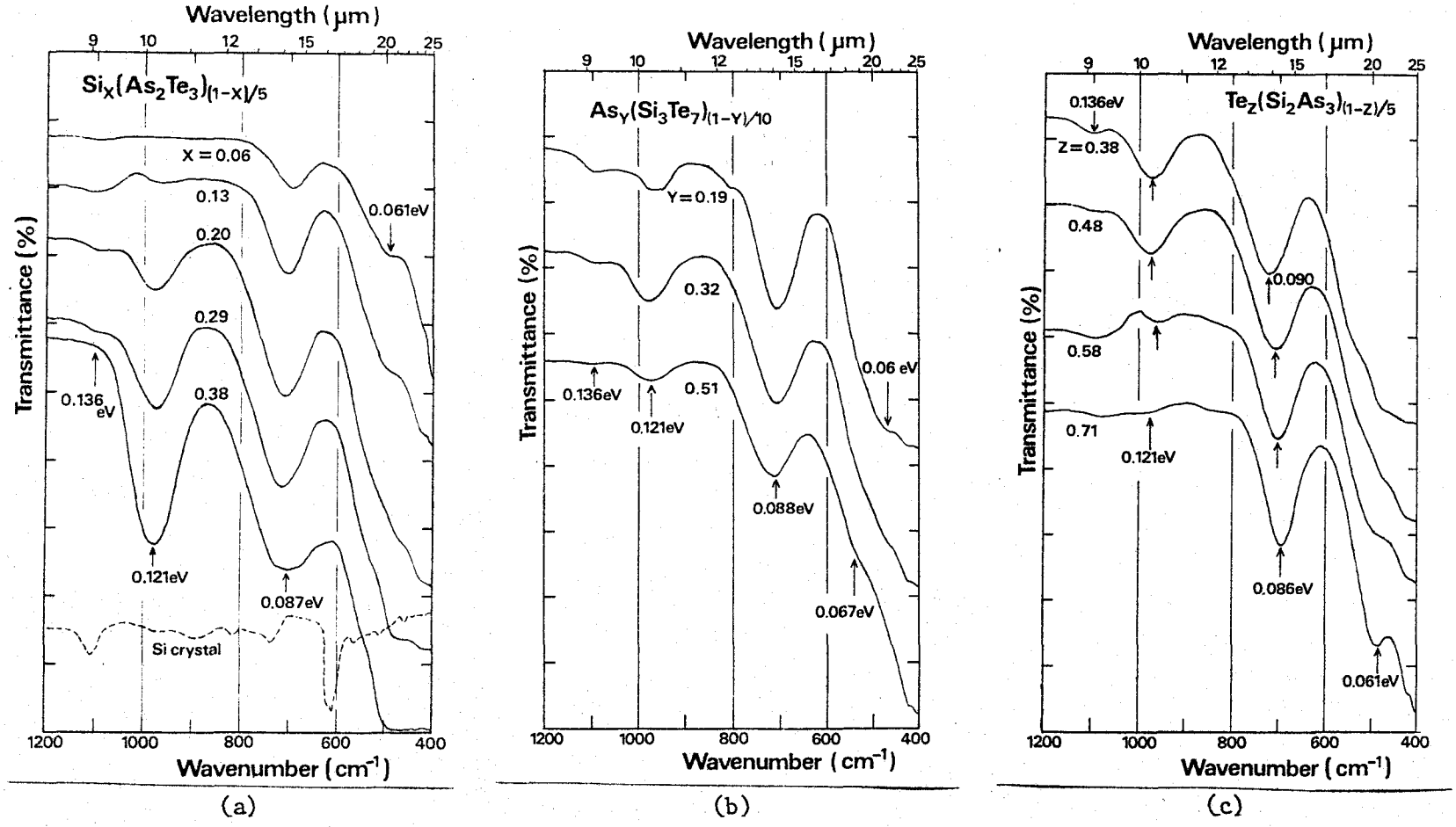

Fig.4-2. Infrared transmission spectra of some Si-As-Te glasses (d≈500μm) at room temperature (a) for different Si contents, (b) for different As contents and (c) for the Te contents.

Another experimental technique aimed at the structural analysis of chalcogenide glasses is infrared spectroscopy. In Figs.4-2(a), (b) and (c), the infrared transmission spectra are shown for some Si-As-Te glasses as a parameter of the contents of Si, As and Te, respectively. The transmission curves exhibit a few absorption bands at 960 and 680 cm^{-1}. Usually infrared absorptions in a solid are associated with three main sources, i.e., impurity absorption, molecular vibration of constituent elements, as well as fundamental absorption described in the previous section. Impurity oxygen bound chemically to silicon, arsenic and/or tellurium produce absorption peaks at 1040, 770 and 620 cm^{-1} for Si-O, As-O and Te-O bonds, respectively.[6,7] These impurity absorptions are not observed in Figs.4-2. No conclusive analysis is still done to show whether the absorption bands for the Si-As-Te glasses are due to oxide or not. Judging from the obvious compositional changes in the spectra, they are rather likely to be caused by chemical bonds between the constituents and to suggest the presence of the short-range chemical order. The general aspects in these spectra are very similar rather to that of amorphous Si_1Te_4 than that of amorphous As_2Te_3.[7,8] These facts seem to imply that the basic network of the Si-As-Te glasses consists of mainly tetrahedral $Si-Te_4$ configurational unit; however what chemical bonds are formed in the glasses is still doubtful.

By using the X-ray diffraction and infrared reflection methods, only an attempt to obtain the informations about the short-range order in the Si-As-Te ternary system was made by Hilton *et al.*[9] It has been concluded that zig-zag chains of Si-Te covalent bonds are constructed in these glass networks. Thus, by the refined methods of X-ray diffraction and infrared spectroscopy a qualitative speculatiom about the

short-range configurational order can be represented, but none has succeeded in more exact description of the three-dimensional structure of multicomponent chalcogenide glasses. The purpose of this work is not to investigate the structural nature itself. Here, the author will only give a tentative structural model necessary to discuss the electronic properties in the Si-As-Te amorphous semiconductors from the compositional dependences of electrical, optical and other physical properties.

4-3. Compositional Trends of Thermodynamic Factors and Structural Model

In order to measure compositional dependences of various physical properties, 24 glass specimens of different compositions were prepared along the lines on which the atomic ratio of two elements remains constant within the glass-forming region in the Si-As-Te ternary system, as shown in Fig.2-3.

Weight density is a reciprocal of specific volume which is one of the most basic thermodynamic variables of the substance, and denotes a structural factor of such macroscopically isotropic materials as glasses. The weight density at 25 °C, ρ_{25}, was measured by the Archimedes' method, in which a 3mm thick disk sample (about 2 g) was weighed in air and pure water at 25 °C. The measurement error of ρ_{25} was within ±0.5%. Table-5 shows the results of the density measurements for all the glasses in the Si-As-Te system. Dependences of ρ_{25} on the content of Si, As and Te (in atomic %) are shown in Figs.4-3(a), (b) and (c), respectively, as a parameter of the atomic ratio of the other two constituent elements. As can be seen from the figures, the value of ρ_{25} depends strongly upon each of the contents of Si and Te. Namely, it increases linearly with

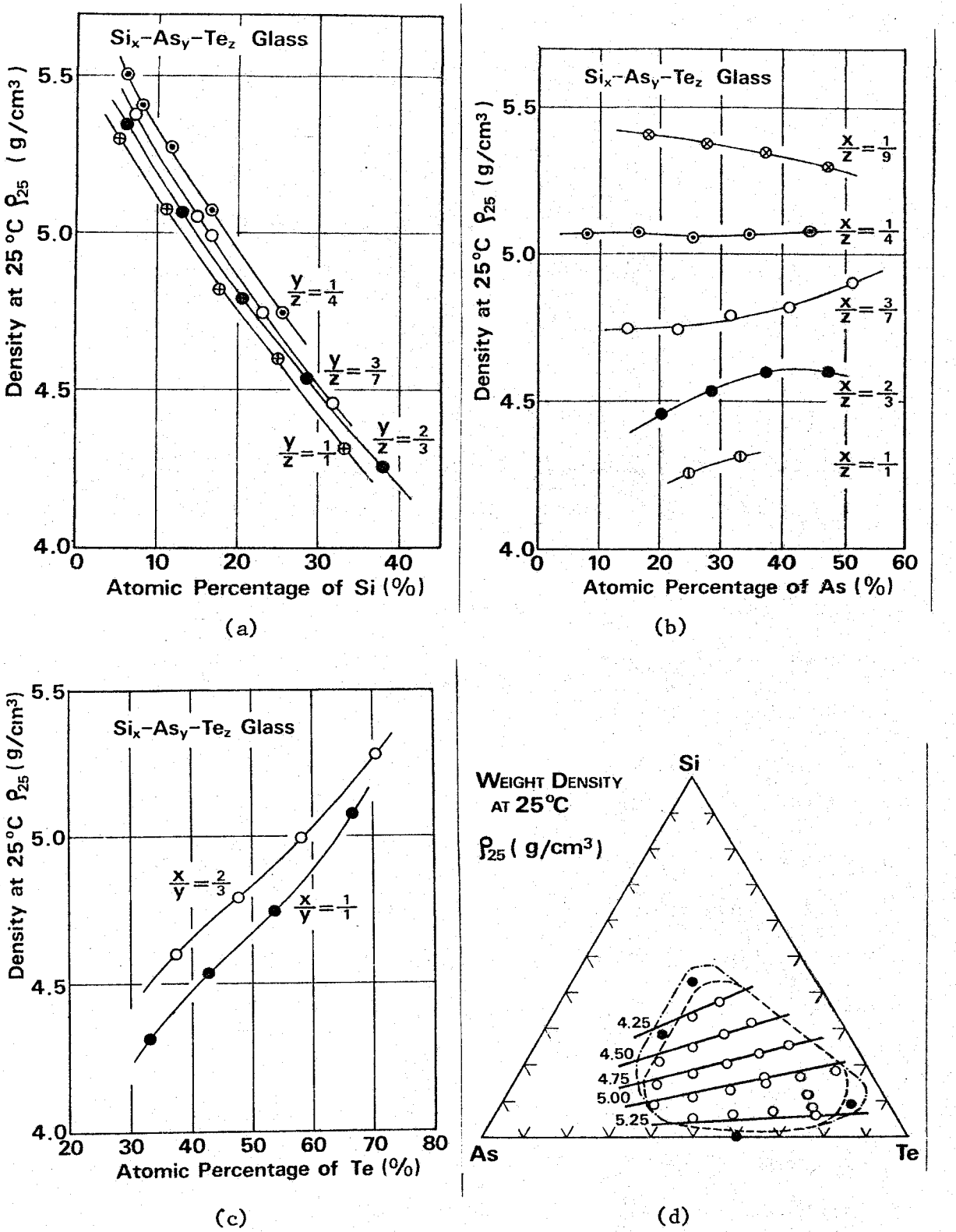

Fig.4-3. Compositional dependences of weight density at 25°C, ρ_{25} in Si-As-Te glass system, (a) for the Si content, (b) for the As content, (c) for the Te content, and (d) compositional trend of ρ_{25} depicted in the Gibbs' triangle.

decreasing the Si content and with increasing the Te content, but is almost independent of the As content. In other words, ρ_{25} seems to depend linearly on only the atomic ratio of Si to Te contents, which is less than 1.0 within the glass-forming region. The aspect of compositional changes of ρ_{25} is again shown in the Gibbs' triangle of

Table-5. Basic Physical Properties of Si-As-Te Glasses.

COMPOSITIONS (Atomic Ratio)	σ_{25} $(ohm.cm)^{-1}$	ρ_{25} (g/cm^3)	T_g (°K)	T_s (°K)	T_{As} (°K)	β $(x10^{-6})$
$Si_1 As_1 Te_9$		5.62	(367)			
$Si_9 As_4 Te_{36}$	1.01×10^{-6}	5.07	430	459		18.5
$Si_1 As_3 Te_{12}$	7.15×10^{-5}	5.50	373	395	523	18.8
$Si_4 As_9 Te_{36}$	3.05×10^{-5}	5.41	387	404		21.3
$Si_2 As_3 Te_{12}$	8.69×10^{-6}	5.28	403	427	478	18.7
$Si_1 As_1 Te_4$	9.65×10^{-7}	5.07	433	463		18.3
$Si_{12}As_7 Te_{28}$	7.11×10^{-9}	4.74	513	552	695	15.8
$Si_7 As_{27}Te_{63}$	2.23×10^{-5}	5.38	396	419		17.9
$Si_{14}As_{24}Te_{56}$	8.15×10^{-7}	5.05	441	473		16.7
$Si_2 As_3 Te_7$	3.10×10^{-7}	4.99	453	488		16.5
$Si_3 As_3 Te_7$	1.60×10^{-8}	4.74	513	550		14.9
$Si_{14}As_9 Te_{21}$	1.45×10^{-10}	4.46	606	646		11.6
$Si_1 As_6 Te_9$	1.46×10^{-5}	5.35	409	436	502	18.1
$Si_3 As_8 Te_{12}$	6.39×10^{-7}	5.07	450	489		15.9
$Si_9 As_{14}Te_{21}$	2.05×10^{-8}	4.79	506	550	633	14.8
$Si_2 As_2 Te_3$	4.52×10^{-10}	4.54	580	629		11.4
$Si_3 As_2 Te_3$	1.29×10^{-11}	4.26	673	721	730	8.8
$Si_1 As_9 Te_9$	1.04×10^{-5}	5.30	417	445		15.4
$Si_1 As_4 Te_4$	5.81×10^{-7}	5.08	458	491	493	14.0
$Si_3 As_7 Te_7$	2.96×10^{-8}	4.82	512	548		12.1
$Si_2 As_3 Te_3$	9.94×10^{-10}	4.60	569	619	710	11.1
$Si_3 As_1 Te_1$	7.76×10^{-11}	4.32	650	695		9.2
$Si_1 As_6 Te_4$	3.44×10^{-7}	5.05	477	510		12.7
$Si_6 As_{21}Te_{14}$	2.17×10^{-8}	4.91	508	550	535	12.2
$Si_4 As_9 Te_6$	9.10×10^{-9}	4.60	567	617		10.9
$Si_2 As_3 Te_2$		4.28	(645)			
$Si_{12}Ge_{10}As_{30}Te_{48}$	4.05×10^{-8}	5.07	502	550		12.6
$Si_{44}Ge_{46}As_{14}Te_{21}$	1.20×10^{-7}	5.06	489	531		
$Ge_1 As_4 Te_4$	3.00×10^{-6}	5.38	453	478		

Fig.4-3(d). In the vitreous materials, the density may be determined statistically from the atomic geometrical arrangement (packing density) and the atomic weight of the constituents. The mean interatomic distance can be estimated to be about 3.5 Å from the measured value of ρ_{25} on the assumption of a close-packed network structure and from the maximum peak on the X-ray diffraction pattern. This value is considerably greater than about 2.5 Å bond length in the Si-Te zig-zag chains indicated by Hilton *et al.*[9] These facts infer that the two atoms, Si and Te, tend to link together preferentially and more closely to form a basic cross-linked network structure, whereas most As and excess Te atoms seem to be loosely bound in the basic voided network as intermediators. Therefore, the packing density of the network structure is considerably smaller than that of crystalline solids.

Glass transition temperature T_g, glass softening temperature T_s and thermal linear expansion coefficient β were determined from the linear expansion curves measured at a heating rate of 20 deg/min with the Parkin-Elmer TMS-1 or the Leitz Dilatometer model-UBD. As shown in Section 2-4, T_g was obtained from the cross point of two extrapolated lines out of the smaller and larger expansivity regions, and T_s was determined as the temperature at which the glass specimen begins to be shrinked by the measuring probe about 5 g in weight on the experimental curves. The coefficient β was estimated from the slope of the curve in the glassy phase below T_g. The values of T_g were also confirmed by the method of the scanning calorimetric trace (Perkin-Elmer DSC-1) at the same heating rate of 20 deg/min. The difference between the values of T_g by both methods did not exceed 10 degrees. These basic thermodynamic factors determined for all the Si-As-Te glasses are listed up in Table-5.

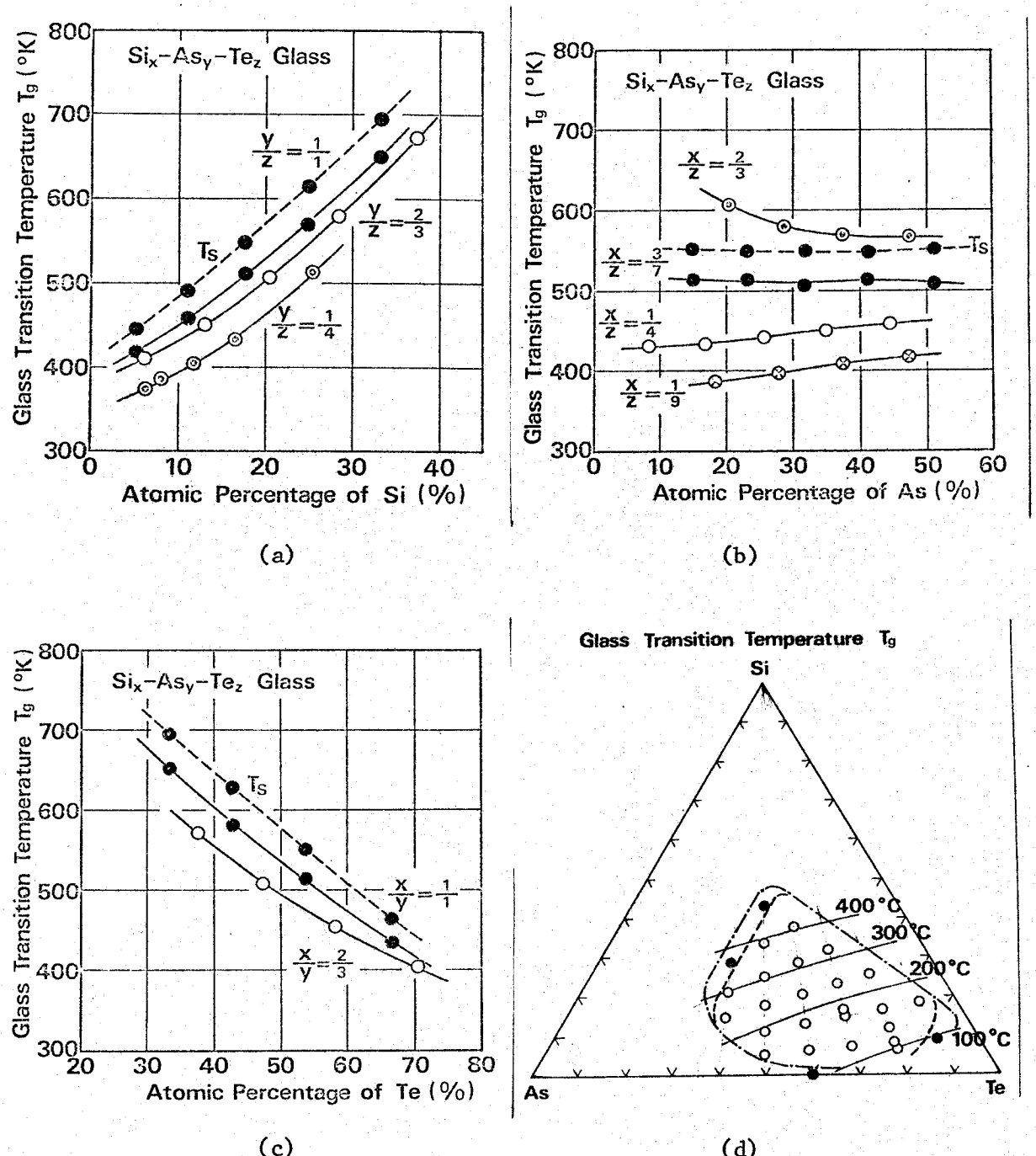

Fig.4-4. Compositional dependences of glass transition temperature T_g and of softening temperature T_s in Si-As-Te ternary system, (a) for the Si content, (b) for the As content, and (c) for the Te content, as a parameter of atomic ratio between the other two element contents. (d) Compositional trend of T_g within the glass forming region in the Gibbs' triangle.

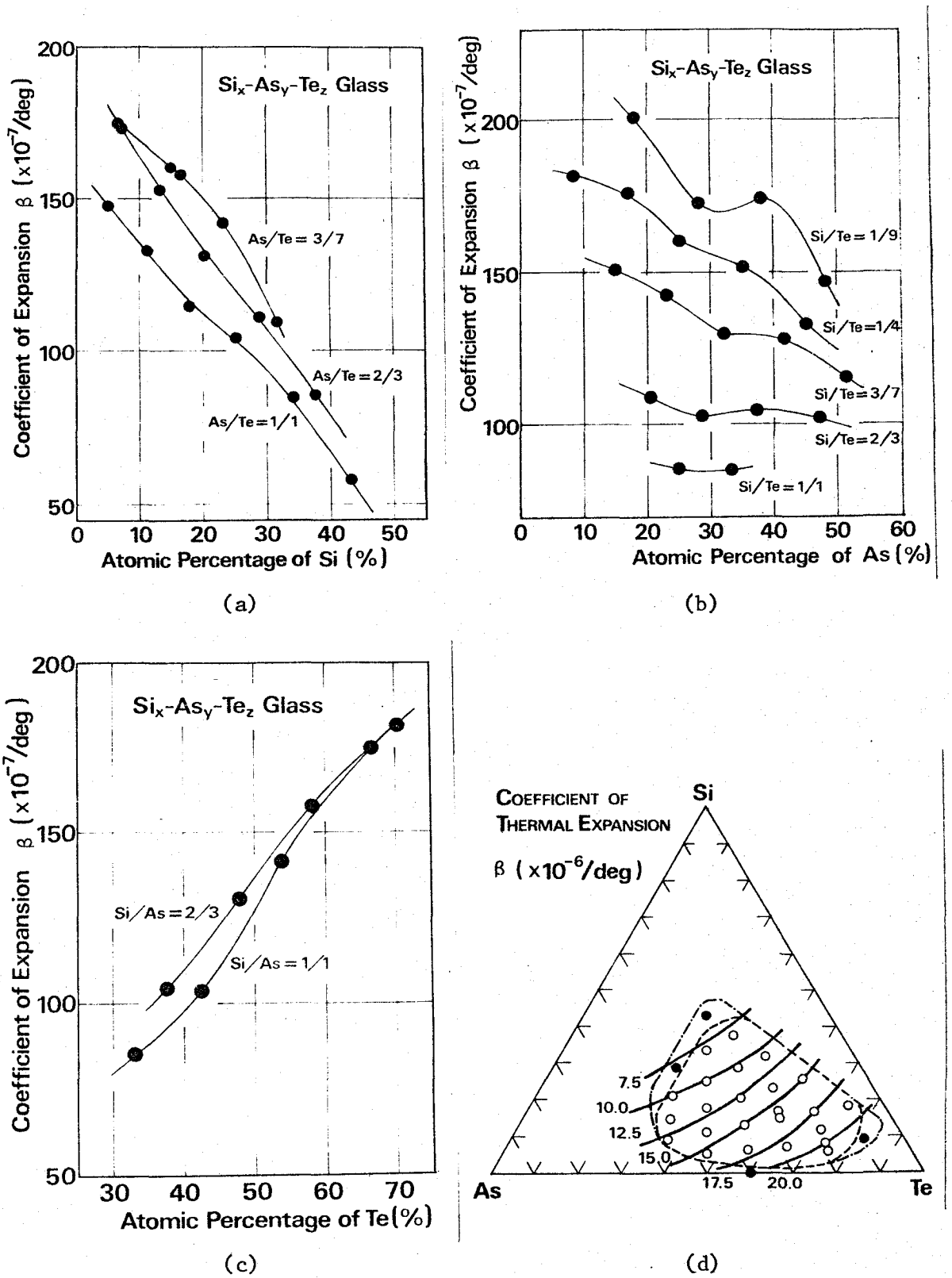

Fig.4-5. Compositional dependences of linear thermal expansion coefficient β for the glassy phase in Si-As-Te glass system, (a) for the Si content, (b) for the As content, and (c) for the Te content, as a parameter of atomic ratio between the other two element contents. (d) Compositional trend of β within the glass forming region in the Gibbs' triangle.

Compositional dependences of T_g and T_s in the Si-As-Te system are shown in Figs.4-4(a), (b) and (c). As shown in Fig.4-4(a), T_g increases remarkably with the increase of the Si content, and Fig.4-4(b) shows that T_g decreases monotonously with the increase of the Te content. In Fig.4-4(c), however, T_g is almost insensitive to the As content. Fig.4-4(d) illustrates the whole aspect of the compositional changes of T_g within the glass-forming region in the Si-As-Te ternary system. As shown by the dotted lines in Figs.4-4(a,b,c), T_s has the completely same compositional changes as T_g with the constant ratio of $T_g/T_s \fallingdotseq 0.94$ (T in °K). The highest values of T_g seem to lie along the line connecting Si-Te to As with average coordination number 3 and within the chalcogen deficient region of the Si-As-Te system. These compositional dependences of T_g and T_s are almost similar to the results of Minami *et al.*[10] and de Neufville[11]. Since T_g measures the onset of diffusive motions, it closely corresponds to a fixed value of viscosity; i.e., another definition of T_g is empirically adopted as the temperature at which the viscosity is $10^{14.6}$ poise.[12] Likewise, these T_g and T_s depend linearly upon the value of Knoop hardness, which as physical strength of a glassy material, of course, reflects strength of the chemical bonds in the glass.[13] Turnbull and Cohen have suggested that T_g and T_s depend directly on the average cohesive energy for a molecular type in a given vitreous material.[14] In a multicomponent glass, the cohesive energy is strongly dependent on the molecular configuration and the composition; the temperature T_g should be also very structure-sensitive. From the compositional dependences of T_g, this Si-As-Te glass consists of a three-dimensionally cross-linked network structure rather than of two-fold chain-like molecular complexes of large size

which are held together with weak van der Waals forces.

The expansion coefficient β is estimated for the glassy phase on the linear thermal expansion curve observed at the constant heating rate, as shown in Fig.2-6. Figs.4-5(a),(b),(c) and (d) illustrate compositional dependences of β in the Si-As-Te system. The value of β tends to decrease rapidly with increasing the Si content but with decreasing the Te content, and it seems almost independent of the As content. Therefore, high softening glass has generally low coefficient β. The behavior of β of these glasses is similar to that for the specific heat C_p. As in the case of the β value, it follows that the thermally oscillatory motion is essentially responsible for the specific heat C_p in the vitreous state.[15] It has been found in the vicinity of T_g that C_p also changes remarkably accompanying the change in β. Thus, this β coefficient has obviously compositional changes similar to the density ρ_{25} and other properties.

In looking through the compositional dependences of thermodynamic properties, it can be speculated that the glass network structure of the Si-As-Te glass is three-dimensionally cross-linked and is based mainly on the tetrahedral molecular unit of $Si\text{-}Te_4^{-4}$ (or $Si\text{-}Te_2$), not on the two-dimensional Si-Te zig-zag chain. Fig.4-6 demonstrates a three-dimensionally structural model for the Si-As-Te glass. As shown by Ovshinsky *et al.*[16] a notable point is the heavy cross-linking and lack of long tellurium chains in this model. In such a chalcogenide substance, a chalcogen, i.e. tellurium, can be chemically incorporated into the basic network through its covalent bonding properties and those of its alloying elements, following the chemical rule. Tetravalent silicon and trivalent arsenic act to cross-linked the tellurium. It is

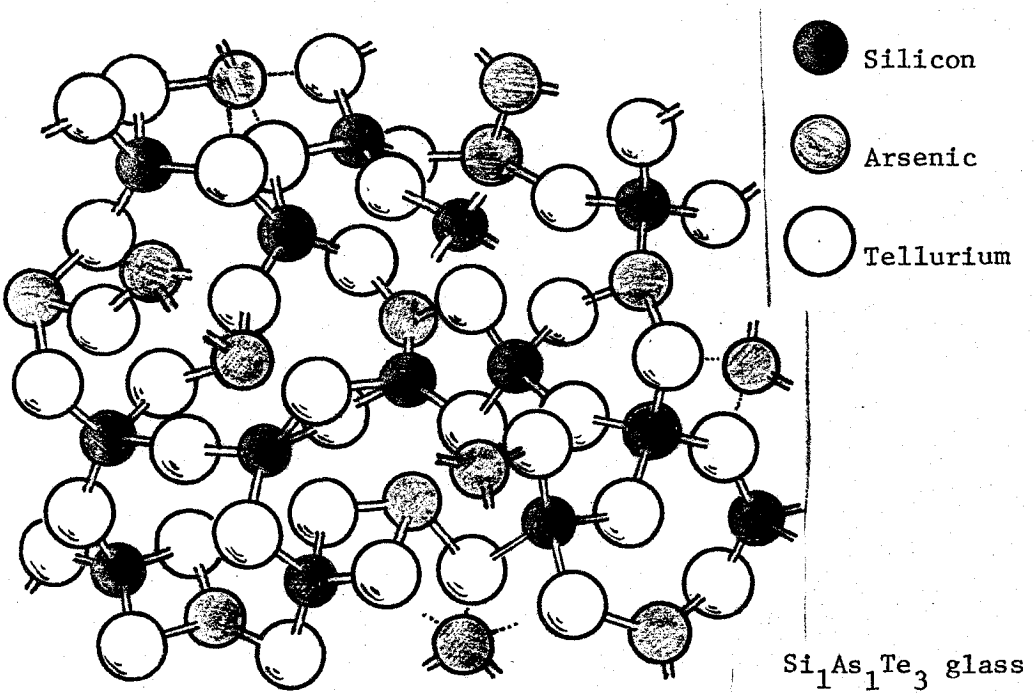

Fig.4-6. A three-dimensional structural model for Si-As-Te glass. Light balls represent Te atoms and the dark balls are Si and As atoms. The coordination can vary from site to site; however, in this model Si and As are shown as 4- and 3-coordinated, respectively.

natural that Si-Te covalent bonds having the highest bonding energy of heteropolar bonds between the constituents play a predominant role in formation of the basic network structure in the Si-As-Te system. The Te and As atoms in excess would be combined relatively loosely with the basic network as network-modifier atoms. At the chalcogenide deficient compositions, of course, Si-As, Si-Si and As-As bonds also exist in substantial concentrations.[11] Such a structural model based on the three-dimensionally cross-linked network seems to account nicely for the observed compositional dependences of T_g, ρ_{25} and other basic properties of the Si-As-Te vitreous materials. It also is concluded that these glasses have a short-range configurational order built around the Si atoms mainly in the form of the tetrahedral molecular configuration

of $Si\text{-}Te_4^{-4}$.

In order to obtain another evidence for the chief contribution of the Si-Te covalent bonds to the basic network, a qualitative study of vaporization or sublimation from the Si-As-Te glasses was made with the quadrupole mass spectro-analyser (Mitsubishi Ele. Co.) over the temperature range from 25 to 500 °C. Glass samples were put into a small fused silica furnace fitted in the cavity of a high vacuum ($\sim 10^{-7}$ Torr), and the temperature was very slowly raised at about 1 deg/min. Ionization of the vaporized atoms or molecules was done by an electron beam. Fig.4-7 illustrates typical mass-spectrometric curves obtained for pure arsenic, tellurium and the $Si_9As_{14}Te_{21}$ glass. The detectable sensitivities were calibrated with the pure arsenic and tellurium under the same experimental conditions, and are about 7×10^{-8} Torr for the vapor of As ions and 4×10^{-7} Torr for the Te ions. The sensitivity for the Te ions is relatively low and the vaporization of silicon can not be detected in this temperature range. In Fig.4-8, detectable temperatures, T_{As} and T_{Te} for the As^+, As^{++} and Te^{++} observed first with the above sensitivities are plotted for the different As fraction of the Si-As-Te system. T_{As} for several glasses is also shown in Table-5. As can be seen from the figure, these T_{As} and T_{Te} decrease rapidly with increasing the As content in spite of no change of T_g and T_s. This low-temperature appearance of As and Te in the vapors over the heated ternary glasses indicates that the considerable part of As and Te atoms is only weak and loosely bound in the basic glass network. This fact supports the structural model in Fig.4-6 speculated from the compositional dependences of the basic properties of the Si-As-Te vitreous materials.

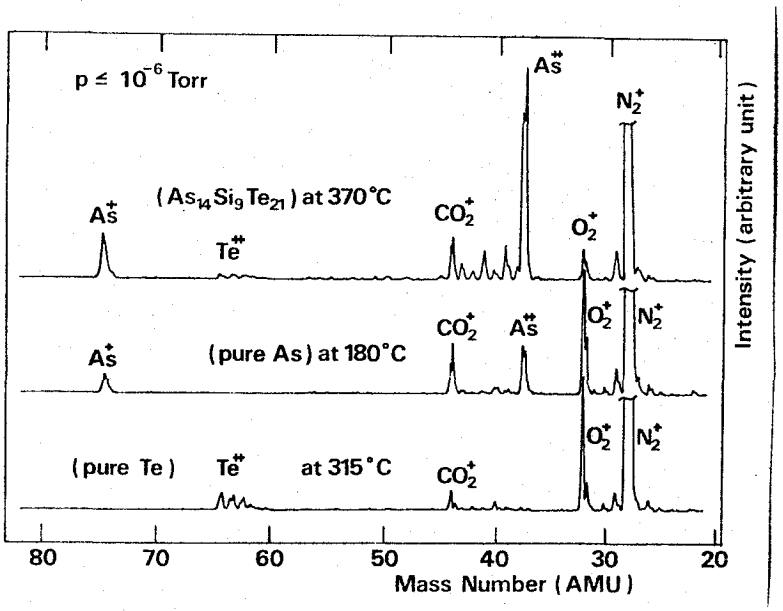

Fig.4-7. Typical mass-spectrometric curves obtained for pure arsenic, tellurium and $Si_9As_{14}Te_{21}$ glass.

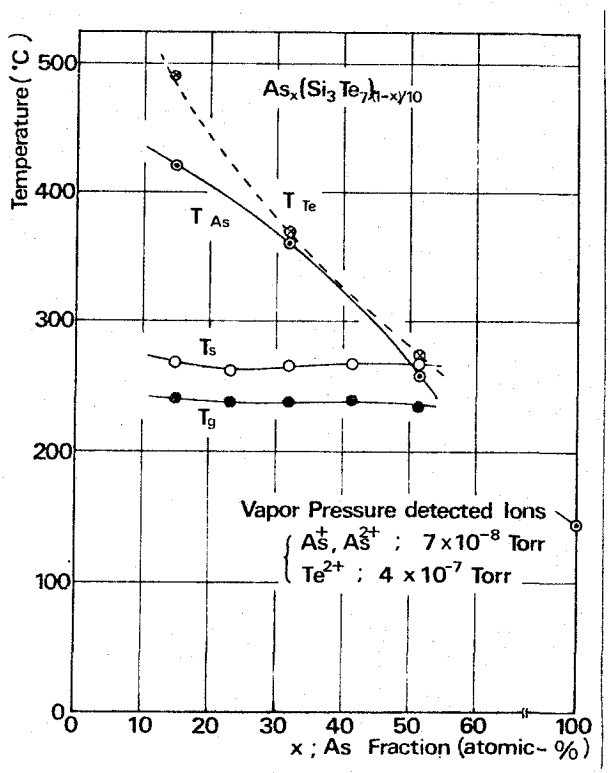

Fig.4-8. Detectable temperatures, T_{As} for As^{+}, As^{++} and T_{Te} for Te^{++}, observed for several Si-As-Te glasses of different As fraction as compared with their T_g and T_s.

4-4. Compositional Dependences of Electrical and Optical Gaps

As shown in Table-4 and Figs.4-9(a,b,c), the electrical gap $E_{g(el)}$ and the optical gap $E_{g(op)}$ also are strongly sensitive to the glass compositions. Both gaps increase linearly with increasing the Si content but with decreasing the Te content, while they are almost independent of the As content. Therefore, the value of gaps is determined only by the atomic ratio of Si to Te, in common with T_g, T_s, ρ_{25}, etc. The whole aspects of compositional changes of both gaps are shown in the Gibbs' triangles of Figs.4-10 and 4-11, again.[17]

As shown in Fig.4-12, a linear relation is found between the gap $E_{g(el)}$ and the density ρ_{25} for all the Si-As-Te vitreous semiconductors. The empirical relationship is given by $E_{g(el)}$ in eV and ρ_{25} in g/cm^3 as

$$E_{g(el)} = 4.5 - 0.65\ \rho_{25}\ , \text{ in eV.} \quad \ldots\ldots \quad (4\text{-}1)$$

For amorphous Ge films[18] and dense Hg vapor[19], essential relations between the band gap and the density have been discussed on the basis of their average interatomic separations. Even in the multicomponent glass system, there is an obvious correlation between the prevailing type of chemical bonds and the resulting glass network structure. The linear relationship in Fig.4-12 manifests that the band gap in the Si-As-Te amorphous semiconductors is governed by electronic configurations of the same chemical bonds that construct predominantly the inherent three-dimensionally cross-linked network. Especially, the Si-Te covalent bonds in the tetrahedral molecular unit preserved as the short-range chemical and configurational order play an important role in the static electronic properties of the Si-As-Te glasses. As shown by the dotted line with these black circlets in Fig.4-12, the experimental results on other glass system containing germanium for silicon by 10 atomic % seem to lie on a

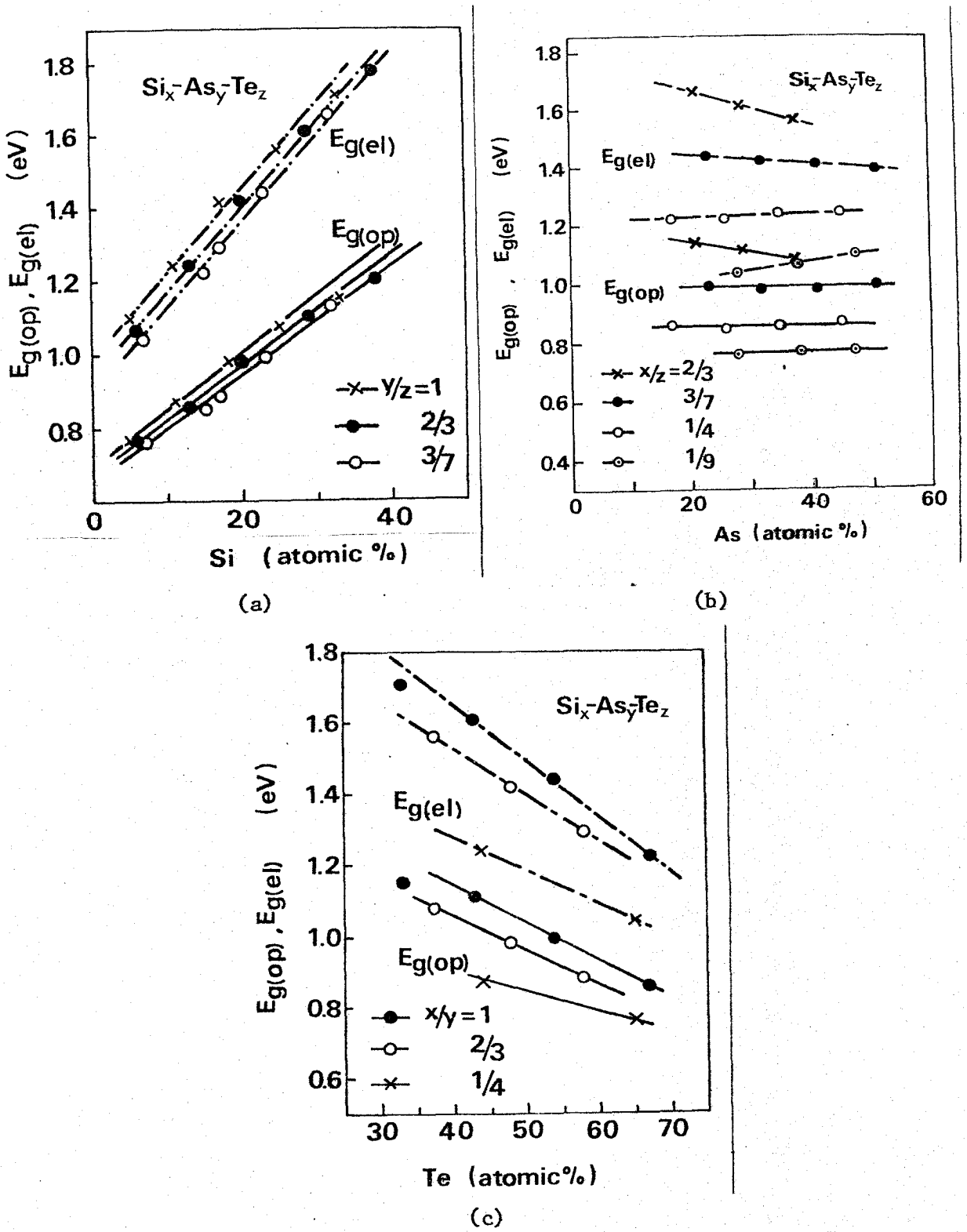

Fig.4-9. Compositional dependences of electrical gap $E_{g(el)}$ and optical gap $E_{g(op)}$ in amorphous Si-As-Te system. (a)$E_{g(el)}$ and $E_{g(op)}$ as a function of the Si content, (b) both gaps as a function of the As content, and (c) the both gaps as a function of the Te content, with a parameter of atomic ratio of the other constituent elements.

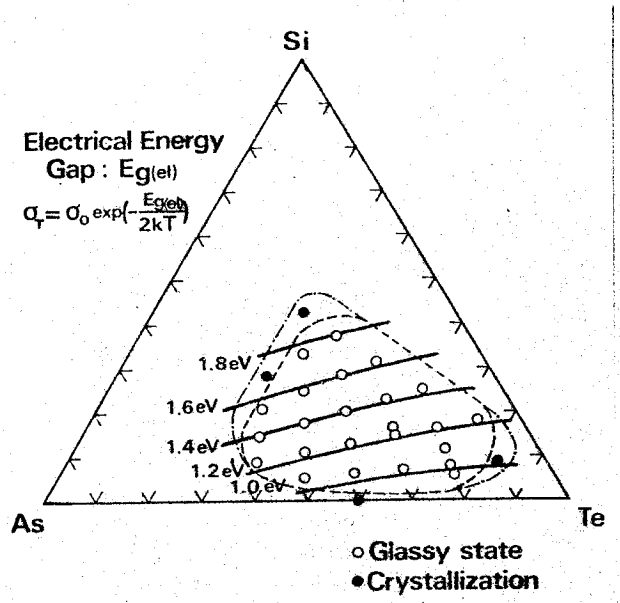

Fig.4-10. Compositional dependence of electrical gap $E_{g(el)}$ in amorphous Si-As-Te ternary system.

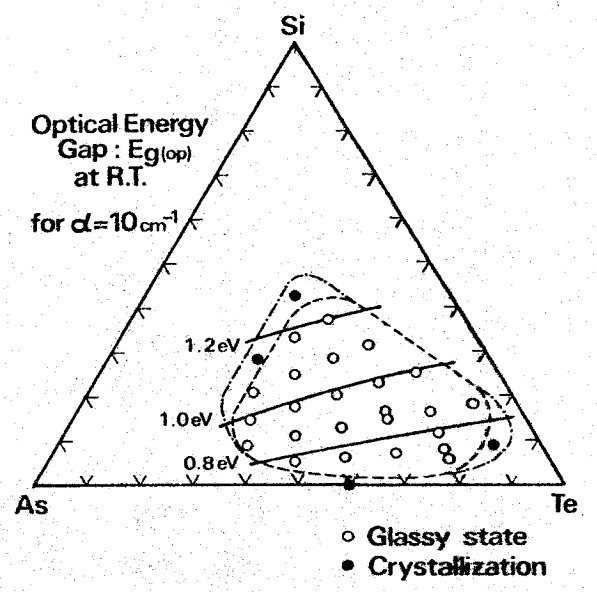

Fig.4-11. Compositional dependence of optical gap $E_{g(op)}$ in amorphous Si-As-Te ternary system.

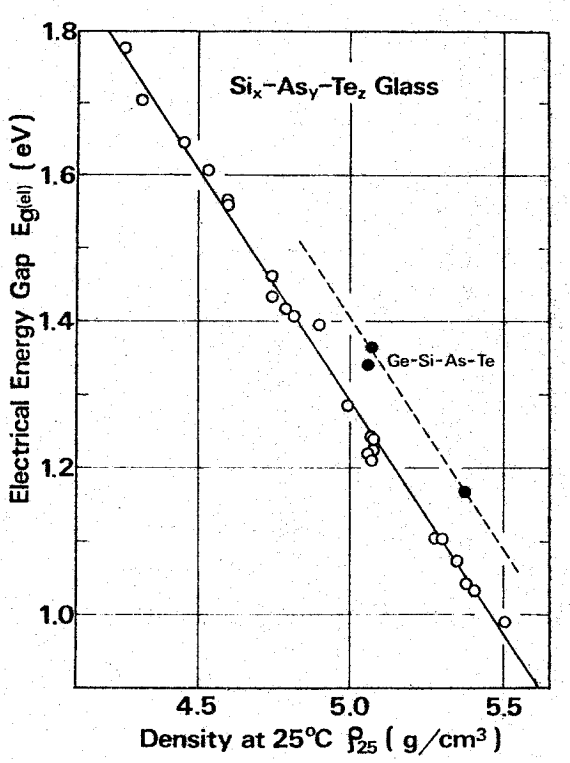

Fig.4-12. Relation between electrical gap $E_{g(el)}$ and weight density at 25°C ρ_{25} for amorphous semiconductors in Si-As-Te and Ge-Si-As-Te systems.

line in parallel with that for the Si-As-Te system. This substitution effect causes a decrease of $E_{g(el)}$ and an increase of ρ_{25} by about 5 %, which may be respectively due to differences of the bond strength and the atomic weight between Si and Ge atoms.[3)]

An attempt to plot the gap $E_{g(el)}$ against each of the two thermodynamic parameters, T_g and T_s, is made for all the Si-As-Te glass, as shown in Fig.4-13. Simple relationships are expressed as follows:

$$T_g = 178 \cdot \exp[0.75 \cdot E_{g(el)}],$$
$$T_s = 190 \cdot \exp[0.75 \cdot E_{g(el)}], \text{ in } °K. \quad \cdots\cdots \quad (4\text{-}2)$$

These simple relationships hint at the underlying correlation between the bond energy and the glass transition. Likewise, they will supply valuable information regarding the static electronic process in the three-dimensionally cross-linked network structure of the Si-As-Te glasses.[2)]

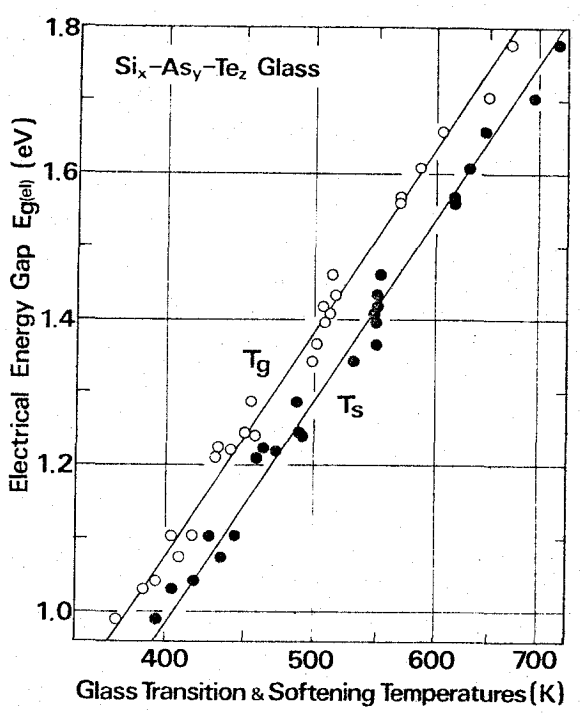

Fig.4-13. Relationships between electrical gap $E_{g(el)}$ and each of two characteristic temperatures, i.e. glass transition temperature T_g and softening temperature T_s, for Si-As-Te vitreous semiconductors of different composition.

Recently, deNeufville *et al.*[20] have introduced a concept of *connectedness C* defined by the average coordination number for covalently bonded materials, to classify relationships of $E_{g(op)}$ versus T_g for a wide variety of stoichiometric chalcogenide glasses. For two-fold coordination materials of $C=2$, T_g is substantially independent of $E_{g(op)}$ due to the covalent bond strength because T_g is associated with the breaking of weak van der Waals bonds between chains and rings. In rather three-dimensional glasses with $C>2$, the gap $E_{g(op)}$ has a linear relationship with T_g for the same C value. This fact suggests that the three-dimensional network structure of the Si-As-Te glasses is heavily cross-linked and almost lacking in long Te chains as shown in Fig.4-6. In these glassy materials, bonds taking part in the static electronic process are no longer distinguished from those forming the basic cross-linked network structure. A similar procedure was successfully employed by Kastner to correlate the band gap and the melting point T_m for numerous crystalline semiconductors.[21]

Contribution of the Si-Te bonds to the band gap can be made clear by re-plots of $E_{g(el)}$ against the mole fraction of the Si-Te for the As-Te bonds as shown in Fig.4-14. An increase of the mole fraction leads to a linear increase of $E_{g(el)}$ and a decrease of ρ_{25}. Therefore, the value of $E_{g(el)}$ or $E_{g(op)}$ is determined by the concentration of the Si-Te covalent bonds in the Si-As-Te amorphous semiconductors. Further, Fig.4-15 shows dependences of $E_{g(el)}$ on the contents of Si and of other substituent atoms, germanium or thallium in place of silicon, in the (As_2Te_3)-based ternary glasses.[22] For the glass system containing Ge atoms, $E_{g(el)}$ increases rather gently with the Ge content as compared with the glasses having Si atoms because the binding energy of Ge is

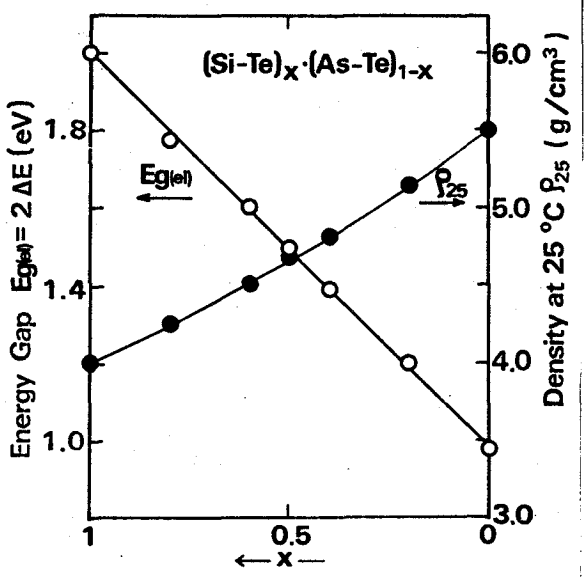

Fig.4-14. Electrical gap $E_{g(el)}$ and weight density ρ_{25} as a function of mole fraction of Si-Te for As-Te bonds.

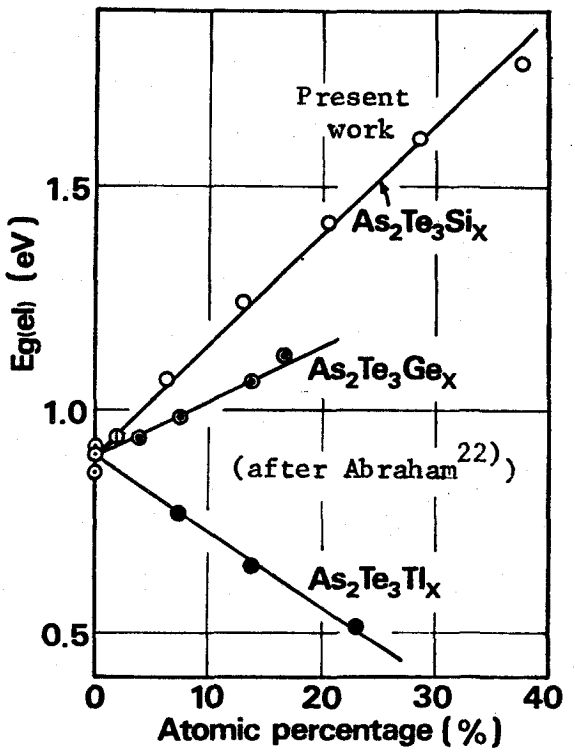

Fig.4-15. Electrical gap $E_{g(el)}$ versus composition of As_2Te_3 with Si, Ge and Tl respectively.

smaller than that of Si by about 0.2eV. In the case of the $Tl_xAs_2Te_3$ glasses, since the Tl atoms of valency 3 have lower binding energy than the As atoms, $E_{g(el)}$ rather decreases with increasing the Tl content. Thus, the Si-Te covalent bonds play a predominant role not only in the construction of the three-dimensionally cross-linked network structure but also in the presence of the band gap in the electronic spectrum as the short-range chemical and confugurational order preserved in such a disordered Si-As-Te system.

4-5. Chemical Basis of Static Electronic States

Little is known in detail about chemical characters of the heavily cross-linked network structure which governs the electronic properties in the multicomponent Te-based vitreous semiconductors. According to

the Pauling's theory about the chemical bonds,[23] the chemical trend of bonds is given by the following fractional ionicity f_i;

$$f_i = 1 - \exp[-(x_A - x_B)^2/4] \ , \qquad \ldots\ldots \qquad (4\text{-}3)$$

where x_A and x_B are the electronegativities of atoms A and B. Since the electronegativities are given to be 1.8, 2.0 and 2.1 for the respective constituent atoms, Si, As and Te, the fractional ionic character of this chalcogenide alloy can be estimated to be 2.2% at maximum. In addition, the binding energy E(A-B) of a heteropolar bond between two atoms, A and B, is approximated by the following form:

$$E(\text{A-B}) = \frac{1}{2}[\ E(\text{A-A}) + E(\text{B-B})\ ] + (x_A - x_B)^2 \ , \quad \ldots\ldots \qquad (4\text{-}4)$$

where E(A-A) and E(B-B) are the covalent bond energies of homopolar bonds. By using the homopolar bond energies of Si, As and Te, the heteropolar bond energies between the constituent elements in the Si-As-Te system can be obtained as follows:

$$\begin{aligned} E(\text{Si-Te}) &= 1.72 \text{ eV} \ , \\ E(\text{Si-As}) &= 1.65 \text{ eV} \ , \\ E(\text{As-Te}) &= 1.43 \text{ eV} \ . \end{aligned} \qquad (4\text{-}5)$$

From the physico-chemical viewpoint, thus, it can be concluded that the covalent bonds between Si and Te atoms should combine in preference to the other covalent bonds so as to maximize total bond energies of the network. Such a covalent bond is in general characterized by the firm restriction of valency and the spatial orientation for the valence-electronic configuration of each atom, which is given by a concept of so-called *orbital*. Each atom tends to surround itself with the number of nearest neighbors required by its valency and bonding configuration. In the case of the Si-As-Te ternary glass with atoms of different valency, therefore, the three-dimensionally cross-linked and strongly covalently bonded network structure can be formed naturally with as few

misfits as possible, as shown in Fig.4-6. The valency satisfaction of each atom gives rise to short-range chemical ordering effects like the tetrahedral $Si-Te_4^{-4}$ molecules in the disordered Si-As-Te system.

As recently pointed out by Phillips,[24] chemical bond arguments can be available in describing the electronic properties in covalently bonded crystalline and amorphous materials by some average over their valence electrons. For example, Fig.4-16 shows a relation between the gap $E_{g(el)}$ and the average coordination number corresponding to the connectedness C introduced by deNeufville *et al.*[20] The gap $E_{g(el)}$ increases linearly with increasing the number C by the content of cross-linking Si atoms, while for the As content the increase of C leads to a rather decrease of the gap $E_{g(el)}$. Accordingly, the number C is not so

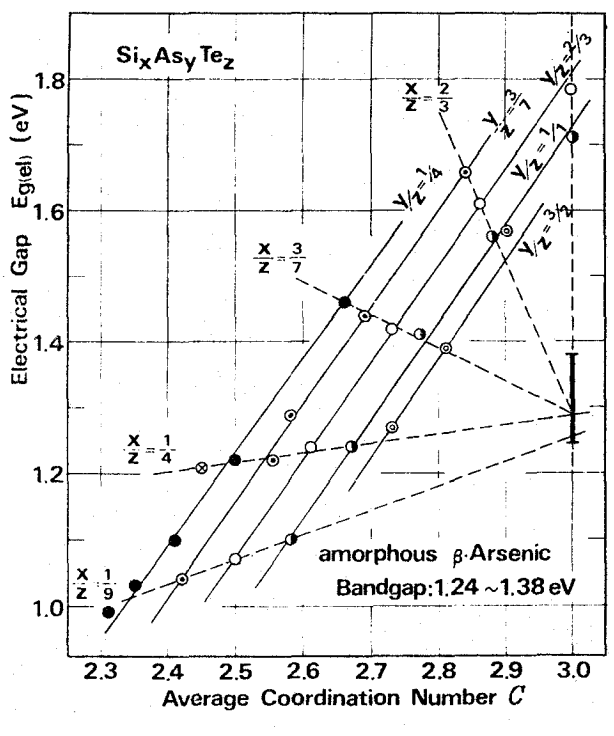

Fig.4-16. Relation between the gap $E_{g(el)}$ and average coordination number C in Si-As-Te amorphous system.

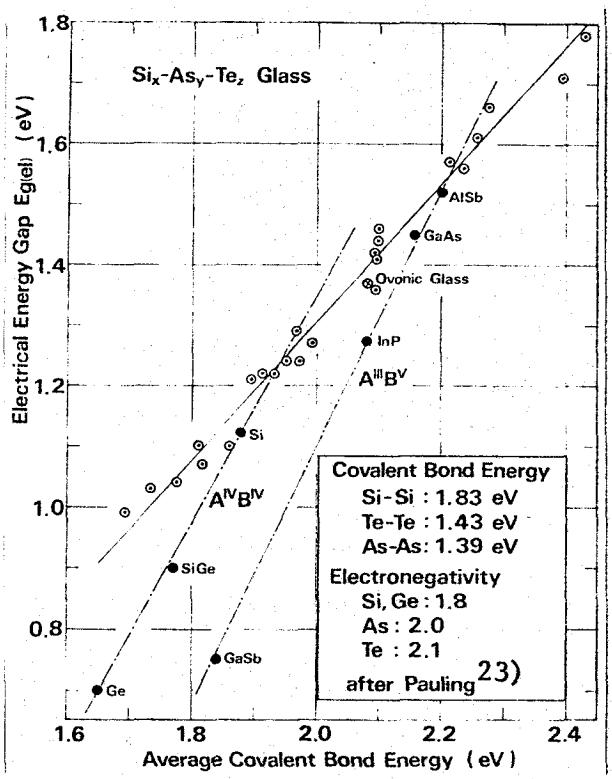

Fig.4-17. Relation between the gap $E_{g(el)}$ and average covalent bond energy in Si-As-Te amorphous system and some crystalline semiconductors.

suitable for the factor indicating the band gap. In Fig.4-17, the gap $E_{g(el)}$ is plotted against the average covalent bond energy per one covalency for all the Si-As-Te vitreous semiconductors. As can be seen in the figure, there is found a good linear correlation between the gap energy $E_{g(el)}$ and the average bond energy, despite of neglecting the ionic bonding character. Some similar relationships were found for some groups of diamond and zincblende type semiconductors by Manca[25] and Vijh.[26] Such a good linear correlation suggests that the glass within the glass-forming region has the same kind of network structure. The short-range chemical ordering effects only between nearest neighbors can give clues to calculate statistically the gap energy in the disordered semiconductors. Therefore, the chemical-bond approach is essentially valuable in interpreting microscopic electronic processes in such covalently bonded amorphous materials. The basic assumption in the approach developed by Mooser and Pearson[27] is that the electronic band-states of the solid are a broadened superposition of molecular-orbital states arising from the constituent atoms. Kastner[28] and Chen[29] have recently discussed the electronic structures of some chalcogenide semiconductors in terms of bonding bands and lone-pair bands by using this molecular-orbital method. As well known, the Si atoms in four-fold tetrahedral coordination have hybridized sp^3 orbitals, which are split into bonding (σ) and antibonding (σ^*) states. In tetrahedral semiconductors the σ- and σ^*-states are broadened into the valence and conduction bands, respectively, as the nearest-neighboring distance decreases. For the group-VI elements such as Te atoms, only two of the six p-state valence electrons participate in the two-fold coordinated bonding (σ) within their molecules, and the other four electrons form two sets of

lone-pair non-bonding (LP) orbitals. The As atoms have three bonding (σ) and one LP hybridized orbitals. The covalent bonds in the Si-As-Te vitreous alloy are formed by the molecular orbitals between the bonding hybrids of Si and Te and between the other σ-orbitals. In the common chalcogenide glasses, the σ-orbital states lie considerably lower in energy than the LP states, so that the σ-states seem no longer to act as the valence band and this role may be played by the LP band. As observed in real amorphous Se, Te, As_2S_3, GeTe, etc. from photoemission[30] and other experiments, however, the σ-orbital and the LP-orbital levels are sufficiently closed and intermixed in the valence band, and seem to contribute together to the upper valence band edge.[31] It is speculated for the multicomponent chalcogenide alloys that the σ- and LP states of various molecular orbitals are mixed still more within the valence band. The speculation is also made from the identified compositional dependences of the structural factors and of the band gap in the Si-As-Te system. The unoccupied σ^*-states of all the constituent atoms are of course broadened and intermixed into the conduction band. Then, the band gap is corresponding to the average energy value necessary for excitation of electrons from the valence to the conduction bands. The basic electronic properties of the Si-As-Te amorphous semiconductor alloys are governed by the short-range chemical order based on the chemical characters of Si-Te covalent bonds, not by the long-range ordering. So far, more detailed discussions can not be promoted because of the lack of both the theoretical and experimental studies about the electronic states in such a multicomponent semiconducting glass system.

4-6. Summary

In this chapter, the compositional dependences of the electrical and optical gaps, in common with those of other structural parameters like the weight density, the glass transition temperature, the thermal expansion coefficient, have been measured systematically for a series of Si-As-Te amorphous semiconductors prepared within the wide glass-forming composition region. Similar compositional trends have been found out for all the electronic and configurational properties, which depend strongly upon the contents of Si and Te, i.e. only on the atomic ratio of Si to Te contents, but are almost insensitive to the As content. In this glass system, particularly, linear relationships of the band gap to the weight density, the glass transition temperature and the softening temperature have been found. In taking account of these compositional dependences observed and the chemical characters of the constituent atoms, a three-dimensionally cross-linked and heavily covalently bonded structural model has been tentatively demonstrated for the Si-As-Te glass. It has been made clear that the basic electronic properties such as the valence- and conduction-band states and the band gap can be determined only by the short-range chemical order like the tetrahedrally bonded $Si-Te_4^{-4}$ molecules which remains relatively unaffected by disordering. Qualitative discussions have been done about the electronic states in the Si-As-Te vitreous semiconductor from a viewpoint of the molecular-orbital of covalent bonds.

REFERENCES-IV

1) A. F. Ioffe and A. R. Regel, in *Prog. Semiconductors* 4, 239 (1960).

2) M. Nunoshita and H. Arai, Solid State Commun. 11, 213 (1972).

3) M. Nunoshita and H. Arai, *ibid.* 11, 337 (1972).

4) M. Nunoshita, H. Arai, T. Taneki and Y. Hamakawa, J. Non-Cryst. Solids 12, 339 (1973).

5) B. E. Warren *et al.*, J. Amer. Ceram. Soc. 19, 202 (1966).

6) J. A. Savage and S. Nielsen, Phys. Chem. Glasses 7, 56 (1966).

7) L. Štourač *et al.*, in *Proc. 5th Intl. Conf. on Amor. and Liquid Semi., Garmisch,* (Taylor & Francis, London, 1974) Vol.1, p.297.

8) K. E. Petersen *et al.*, Phys. Rev. B8, 1453 (1973).

9) A. R. Hilton and C. E. Jones, Phys. Chem. Glasses 7, 112, 116 (1966).

10) T. Minami and M. Tanaka, *Yōgyō-Kyōkai-Shi* 77, 372 (1969).

11) J. P. deNeufville, J. Non-Cryst. Solids 8-10, 85 (1972).

12) E. U. Condon, Amer. J. Phys. 22, 43 (1954).

13) A. R. Hilton, C. E. Jones and M. Brau, Phys. Chem. Glasses 7, 105 (1966).

14) D. Turnbull and M. H. Cohen, in *Modern Aspects of the Vitreous State,* Ed. by J. D. Mackenzie (Butterworths, London, 1960) Vol.1, p.38.

15) G. Rehage and W. Borchard, *The Physics of Glassy Polymers,* Ed. by R. N. Haward (Appl. Science Pub., London, 1973).

16) S. R. Ovshinsky and K. Sapru, in *Proc. 5th Intl. Conf. on Amor. and Liquid Semi., Garmisch,* (Taylor & Francis, London, 1974) Vol.1, p.447.

17) M. Nunoshita, H. Arai, Y. Hamakawa and T. Fujimoto, in *Proc. 10th Intl. Congress on Glass, Kyoto* (Cer. Soc. Japan, Kyoto, 1974) 7, p.37.

18) F. Harman and J. P. van Dyke, Phys. Rev. Letters 21, 1575 (1968).

19) F. Hensel and E. U. Frank, Rev. Mod. Phys. 40, 697 (1968).

20) J. P. deNeufville *et al.*, in *Proc. 5th Intl. Conf. on Amor. and Liquid Semi., Garmisch* (Taylor & Francis, London, 1974) Vol.1, p.417.

21) M. Kastner, Phys. Rev. B7, 5237 (1972).

22) A. Abrahám *et al.*, Czech. J. Phys. B22, 1168 (1972).

23) L. Pauling, *The Nature of the Chemical Bonds*, 3rd ed. (Cornell Univ. Press, Ithaca, 1960).

24) J. C. Phillips, Rev. Mod. Phys. 49, 317 (1970).

25) P. Manca, J. Phys. Chem. Solids 20, 268 (1961).

26) A. K. Vijh, J. Phys. Chem. Solids 30, 1999 (1969).

27) E. Mooser and W. B. Pearson, in *Prog. Semiconductors* 5, 104 (1960).

28) M. Kastner, Phys. Rev. Letters 28, 355 (1972).

29) I. Chen, Phys. Rev. B7, 3672 (1973), *ibid.* B8, 1440 (1973).

30) J. Stuke, J. Non-Cryst. Solids 4, 1 (1970).
R. E. Drews *et al.*, Solid State Commun. 10, 293 (1972).
N. J. Shevchik *et al.*, Phys. Rev. B8, 2833 (1973).

31) L. Ley *et al.*, Phys. Rev. Letters 29, 274 (1972).

Chapter-V

ANNEALING EFFECTS ON ELECTRICAL AND OPTICAL PROPERTIES OF Si-As-Te GLASSY MATERIALS

5-1. Introduction

A vitreous material is believed to be in a metastable configurational state, but is indeed realized in a thermal non-equilibrium state below its glass transition temperature T_g.[1] Such a glassy substance is relaxing towards a more stable state through the kinetic process called the *glass transition*. Physical properties of a vitreous semiconductor are closely associated with its excess stored energy and internal deformations, so that they may be sensitively affected by the stabilization process. Thus, in addition to structural, compositional, or topological disorders in an *ideal* amorphous solid, there usually exist ionized impurities and other electronic active centers originated from deformations, voids and other defects in a *real* vitreous semiconductor. These long-range disorders cause potential fluctuations on an atomic scale, which affect the electronic properties not only as scatterers of electron waves but also as localized carrier-trapping states in the band gap. Nevertheless, few investigations have been done on the kinetic correlation between thé electronic and configurational systems in amorphous and vitreous states on the basis of the glass transition process.[2,3]

In this chapter, some systematic investigations about annealing effects on the electrical and optical properties in the Si-As-Te glasses have been carried out. To study the annealing effects, several steps of the stabilization were realized as a function of the annealing time

during heat treatment at a temperature slightly below the T_g. Besides the dc and ac conductivities and the optical absorption, other physical properties such as thermal expansion, weight density and heat capacity have been measured for various grades of stabilization. Discussions will be given about the correlation between the relaxation kinetics of the internal strains and excess stored energy and the localized electronic states within the band gap in the Si-As-Te amorphous semiconductors.[4,5)]

5-2. Glass Transition Phenomenon

When a melt is cooled, it is well known that the substance can crystallize or solidify into a glass state according to experimental conditions; i.e., by different cooling or heating rates or by producing isothermal after-effects. Fig.5-1 depicts (a) a volume-temperature dependence and (b) a schematic of the physico-chemically configurational energy states of the crystalline and vitreous phases. As represented schematically for the crystallization in Fig.5-1(a), it is found that at the melting point T_m a jump occurs in the volume, which usually decreases. On the other hand, in the glass formation the expansion coefficient of the melt is unchanged near the T_m, and below the T_g the substance will be solidified from the metastable supercooled melt into a rigid glass phase because of a rapid increase of the viscosity. As shown in Fig.5-1(b), the idea of equilibrium metastability in the temperature range between T_m and T_g requires free energy barriers impeding the transtion of the system from the metastable into the stable states. These barriers for the amorphous-crystalline phase transition may be determined from crystal nucleus formation and from crystal growth.

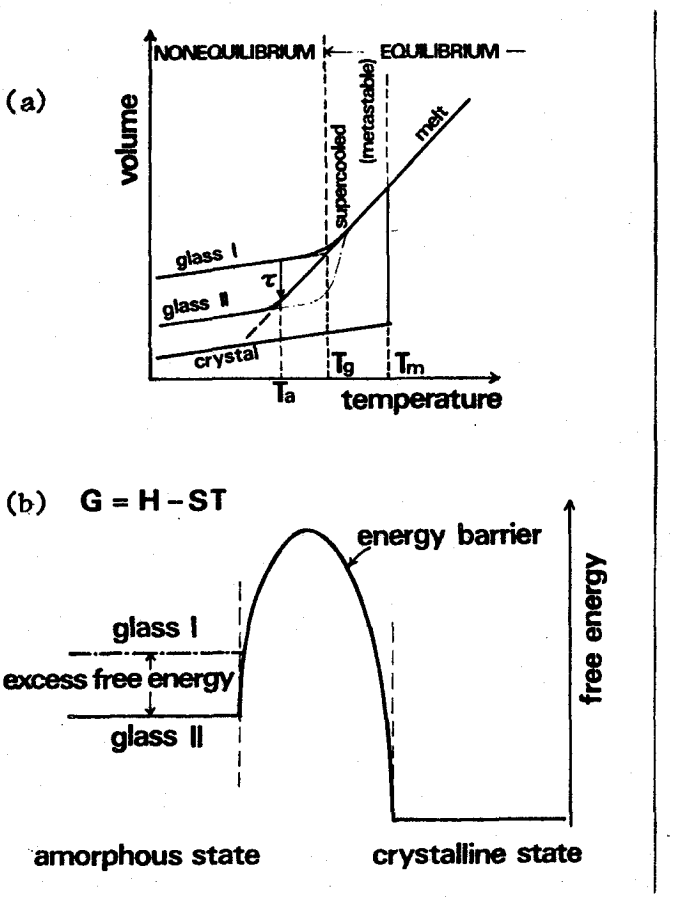

Fig.5-1. (a) Schematic of a volume-temperature dependence of a material in various states. (b) Schematic of physico-chemical configurational energy states of vitreous and crystalline phases of a material.

Strictly speaking, a glass or vitreous substance is in a thermodynamic non-equilibrium state below the temperature T_g at which a certain *transition* takes place. The question whether glassy solidification can be a thermodynamic transition has been frequently discussed. Since the early stage of this kind of investigations, the glass transition has been confused more or less with a thermodynamic second-order transition by reason of their formal similarity. However, because the glassy state is essentially in non-equilibrium, the vitreous solidification or vitrification cannot be identified as second-order transition in the thermodynamic sense, and is realized by an inhibition of pure

kinetic processes.[6] It is widely agreed that this *glass transition* is caused by a relaxation effect, through which some kinetic process in amorphous materials occurs too slowly at low temperatures to permit thermodynamic equilibrium. The evidence that the transition is really a relaxation phenomenon accompanied with structural changes in the glass networks will be presented in this chapter. These changes occur over a relatively wide temperature range in the vicinity of T_g; therefore it would be better to use the term of *glass transition interval*. Such a relaxation process is called *stabilization* phenomenon of glassy materials.

In order to investigate such kinetic processes of the glass transition, the most fruitful experiment has been carried out by measuring annealing effects on various properties of vitreous phase materials. For the purpose, several steps of **stabilization process** in the Si-As-Te vitreous substances were realized as a function of the annealing time during heat treatment at a temperature near the T_g. Most of measurements in this chapter were made for the $Si_9As_{14}Te_{21}$ glass (in atomic ratio)

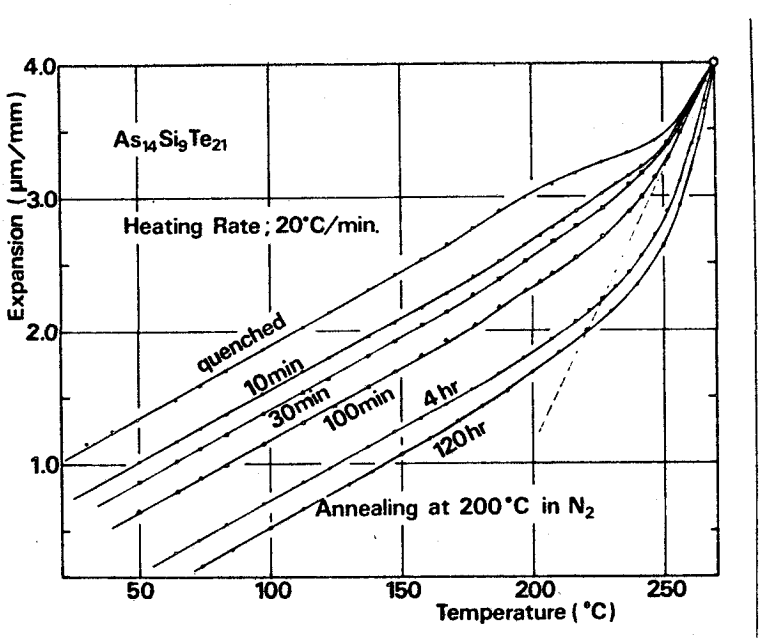

Fig.5-2. Thermal expansion curves on some steps of stabilization.

having the T_g of 233 °C, located in the center of the glass-forming region. The heat treatment was continued for the required hours mainly at 200±3°C below the T_g in atmosphere of dry nitrogen. After that, the samples were rapidly cooled in air. The linear thermal expansion curve was obtained with the Perkin-Elmer TMS-1. The thermal analysis in the glass transition region was made by using a differential scanning calorimeter, the Perkin-Elmer DSC-1. Because arsenic and tellurium have high vapor pressures, the specimen was sealed in an aluminium capsule. The weight density was again measured by the Archimedes' method. As shown in Fig.5-2, the thermal expansion curves for different steps of stabilization of the $Si_9As_{14}Te_{21}$ glass vary clearly with the annealing time at 200 °C. During the heat treatment a continuous contraction of the glass specimen was observed until the glassy state approaches equilibrium at a given annealing temperature, as displayed in Fig.5-3. The rate of the contraction increases rapidly as the annealing temperature T_a decreases, and is corresponding to a stabilization (or relaxation) rate τ shown in Fig.5-1(a). Therefore, the dimensions, specific volume and weight density of the specimen at room temperature are strictly dependent on the the grade of stabilization reached by the annealing. Fig.5-4 shows changes of the weight density ρ_{20} as a function of the annealing time at 200 and 225 °C. As seen in the figure, the density increases logarithmically with the time on the early stages of annealing, and eventually approaches a constant value for a given annealing temperature. This saturation appears at the earlier time and the smaller density value for the higher annealing temperature. From these results on the expansion and density, the full annealing makes the vitreous substance a more stable and close-packing network structure. It has been confirmed by

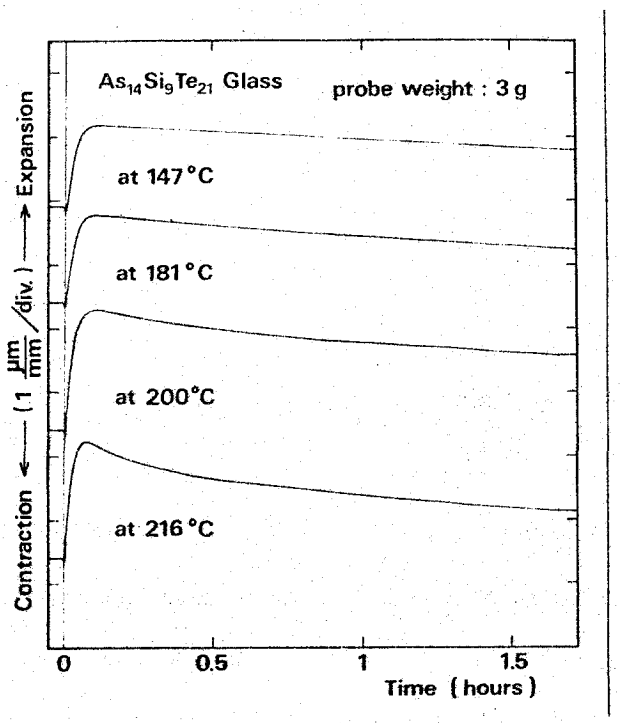

Fig.5-3. Continuous stabilization curves of length of $Si_9As_{14}Te_{21}$ glass during heat treatments at several annealing temperatures within glass transition region.

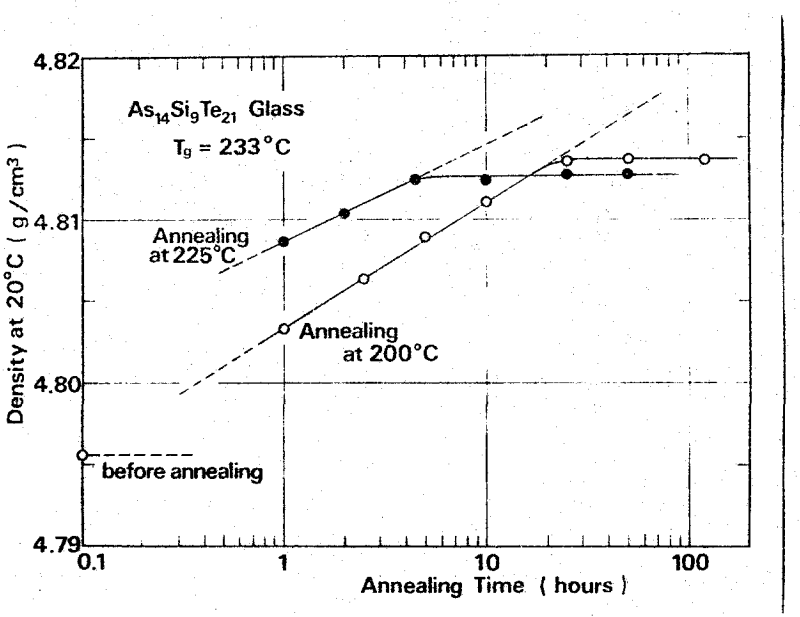

Fig.5-4. Variation of weight density ρ_{20} of $Si_9As_{14}Te_{21}$ glass plotted against annealing time during heat treatments at 200 and 225°C.

the X-ray diffraction measurement that the phenomenon is not due to a phase transition from the amorphous to crystalline states, and it may be due to certain structural changes in the amorphous phase. For the well-annealed glass, the thermal expansion curves observed depart from the complete equilibrium curve which is denoted by a dashed line in Fig.5-2. This behavior is attributed to a large overshoot by a *plastico-viscous* nature of the network structure at the finite heating rate.[7] It would be expected therefore that such a large overshoot results in a high endothermic peak on the increasing heat capacity versus temperature curve of the DSC analysis. The endo- and exo-thermic effects of the glass transition on the DSC traces at the constant heating rate of 20 deg/min are illustrated in Fig.5-5(a) as a parameter of the annealing time at 200 °C for the $Si_9As_{14}Te_{21}$ vitreous material. As can be seen in Fig.5-5(a), the height of the anomalous heat-capacity peak in this region increases with the annealing time. The area of the peak corresponding to the

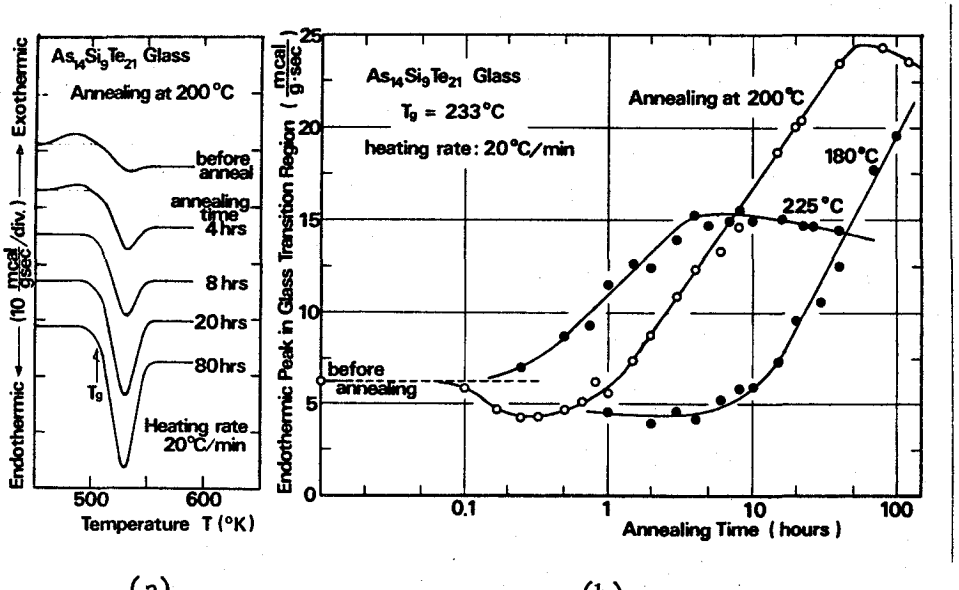

(a) (b)

Fig.5-5. (a) Variation of DSC traces in glass transition temperature region for $Si_9As_{14}Te_{21}$ glass as a parameter of annealing time at 200 °C. (b) Plots of endothermic peak of glass transition against annealing time at some annealing temperature for $Si_9As_{14}Te_{21}$ glass. The measurements were made at a constant heating rate of 20 deg/min.

enthalpy difference ΔH is considered to depend closely upon the release of internal configurational energy, chiefly the decrease of excess-stored energy, during the annealing.[8] On the assumption that the temperature width of the glass transition interval is constant regardless of annealing conditions, an attempt is made to plot the peak height as a function of the annealing time. Fig.5-5(b) shows variations of the peak height by annealing. As shown in the figure, with increasing the time at a given annealing temperature the height of anomalous heat capacity in the vicinity of the T_g seems to increase also logarithmically. Once equilibrium has been attained at an annealing temperature, an increase of the peak height occurs no longer on further heating. As shown in Fig.5-5(b), the higher the annealing temperature is, the earlier and smaller saturation of the peak is observed. On annealing at 200 °C, the height is saturated for about 50 hours. Low annealing temperatures can make the glassy substance attain finally to a more stable and lower energy state, in spite of a decrease of the relaxation rate.

A real vitreous substance maintains essentially more or less the order and disorder of the supercooled melt. Glasses having the same composition do not always lie in one inherent metastable state, but can be realized in various physico-chemical energy states depending on their own thermal history. Especially, an as-quenched glass has considerably low packing density and high configurational energy. During stabilization through glass transition processes, the as-quenched glass can be stabilized towards a more stable and close-packing state, i.e., from glass-I to glass-II as shown schematically in Fig.5-1. Recently Tool has attempted to interpret the kinetic nature of such a glass transition by introducing a concept of *fictive temperature*, at which

the glass would be in thermodynamic equilibrium.[9] As suggested by a few experimental results,[2,10] however, the excess configurational energy stored in non-stabilized glasses can be regarded mainly as local stresses and deformations. The stabilization process by annealing may be governed by releases of the local stresses and deformations through local rearrangements of chemical bonds, and rather as the result an increase of the packing density occurs. When the kinetic process of the glass transition take place, the glassy material is stabilized and experiences a contiuous increase of the degree of ordering. The simplest conception of the release of thermally induced internal stress in non-stabilized glasses may be derived from the Maxwell relation as follows:

$$S(t)/S_0 = \exp(-t/\tau), \quad \tau = G/\eta \ . \qquad \ldots\ldots \qquad (5\text{-}1)$$

Where $S(t)$ is the internal stress or strain at time t, S_0 the initial stress or strain, G the modulus of rigidity, η the viscosity and τ the relaxation time. Indeed, since the viscosity η changes considerably with time during the annealing in the glass transition range, no experimental datum to fit the simple exponential formula has been observed. Therefore, a quantitative explanation of the experimental results obtained in this thesis work can not be made so far.

5-3. Annealing Effects on Electrical and Optical Properties

Structural changes due to the stabilization process should affect sensitively electronic semiconducting properties like dc and ac conductivities and optical absorption of the Si-As-Te glasses. It is very interesting to study about electronic effects of the excess-stored energy and local stresses through the configurational stabilization process by annealing. It is expected that they give rise to potential

fluctuations on an atomic scale, and further contribute to a breakup of long-range order and to a formation of localized electronic states.

A contribution of the localized states to the electronic process can be observed by the measurement of ac hopping conductivity $\sigma(\omega)$.[12] Fig.5-6 shows the influence of annealing on temperature dependence of the ac conductivity $\sigma(\omega)$ as well as the dc one σ_T of the $Si_9As_{14}Te_{21}$ vitreous semiconductor. The annealing was made at 200 °C, too. The $\sigma(\omega)$ was measured with the transformer bridge mentioned previously. The salient features in the temperature dependence are: (i) the $\sigma(\omega)$ approaches the dc conductivity for all frequencies in the high temperature region; (ii) the $\sigma(\omega)$ has a very small activation energy in the low temperature

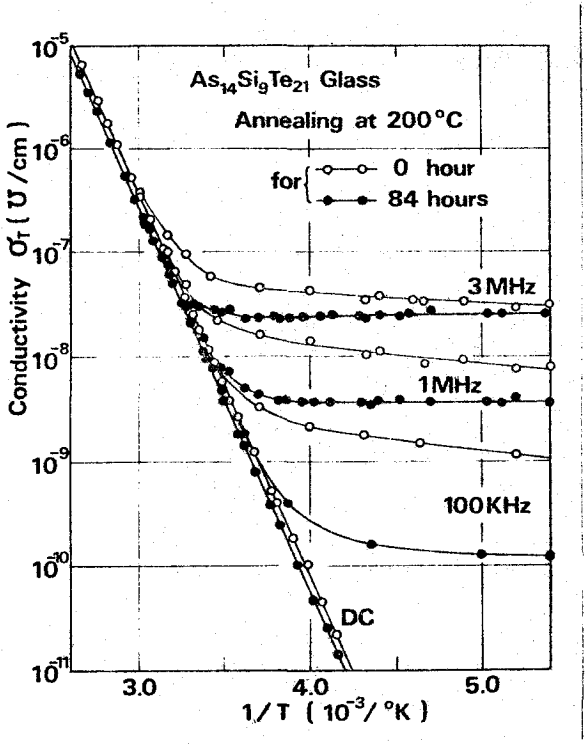

Fig.5-6. Semilog plots of ac and dc conductivities versus reciprocal temperature for as-quenched and full-annealed $Si_9As_{14}Te_{21}$ glasses, at different frequencies.

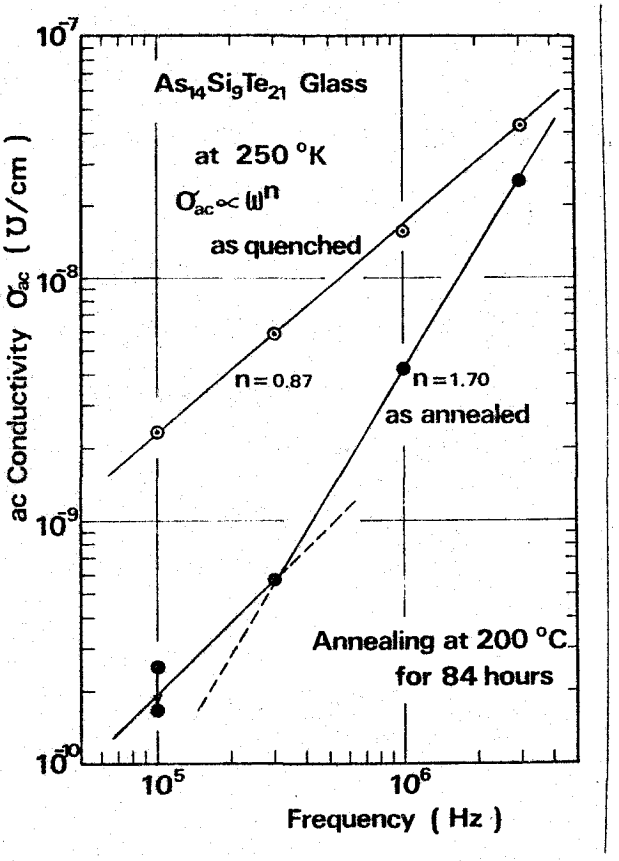

Fig.5-7. Frequency dependence of ac conductivity at 250°K for as-quenched and full-annealed $Si_9As_{14}Te_{21}$ glasses.

region; and (iii) the $\sigma(\omega)$ at low temperatures increases with the frequency. Similar characteristics were observed for amorphous Se, As_2S_3 and As_2Se_3.[13] As seen from the figure, the ac conductivity $\sigma(\omega)$ decreases more remarkably than the dc one by the full annealing under the same experimental conditions. Fig.5-7 shows frequency dependence of $\sigma(\omega)$ at 250 °K for both as-quenched and well-annealed $Si_9As_{14}Te_{21}$ glasses. From the figure, the notable changes of $\sigma(\omega)$ by the annealing are the decrease of activation energy from a finite value to zero and the increase of exponent n from n=0.87 to 1.70 for the frequency dependence expressed by $\sigma(\omega) \propto \omega^n$. The conduction model for the temperature- and frequency-dependent ac conductivity can be described reasonably as thermally activated hopping or tunneling. Pollak and Geballe[12] have pointed out that if the hopping takes place between randomly distributed localized states, then $0.5 < n < 1$. Since the hopping process is phonon-assisted, a small but finite activation energy should be observed for the temperature dependence of $\sigma(\omega)$. In the case of the hopping between identical levels, the value of n is equal to 2 when the frequency ω is smaller than the characteristic hopping frequency. Then the activation energy is nearly zero. In the Si-As-Te vitreous semiconductor, the most likely process seems to occur between localized tail states rather than between midgap states at the Fermi level.[14] As comparing the results in Figs.5-6 and 5-7 with the hopping theory, the author can conclude that the hopping process in the as-quenched glass takes place mainly in a random distribution of the localized tail states, whereas after the glass is well-annealed it occurs rather between identical sites of the regularized tail states. Of course, this arises from the change in distribution of the localized tail states by the annealing.

At the same time, the well-annealing makes the value of tanδ take a figure down one place in the low temperature region. There is found little compositional change of the ac conductivity σ(ω) except only a slight increase of σ(ω) with decreasing the Si content. In contrast to σ(ω), variations of the dc conductivity during the annealing are fairly small as shown in Fig.5-6. In Fig.5-8, the appriciable changes in dc conductivity σ_{25} at 25 °C and the electrical gap $E_{g(el)}$ are plotted as a function of the annealing time at 200 °C. About 30% decrease of σ_{25}, mainly caused by the increase of about 0.04 eV in $E_{g(el)}$, is observed as the annealing time increases. Both values are saturated after about 50 hours, similarly for other properties.

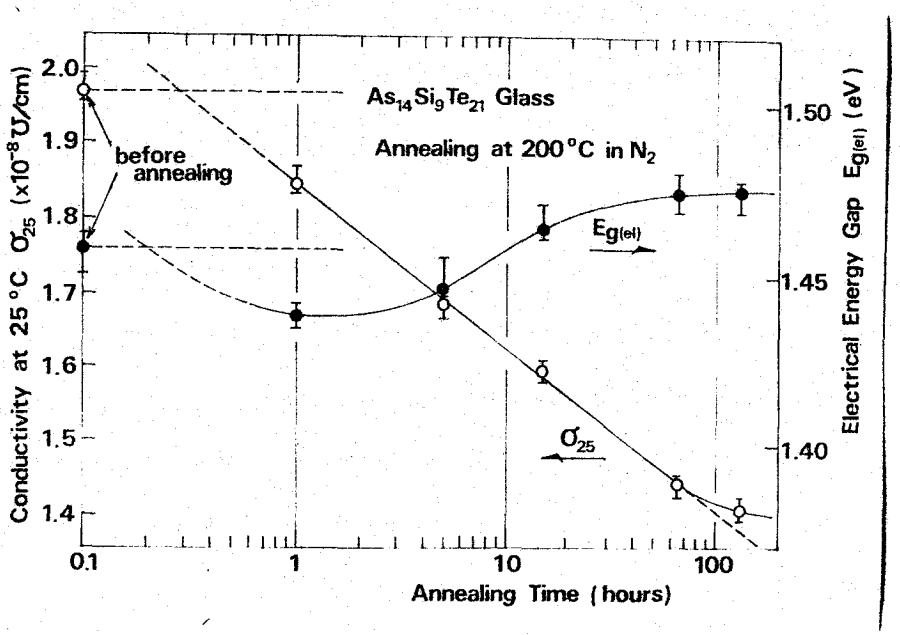

Fig.5-8. Dependences of dc conductivity σ_{25} and electrical gap $E_{g(el)}$ on annealing time.

Figure 5-9 shows the effect of the same heat treatment on the optical absorption spectrum measured for the same glass specimen at room temperature. The exponential absorption edge shifts clearly towards higher photon energy side with increasing the annealing time, as seen

from Fig.5-9. Therefore, the optical gap $E_{g(op)}$, defined as the photon energy $\hbar\omega$ at $\alpha(\omega)=10\ cm^{-1}$, becomes slightly wider ($\sim$0.02 eV) by the annealing. At the same time, the band-tailing factor E_s obtained as the reciprocal slope of the exponential tail is reduced gradually. The changes of $E_{g(op)}$ and E_s by annealing are re-plotted in Fig.5-10.

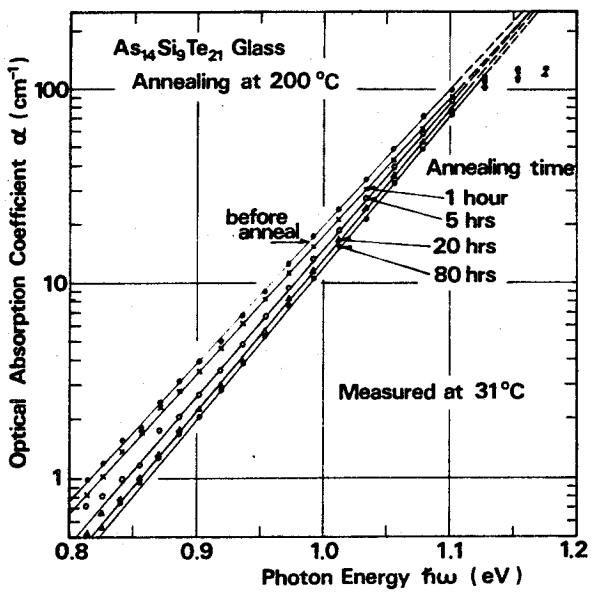

Fig.5-9. Shift of optical absorption edge with annealing time.

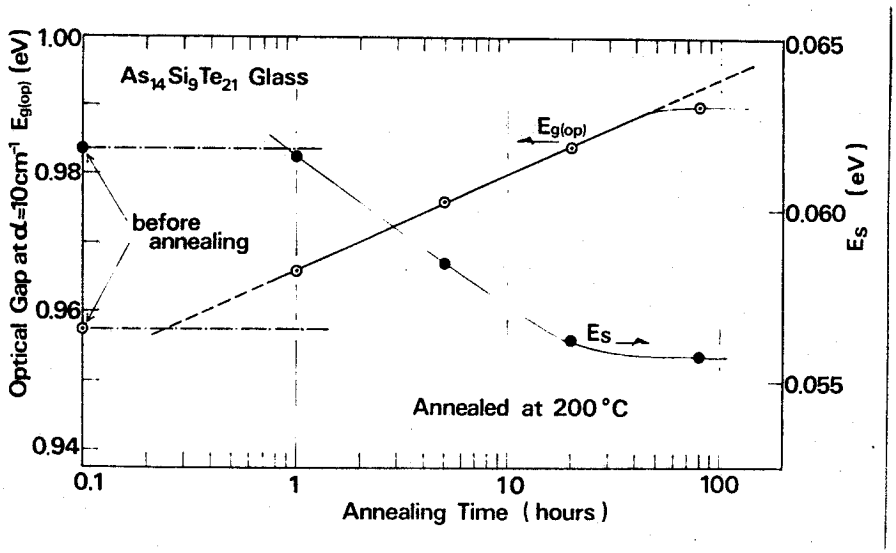

Fig.5-10. Dependences of optical gap $E_{g(op)}$ at $\alpha=10\ cm^{-1}$ and band-tailing factor E_s on annealing time for $Si_9As_{14}Te_{21}$ glass.

Consequently, both values also change logarithmically with the early annealing time and no longer after the complete stabilization by the heat treatment for about 50 hours. The value of E_s would be linearly dependent on the root-mean square of electronic microfields or of potential fluctuations due to the disordering and local stresses.[15,16] The results about the E_s factor in Fig.5-10 implies that the local stress and deformation energy decreases and the internal microfields also weaken during the annealing. In summarizing the above experimental results, the configurational rearrangement during the complete stabilization leads consistently not only to a little increase ($\sim$0.02eV) of the energy-band gap, but also to appreciable reduction and regularization of localized states at the band edges in the Si-As-Te glass. The increase of gap may be almost due to the decrease of localized tail states.

In recent studies about annealing effects on amorphous Ge films, it has been obviously observed that an exponential absorption edge of an as-deposited film changes into a sharp edge and shifts towards higher energy side with an increase of the degree of order by annealing.[17] Its dc conductivity changes from a variable range hopping type obeying the $\log\sigma \propto T^{-1/4}$ law to an intrinsic band-conduction type, and its thermo-electric power starts to change from small positive to large negative values.[18] Photoemission experiment also has shown that the spectrum of valence band states in amorphous Ge films approaches that in the single-crystal form with the grade of annealing.[19] Annealing effects on amorphous Si films reduce the density of localized gap states appreciably as observed in field effect measurements.[20] These annealing effects on the amorphous Ge and Si films agree essentially with the author's conclusions in which the localized tail states

decrease and are regularized with increasing the degree of order in the amorphous Si-As-Te semiconductor during the stabilization process.

5-4. Long-Range Disordering and Localized Tail States

High dense localized states of $10^{18}\sim10^{20}$ $eV^{-1}cm^{-3}$ in the mobility gap play a fundamental and rather characteristic role in electronic properties of amorphous semiconductors. Some knowledges of their nature and distribution are essential for a closer understanding of electrical, optical and magnetic properties of non-crystalline solids. According to Mott's view of amorphous semiconductors, localized states lie in the middle of a band gap in high density of about 10^{19} $eV^{-1}cm^{-3}$ and rather narrow width of a few tenths of 1 eV.[21] Also the CFO model for a chalcogenide alloy has predicted an overlap of band-tails of localized states extending from the mobility edges into the gap.[22] Such high dense localized gap states are assumed only to effectively pin the Fermi level near the center of a pseudogap. As discussed in Sec.3-4, however, many experimental data for the Si-As-Te glasses and other amorphous semiconductors seem to contradict the presence of the high dense localized mid-gap states in these models. For example, the distinctive part of an absorption curve below $\alpha(\omega)=1cm^{-1}$ in Fig.5-9 leads to an estimate of $10^{16}\sim10^{17}$ cm^{-3} for the total density of localized gap states.[16] On the other hand, there is little doubt of the existence of localized states in tails at the band edges. This is evidently supported by many experimental results for the Si-As-Te vitreous semiconductors on the exponential absorption edge, the energy difference between the electrical and optical gaps, the temperature-dependent photo-conductivity and the ac conductivity measured in this thesis work, as well as by the measurements

of Hall mobility and thermo-electric power.[23] The width of tails is consistently obtained to be about 0.1 ∿ 0.2 eV from all the experiments. The density of localized tail states decreases gradually into the gap from $\sim 10^{19}$ to less than 10^{17} $eV^{-1}cm^{-3}$, destroying the sharpness of the valence-and conduction-band edges, as demonstrated in Fig.3-14.

Why the character of eigenstates changes abruptly from localized to extended at certain critical energies remains in question. Anderson has first given a theoretical discussion about the condition under which localization of the electronic eigenstates occurs in a certain kind of irregular lattice, so-called Anderson's transition.[24] Mott has pointed out that if the Anderson's criterion is satisfied, the dc conductivity $\sigma(E)$ at T=0°K can be adopted as a criterion for localization.[25] Because of complexity of real vitreous materials, it is still unknown whether such a standard criterion is applicable to the real systems. Cohen has made a simple plausible arguments on electronic structures in non-crystalline semiconductors on the analogy of a single isolated band in perfect and imperfect crystals.[26] Lack of long-range order in the potential gives a more drastic effect to the eigenstates particularly near the upper and lower edges of the band. As shown as the simplest

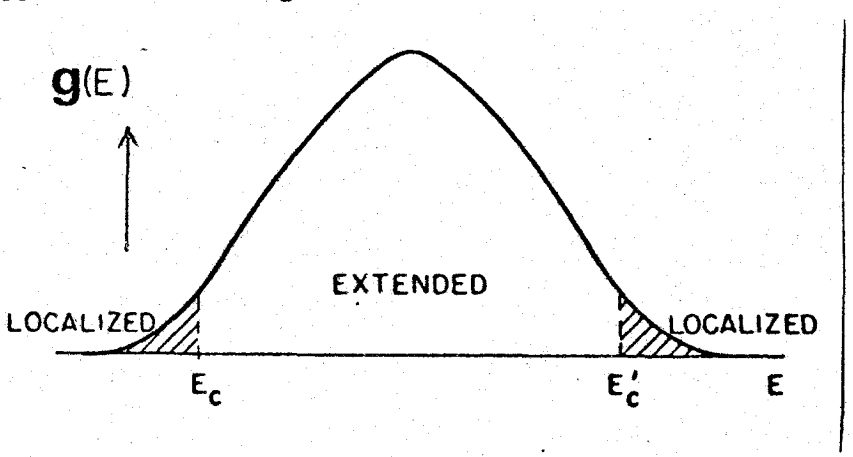

Fig.5-11. The simplest model for the density of states of a single isolated band in a disordered material. (after Cohen[26])

band model in Fig.5-11, for $E_c<E<E_c'$ the electronic states remain extended with a finite phase coherence length, i.e. long-range order in the phase. For $E<E_c$ and $E_c'<E$, the wavefunction is restricted only in a finite region of potential well and its localization can not be destroyed by tunneling, since an overlap of the electronic wavefunctions decreases exponentially with the separation between the nearest states at the same energy level. In the tails of the band, the states all are localized. There exist two characteristic energies E_c, E_c' separating abruptly the regions of localized states from that of extended states, and these energies are called mobility edges.

The basic idea underlying the quantum-mechanical calculations is that in disordered materials the localized tail states are dominated by potential fluctuations but are not in general corresponding directly to individual single-imperfections. The average or superposition of various kinds of disordering effects should act on electrons. It appears important to point out that the potential fluctuations depend self-consistently on the electronic occupation of the localized states. An ideal amorphous substance is thought of as a uniform three-dimensional random network structure in which structural, compositional or topological disorders, based on variations in ionic radius, valency or electronegativity of the constituent atoms, are included in nature. In addition, any real disordered system has usually various kinds of disorders in the the form of dangling bonds, voids, local deformations or other electronic active defects. As mentioned previously, the latter random disorders is closely related to the excess-stored configurational energy and local deformations, and therefore is very sensitive to the thermal history of the material. Both categories of configurational inhomogeneities are

associated with nonuniform charge distributions which cause random potential fluctuations and internal electric microfields introduced by Dow and Redfield.[15]

In order to obtain the magnitude of the internal deformation or stress fields, an attempt to measure an electro-absorption effect was made for the $Si_9As_{14}Te_{21}$ amorphous semiconductor.[4] The specimen of $6\times5\times0.3$ mm^3 having the coplanar electrode gap of 0.5 mm was prepared. The electro-optical measurement was made with a conventional two Lock-In system with a monochromater as employed elsewhere.[27] As shown in Fig.5-12, a linear field-induced change in the optical absorption $\Delta\alpha(\hbar\omega,F)$ near $\alpha(F=0)=10$ cm^{-1} at $\hbar\omega=1.0$ eV was observed on application of an external field $F=1.4\times10^3$ V/cm. By comparing this field-induced energy shift of $\alpha(\omega)$ with that by the full annealing, the excess-stored deformation fields reduced by the full stabilization can be estimated to be about 5×10^4 V/cm. This value is very reasonable in comparison with that in nearly covalent semiconductors doped heavily.[15] According to

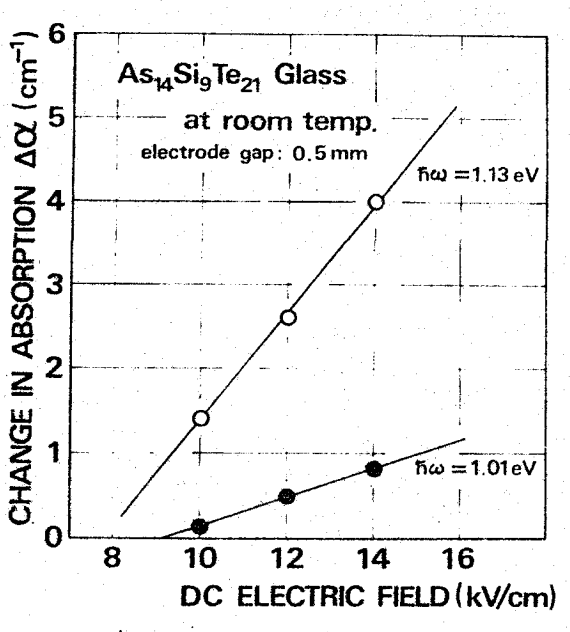

Fig.5-12. Field-induced change in optical absorption $\Delta\alpha(\hbar\omega,F)$ in measurement of electro-absorption effect for $Si_9As_{14}Te_{21}$ amorphous semiconductor.

the theory of internal Franz-Keldish effect by the microfields, estimates of the average field intensity and the barrier height of the potential fluctuations are obtained to be the order of $10^5 \sim 10^6$ V/cm and 0.1∿0.2eV, respectively from the observed exponential absorption edges of amorphous semiconductors.[15,16] From the measurements of Franz-Keldish effect, the root-mean-square value of the microfields has been found to be equal to 4.5×10^6 V/cm for amorphous As_2Se_3.[28] On the other hand, in applying the Poole-Frenkel formula to dc high-field V-I characteristics, the maximum Coulomb potential of ionized centers is estimated in the range of 10^4 to 10^6 V/cm.[29] The photoemission experiment shows that the average value of fluctuations is below the resolution of Nielsen's experiments which he claims to be 0.15 eV.[30] It seems thus likely that the concentration of localized tail states due to the fluctuations extending deep into the gap is small. Most of the potential fluctuations have an average amplitude below 0.1 to 0.2 eV, and the magnitude of microfields may be the order of $10^5 \sim 10^6$ V/cm. It is rather surprising that these values can be estimated nearly equal and experimental aspects like the exponential absorption edge and the ac conductivity of various amorphous semiconductors are closely phenomelogically similar, in spite of having a large variety of possible sources of the random potential fluctuations and internal microfields in real amorphous solids. The observations suggest that there may be some internal electronic mechanism which adjusts the average value of internal fields into relatively narrow limits.

As summarized by Fritzsche[31] and Spear[20], many ambiguities of the character and distribution of localized gap states give rise to considerably different experimental results and conclusions not only by

the compositions and thermal histories of the substances but also by the experimental methods. The quantitative treatment of the transport mechanism as well as of the trapping and recombination kinetics governed by the localized tail states is further difficult at present. There still remain a great number of intensive and challenging problems about the correlation between the configurational states and the localized states in vitreous semiconductors.

5-5. Summary

In this chapter, an effect of annealing on electrical, optical and thermodynamic properties has been systematically investigated for amorphous Si-As-Te system, mainly for the $Si_9As_{14}Te_{21}$ vitreous semiconductor (T_g=233 °C) located near the center of the glass-forming region. Sevral steps of stabilization from an as-quenched to a well-annealed states have been realized as a function of the annealing time by heat treatments at a temperature slightly below the glass transition temperature T_g. As a result of measuring the changes of the thermodynamic and structural properties like the weight density, thermal expansion and heat capacity during the annealing, it has become evident that the $Si_9As_{14}Te_{21}$ glassy substance is stabilized completely until it reaches a more stable and close-packing configurational state by the continuous heat treatment for about 50 hours at 200 °C. The configurational stabilization process in the glass transition is governed by release of the local stresses and deformations corresponding to an excess-stored physicochemical energy through some structural rearrangements, and consequently the degree of orders in a non-stabilized glass increases continuously during the annealing. The decrease of internal electric microfields by

restoring some kind of orders has been estimated to be 5×10^4 V/cm from the electro-absorption measurement. Dc and ac conductivities, electrical and optical gaps and band-tailing factor also have been observed to change consistently with logarithm of the annealing time and to saturate after the continuous annealing for about 50 hours at 200 °C. Especially, notable changes of the ac conductivity $\sigma(\omega)$ by the stabilization have been found: i.e., the decrease of thermal activation energy from a finite value to zero and the increase of exponent n in $\sigma(\omega) \propto \omega^n$ from 0.87 to 1.70 at 250 °K. It follows that the structural change during the stabilization leads to appreciable reduction and regularization of the localized tail states as well as a little increase of the band gap (about 0.02 eV). On the basis of these experimental results, the electronic effects of configurational disordering and the correlation between localized states and random potential fluctuations or internal electric microfields produced by the lack of long-range orders in the Si-As-Te amorphous semiconductors have been discussed.

REFERENCES-V

1) W. Kauzmann, Chem. Rev. 43, 219 (1948).

2) G. C. Das, M. B. Bever, D. R. Uhlmann and S. C. Moss, J. Non-Cryst. Solids 7, 251 (1972).

3) A. Hamada, M. Saito and M. Kikuchi, Solid State Commn. 9, 873 (1971).

4) M. Nunoshita *et al.*, in *Proc. 5th Intl. Conf. on Amorphous and Liquid Semicon., Garmisch* (Taylor & Francis, London, 1974) Vol.2, p.753.

5) M. Nunoshita *et al.*, in *Prog. 10th Intl. Cong. on Glasses, Kyoto* (1974).

6) S. Seki, *Jap. Keshyō-Gakkai-Shi* 14, 335 (1972).
G. Rehage and W. Borchard, *The Properties of Glassy Polymers*, Ed. by R. N. Haward (Appl. Science Pub., London, 1973) p.54.

7) J. E. Stanworth, *Physical Properties of Glass*, (Clarendon Press, Oxford, 1950).

8) Yu. A. Sharonov *et al.*, Soviet Phys. Solid State 5, 429 (1963).

9) A. Q. Tool and C. G. Eichline, J. Amer. Ceram. Soc. 29, 240 (1946).

10) S. Spinner and R. M. Waxler, Appl. Opt. 5, 1887 (1966).
T. Kurosu and M. Kikuchi, in *Proc. 5th Intl. Conf. on Amorphous and Liquid Semi., Garmisch* (Taylor & Francis, London, 1974) Vol.1, p.389.

11) J. DeBast and P. Gilard, Phys. Chem. Glasses 4, 117 (1963).

12) M. Pollak and T. H. Geballe, Phys. Rev. 122, 1742 (1961).

13) A. I. Lakatos and M. Abkowitz, Phys. Rev. B3, 1791 (1971).

14) H. K. Rockstad, J. Non-Cryst. Solids 8-10, 621 (1972).

15) J. D. Dow and D. Redfield, Phys. Rev. B5, 594 (1972).

16) J. Tauc and A. Menth, J. Non-Cryst. Solids 8-10, 569 (1972).

17) M. Theye, Mat. Res. Bull. 6, 103 (1971).

18) W. Beyer and J. Stuke, J. Non-Cryst. Solids 8-10, 321 (1972).

19) W. E. Spicer and T. M. Donovan, J. Non-Cryst. Solids 2, 66 (1970).

20) W. E. Spear, in *Proc. 5th Intl. Conf. on Amorphous and Liquid Semi., Garmisch* (Taylor & Francis, London, 1974) Vol.1, p.1.

21) E. A. Davis and N. F. Mott, Phil. Mag. 22, 903 (1970).

22) M. H. Cohen, H. Fritzsche and S. R. Ovshinsky, Phys. Rev. Letters 22, 1065 (1969).

23) P. Nagels *et al.*, in *Proc. 5th Intl. Conf. on Amorphous and Liquid Semicon., Garmisch* (Taylor & Francis, London, 1974) Vol.2, p.867.

24) P. W. Anderson, Phys. Rev. 109, 1492 (1958).

25) N. F. Mott, Phil. Mag. 17, 1259 (1968).

26) M. H. Cohen, J. Non-Cryst. Solids 4, 391 (1970).

27) Y. Hamakawa, J. Germano and P. Handler, Phys. Rev. 167, 703 (1968).

28) B. T. Kolomiets *et al.*, Soviet Phys. Semicon. 5, 2004 (1972).

29) R. M. Hill, Phil. Mag. 23, 59 (1971).

30) P. Nielsen, Phys. Rev. B6, 3739 (1972).

31) H. Fritzsche, J. Non-Cryst. Solids 6, 49 (1971).

Chapter-VI

ELECTRIC BREAKDOWN PHENOMENON AND THRESHOLD SWITCHING DEVICES OF Si-As-Te-(Ge) AMORPHOUS SEMICONDUCTORS

6-1. Introduction

One aspect of practical interest in the field of non-crystalline chalcogenide semiconductors is the possibility of realizing electronic and opto-electronic active devices by means of thin-film processes.[1] Since the report of Ovshinsky,[2] many intensive efforts have been devoted to the study about two types of useful switching phenomena: i.e. memory and threshold switches. Such two-terminal switches have need of operating at a higher speed and of integrating in a smaller size as one of the most basic elements in the computer and communication systems. The memory effect has been already clarified to be due to *lock-on* process accompanied with a phase transition from amorphous to crystalline forms.[3] A *read-mostly-memory* device with about 10^8 failure-free cycles has been realized by using a $Te_{81}Ge_{15}Sb_2S_2$ amorphous film.[4] In contrast, the field of the threshold switch suffers from a large degree of ambiguity. Its physical process has been explained by thermal,[5-7] electro-thermal[8-12] and electronic models.[13-19] It is still unclear whether it arises from a thermal runaway or from an electronic breakdown. It is very difficult to solve this question exactly because the material parameters and the external effects like device geometries are not only poorly understood but also interact complicatedly one another.[20] The most important thing in practical application is to know what parameters for the thin-film techniques lead to significant improvements of reliability, reproducibility and characteristics of the amorphous thin-film devices.

This chapter describes exclusively about the reversible threshold switching devices made of some Te-based chalcogenide alloys or amorphous thin-films in the Si-As-Te-(Ge) system.[21] Bulk and thin-film switching devices have been fabricated as a trial in the author's laboratory. A series of practical experiments on the pre-switching electric breakdown and threshold switch has been carried out by using parameters of sample thickness, duty cycle of the applied voltage pulses, glass-composition, etc. The primary aim was directed to finding device parameters which can separate the switching mechanism due to the electronic breakdown from that due to the thermal process. Consequently, the performance of the thin-film switching device has attained to a considerably high degree of reliablity and reproducibility in practice. The switching mechanism will be discussed in consideration of influences of the material parameters and the external effects.

6-2. Structures and Fabrication of Threshold Switching Devices

Two types of threshold switching devices shown schematically in Figs.6-2(a) and (b) have been fabricated in the author's laboratory. Fig.6-2(a) presents a typical bulk device of the Si-As-Te-(Ge) amorphous alloys. The disk of alloys used in this work was cut from individual alloy ingots in the form of about 1 mm thick and 15 mm in diameter. One of surfaces of the disk was mirror-polished with 0.3 μm Al_2O_3 powder. By means of vacuum evaporation techniques, molybdenum, gold or platinum thin-film was deposited as the lower electrode onto the whole polised surface. Then the disk was mounted on a metallic block with Ag paste, as exhibited in Fig.6-2(a). This metallic block acts as a good heat sink as well as the lower electrode. The upper surface was

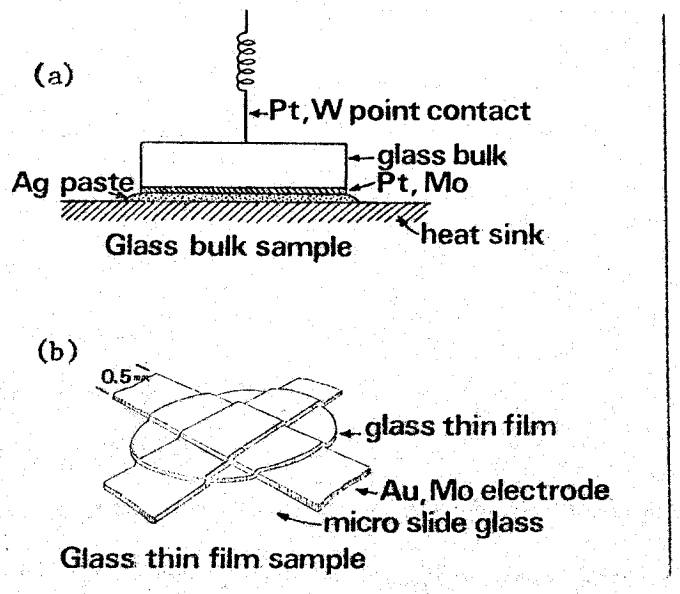

Fig.6-2. Device configurations of threshold switch
(a) point-contact device of bulk threshold switch,
(b) crossover sandwitch-type device of all-film threshold switch.

grinded and polished mechanically with Al_2O_3 fine powder and 0.3 μm diamond paste to prepare desirable thick devices above 20 μm. As the other electrode, a point-contact of a platinum or tungsten needle 0.2mm in diameter was placed on the polished upper surface. Such a point-contact electrode was employed to obtain the better switching characteristics with a high *off-to-on* resistance ratio. Measurements of the switching characteristics were made as soon as the sample was polished and well washed. Little influence of chemical etching and annealing was observed in the characteristics. Fig.6-2(b) illustrates a crossover sandwitch-type device of all-film threshold switch. This thin-film devices up to 12 μm thick were fabricated by means of a vacuum evaporation technique on a microscope slide glass or a BeO ceramic plate. As shown diagrammatically in Fig.6-2(b), the active region of the amorphous thin-film was contacted by thin-film molybdenum or gold crossing

electrodes of 0.5 mm width in the form of sandwitch structure. Compositions of the thin films were chiefly employed near the Ovonic fractions ($Si_{12}Ge_{10}As_{30}Te_{48}$) as the result of vacuum evaporation. To obtain this film composition, the source material of a certain composition was chosen by experience under the fixed evaporating condition. The atomic fractions of films were measured with the atomic absorption analysis (Nippon Jarrell-ASH, Jaco AA-1E) shown in Fig.6-3 with an accuracy of about 2%. For the purpose of preventing the device from worsening, the thin-film device was overcoated with SiO_2 and As_2S_3 amorphous films. The thickness of active material was measured using a Hg spectrum interferometer and an electro-micrometer. The switching characteristics on applying ac and pulse voltages were observed with osciloscope.

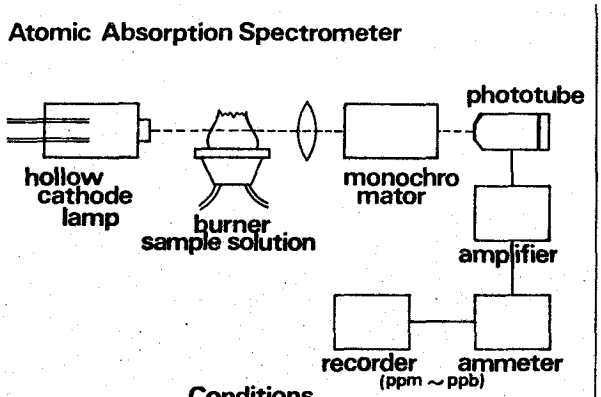

Conditions

element	As	Te	Si	Ge
Source (Å)	1937	2143	2516	2651
Fuel	H_2	C_2H_2	C_2H_2	C_2H_2
Oxidant	Air	Air	N_2O	N_2O
Burner	Hetco	Slit	Slit	Slit

Fig.6-3. Schematic of atomic absorption spectrometer. Chathode lamps of As, Te, Si and Ge are made in Westing Hause Co. Dilution solution of 0.5 N HNO_3 containing 0.05% HF was used.

6-3. Principal Parameters of Threshold Switch and Electric Breakdown

Two different types of non-destructive switching phenomena, memory and threshold switches, have been observed in chalcogenide glasses and films. Figs.6-4(a) and (b) show the schematic current-voltage (V-I) characteristics of the threshold (OTS) and the memory (OMS) switching operations. In both types of switches, first the threshold switching

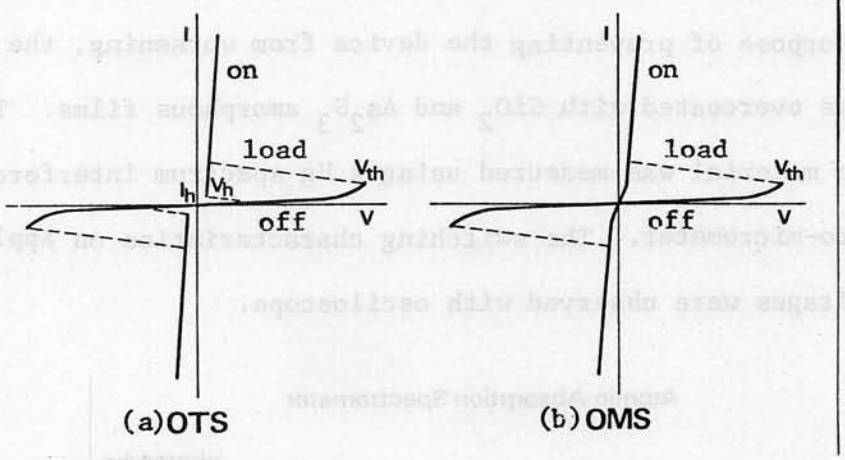

Fig.6-4. Idealized current-voltage characteristic of (a) an Ovonic threshold switch (OTS) and (b) an Ovonic memory switch (OMS).

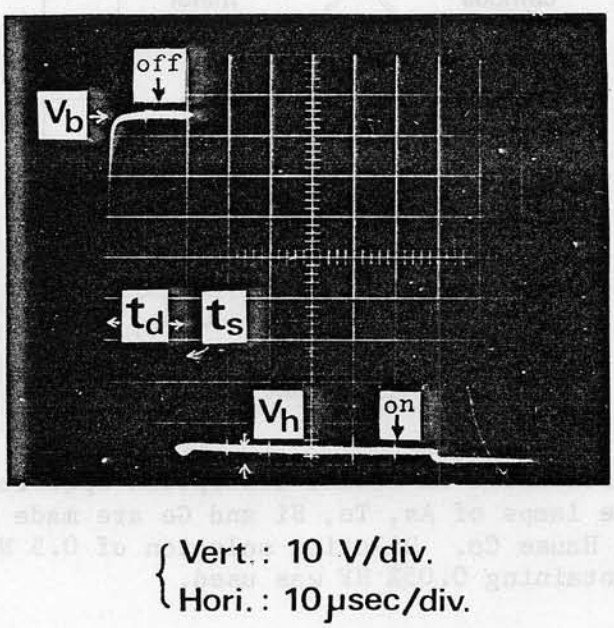

Fig.6-5. Time responce to a voltage pulse applied to a threshold switching device. Vertical voltage scale: 10 V/div; horizontal time scale: 10 μsec/div; series load: 100 kΩ; repetition rate: 1 kHz; temperature: room temperature; thickness: 5 μm.

process occurs when the applied voltage exceeds a threshold voltage V_{th} (or breakdown voltage V_b). As shown in Fig.6-5, this process proceeds very rapidly within a transit time $t_s \lesssim 10^{-10}$ sec along a load line from high-resistance *off*-state in the range $10^6 \sim 10^7$ Ω to the conductive *on*-state. However, it does not occur simultaneously with the application of pulse voltage, but after a delay time t_d which is observed as a relatively large statistical value for the applied overvoltage. In the conducting state the voltage drop is about equal to $V_h \simeq 1$ V. Such a switching behavior is led by an electric breakdown accompanying with a current-controlled differential negative resistance, and during the breakdown a transverse spatial instability contracts the current flow to a filament of high current density.[22] The principal difference between two switches is that OTS returns to its original *off*-state when the *on*-current falls below the holding (or sustaining) current I_h, whereas the OMS retains its *on*-state if it allows sufficient time for *lock-on* process to occur after being switched. The OMS effect is obviously due to crystalline filament growth of a Te-based crystal in the *lock-on* process, and then the memory reset is achieved by revitrification of the crystal.[1] The OTS seems to involve no structural or compositional changes during the switching operations.

The threshold switching behavior is either explained as a thermal process or as an electronic one, but the purely thermal effect is no longer available for reliability and operating life of the practical OTS devices. Since the external parameters like ambient temperature and device geometries are still poorly understood in amorphous semiconductor devices, the mechanisms leading to the high-field breakdown as well as the dynamic process taking place once the breakdown has occurred,

are very difficult to be identified. It is therefore indispensable to take these parameters as well as the material properties into sufficient consideration for the device design. At the same time these remarks may suffice as warning against accepting the experimental data on the OTS without explicit cross-checks of the physical conditions of the amorphous materials and device structures.[23)]

Fig.6-6 shows typical dc V-I characteristics in the high-resistance *off*-state for bulk and thin-film devices of OTS with the fractions nearly equal to the Ovonic $Si_{12}Ge_{10}As_{30}Te_{48}$ (atomic %).[2)] From this figure, it can be seen that the Ohmic region appears at low electric fields and that the non-Ohmic current increases rapidly for the high fields larger than $F = 10^4$ V/cm. When the pre-breakdown current increases still more and the applied voltage exceeds a threshold value V_{th}, a sudden electric

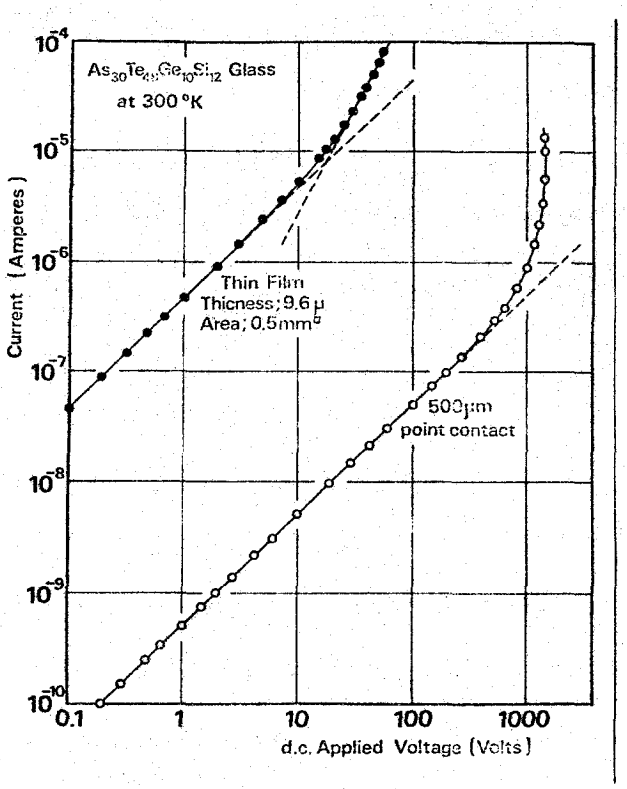

Fig.6-6. Current-voltage characteristics of bulk and thin-film OTS devices of $Si_{12}As_{30}Te_{48}Ge_{10}$ glass in high-resistance *off*-state.

breakdown takes place and then the device switches from the *off*- to the conducting *on*-state. Such characteristics are almost unchanged by the polarity of applied voltage and by the electrode metals. A similar behavior has been found in many kinds of amorphous semiconductors and insulators.

In order to understand the switching process and to obtain the desirable amorphous devices, experiments have been firstly carried out on influences of the external parameters and the material properties upon the high-field transport and pre-switching breakdown. Fig.6-7 shows oscilloscopic photographs of the switching V-I characteristics for the $Si_3As_8Te_{12}$ bulk devices having different area of the upper electrode. As be seen from the pictures, an electrode area as small as the point contact is suitable to reduce a pre-breakdown leakage current and a capacitive stored energy and to realize a better switching characteristic with a high *off-to-on* resistance ratio. This reason is that the diameter of an active area of the filamentary breakdown is the order of 10 μm.

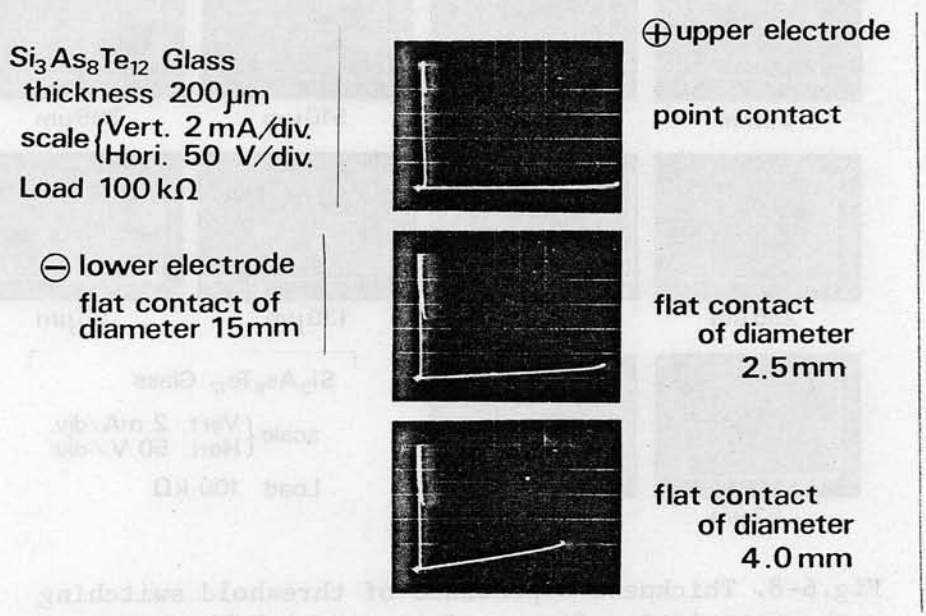

Fig.6-7. Dependence of switching characteristic on upper electrode area for $Si_3As_8Te_{12}$ bulk device. Vert. scale:2mA/div; Hori. scale: 50V/div.

The much leakage current and stored charges bring on destroying the electrodes and on shortening the operating life of the devices. Fig.6-8 displays photographs of the switching operation for point-contact devices of different thickness. Apparently the switching characteristics, e.g. breakdown voltage, resistances in the *on* and *off* states, change with the device thickness or electrode separation. The threshold switch for the sample thickness less than about 200 μm is at a glance superior to that of the thicker devices. In Fig.6-9, the *off*-state resistance R in the Ohmic region is plotted against the thickness d of the bulk devices. It follows that R remains constant for d > 150 μm and decreases linearly with decreasing d below 150 μm. The point-contact area is estimated to be about 50 μm in diameter. The affect of such a point-contact seems to spread over into the bulk 150 μm deep and must be closely related to the mechanism of the threshold switches. Fig.6-10 represents plots of the initial breakdown voltage V_b as a

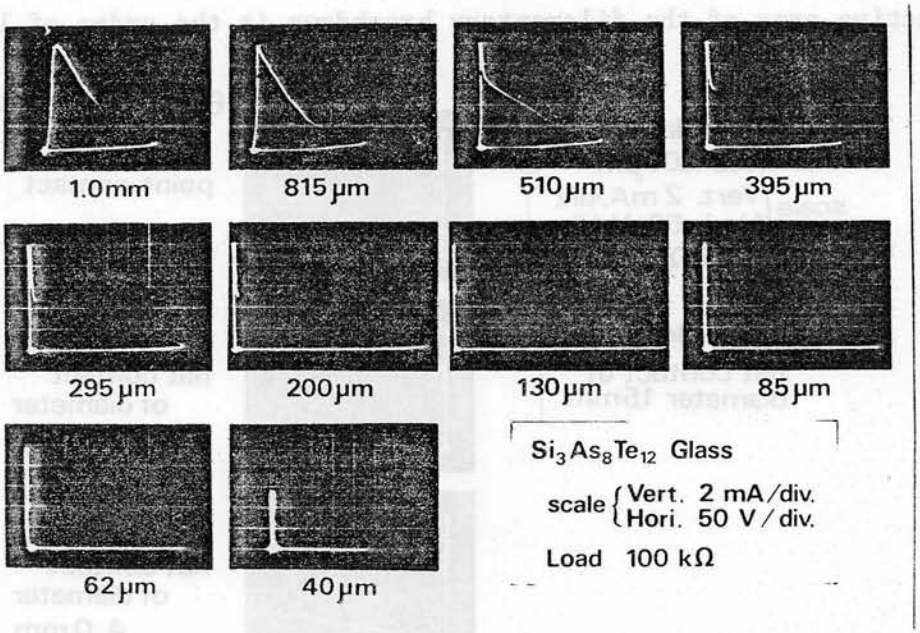

Fig.6-8. Thickness dependence of threshold switching characteristics for a point-contact bulk devices of $Si_3As_8Te_{12}$ amorphous semiconductors.

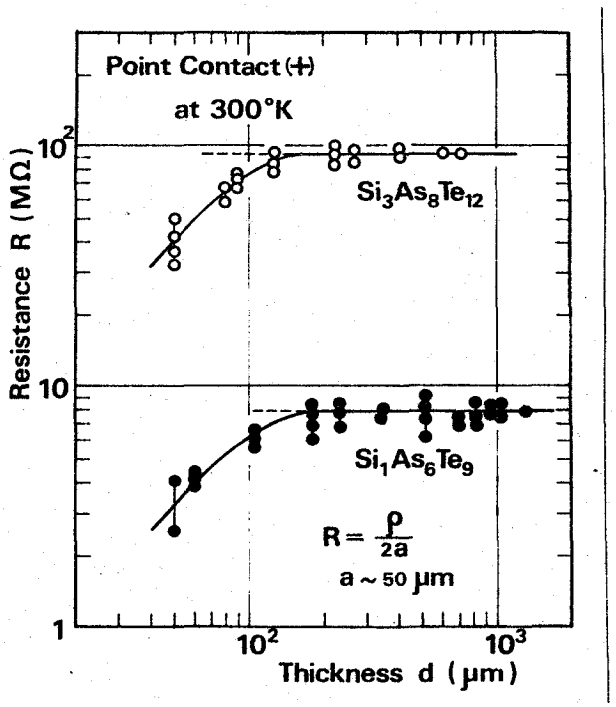

Fig.6-9. *Off*-state resistance R in Ohmic region as a function of sample thickness d for point-contact devices of $Si_3As_8Te_{12}$ and $Si_1As_6Te_9$ amorphous alloys.

function of d for the applied voltages of various waveforms; dc, rectified 60 Hz ac and 1 msec wide square pulse voltages, respectively. Likewise, thickness dependence of the average breakdown field $F_b=V_b/d$ is plotted in Fig.6-11 as a parameter of duty cycle of the applied pulse voltage. As shown in Figs.6-10, 6-11 and 6-12, identical thickness dependences of V_b and F_b have been observed for other glasses in the Si-As-Te and Si-As-Te-Ge systems. From the results, it can be seen that F_b remains almost independent of d below about 100 μm and it follows the empirical relationships in the thickness region above 200μm:

$$F_b \propto d^{-2/3} \quad \text{for impulse breakdown,}$$

$$F_b \propto d^{-1\sim-3/2} \quad \text{for steady-state breakdown.} \qquad \ldots\ldots \qquad (6\text{-}1)$$

These results differ fairly from the datum of Kolomiets *et al.*[24] for a Si-As-Te-Ge glass, as shown in Fig.6-12. Because of no description about the glass composition and the device structure in their report,

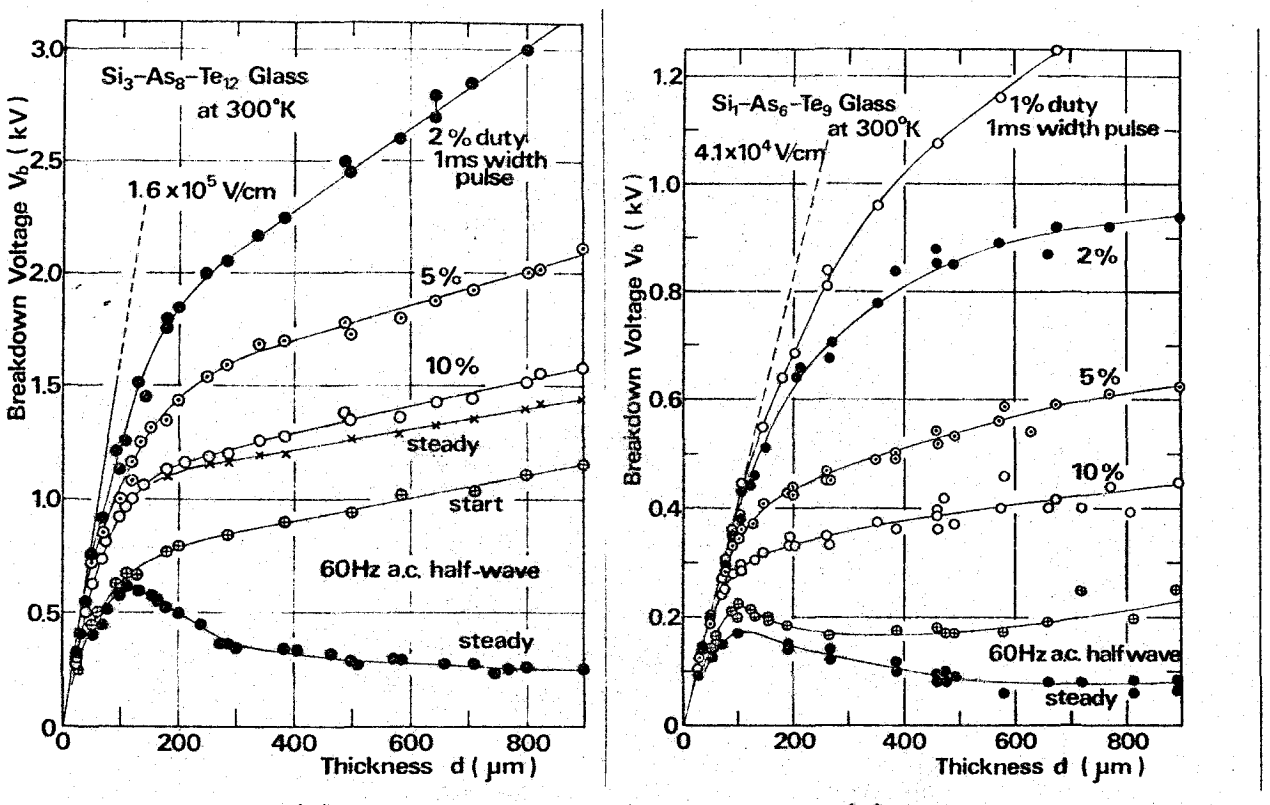

(a) (b)

Fig.6-10. Dependence of breakdown voltage V_b on sample thickness d for threshold switch (a) of $Si_3As_8Te_{12}$ glass and (b) of $Si_1As_6Te_9$ glass as a parameter of duty cycle of applied voltage pulse.

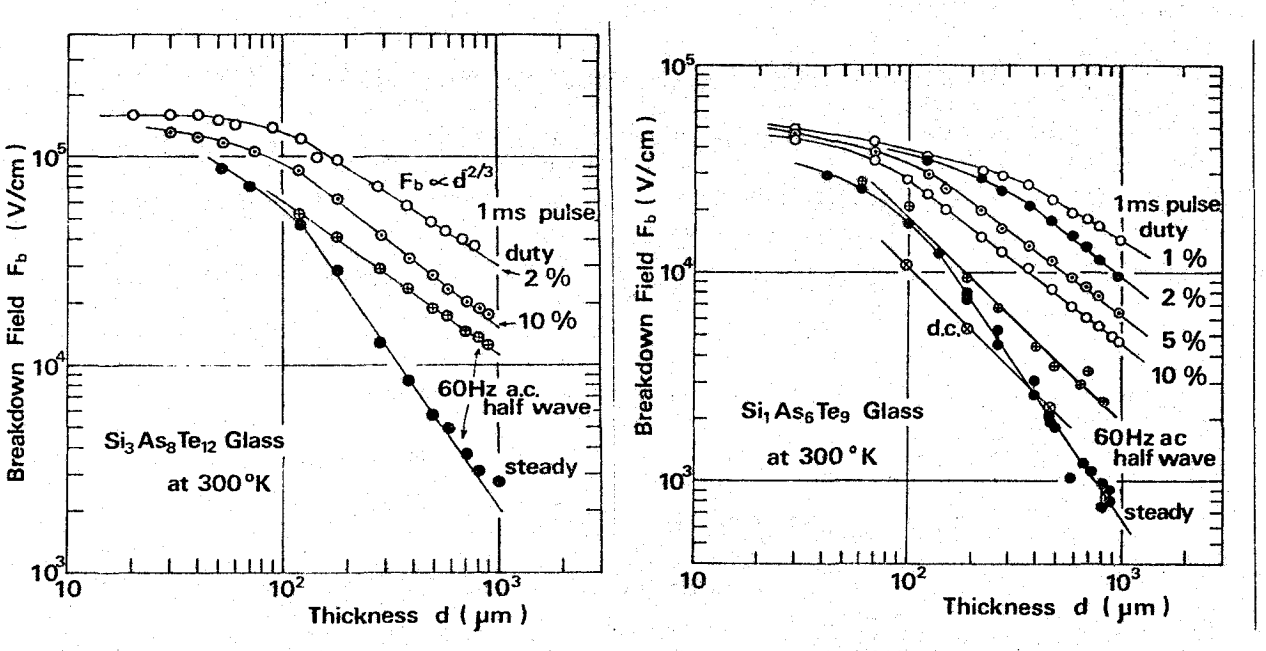

(a) (b)

Fig.6-11. Dependence of average breakdown field F_b on sample thickness d for threshold switch of (a) $Si_3As_8Te_{12}$ glass and of (b) $Si_1As_6Te_9$ glass as a parameter of duty cycle of applied pulse.

this disagreement cannot be solved. For the thick devices, V_b and F_b are strongly affected by thermal boundary conditions due to the contact and shape of the devices, well connected to a heat sink. For example,

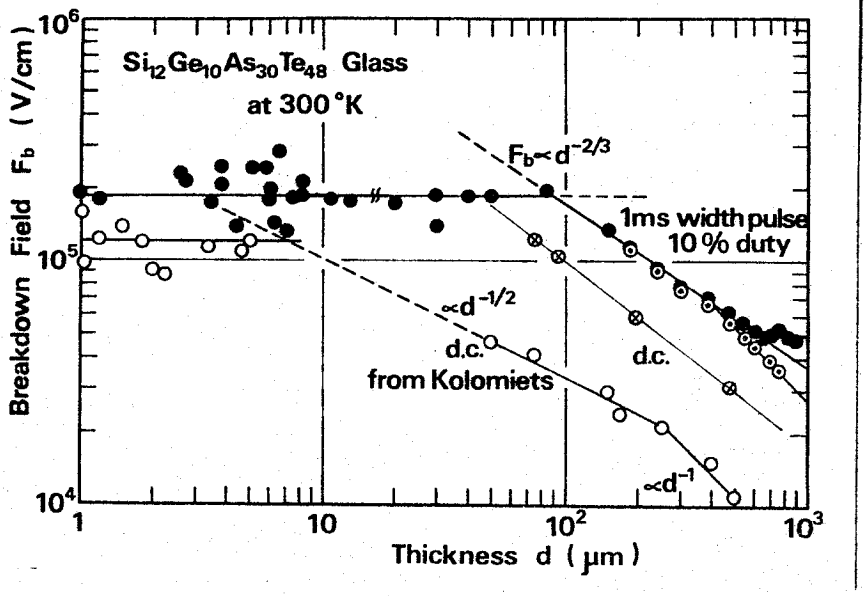

Fig.6-12. Average breakdown field F_b as a function of sample thickness d for Si-As-Te-Ge glassy semiconductors as compared with the datum of Kolomiets *et al.*[24]

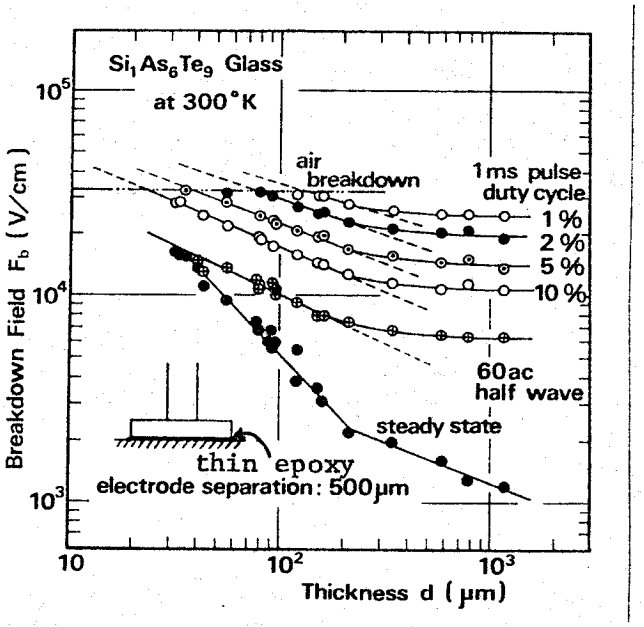

Fig.6-13. Average breakdown field F_b as a function of sample thickness d for two-point-contacts devices of $Si_1As_6Te_9$ amorphous semiconductors. The electrode gap is 500 μm.

another experimental result obtained for a different structure of $Si_1As_6Te_9$ OTS device with two point-contacts separated by 500 μm on the upper surface is shown in Fig.6-13. As compared the result with Fig.6-11, the aspects are quite different. For this device structure, the field F_b is almost independent of d above 200 μm, and $F_b \propto d^{-1/3}$ for small thickness below 200 μm. Unfortunately the breakdown measurement in excess of $F_b = 3 \times 10^4$ V/cm is hindered by a glow discharge between the two needles. This result comes from only the thermal condition of the active region, and therefore the heating-up region between the two point-contacts is likely to be localized within the depth of about 200 μm from the surface, because of relatively small thermal conductivity of these chalcogenide glasses. Below 200 μm a release of heat from the active region to the heat sink may be predominant. Therefore, it is considered that the crytical value of 100∿200 μm is due to the cooling condition rather than due to the electrode separation and the spreading resistance of a point-contact. The critical value is of course shifted by the device structure. In the thin-film devices on a microscope glass substrate, F_b does not remain independent of d beyond about 10 μm as shown by Kolomiets *et al.*[24] No unique functional dependence of F_b on d can be given for the thicker devices since it is influenced by the thermal boundary conditions set by the contacts and device geometries. Thus, the glass thickness, electrode area and separation are very important for the OTS devices.

The thick devices having d >100 μm are affected strongly by the duty cycle, i.e., the mean power of the applied pulse voltage. On applying 60 Hz half-wave voltage, the steady-state breakdown voltage drops relatively lower than the initial threshold value because of heating-up

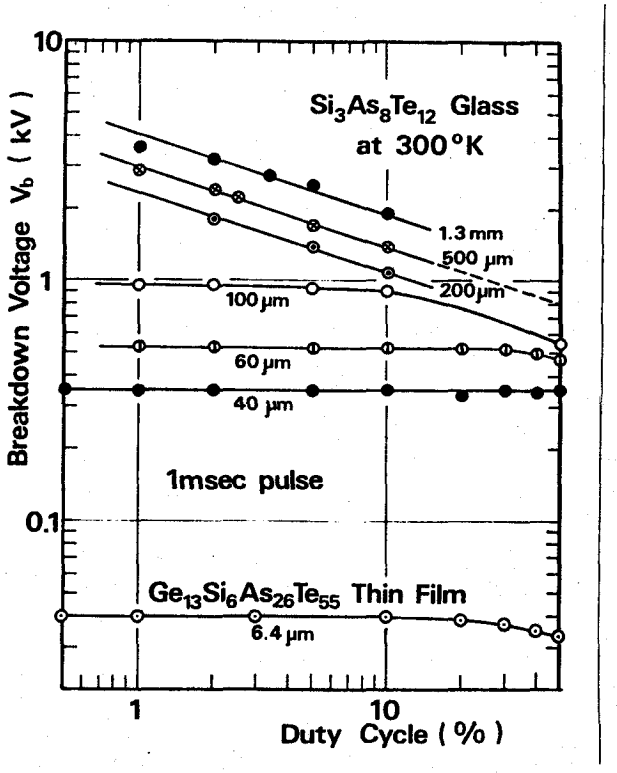

Fig.6-14. Relation between breakdown voltage V_b and duty cycle of applied pulses as a parameter of thickness d for $Si_3As_8Te_{12}$ bulk and $Si_6Ge_{13}As_{26}Te_{55}$ thin-film devices at room temperature.

by steady-state *on*-current. In Fig.6-14, a relation between V_b and the duty cycle is plotted as a parameter of the sample thickness d for the $Si_3As_8Te_{12}$ bulk and the $Si_6Ge_{13}As_{26}Te_{55}$ thin-film devices. As be seen in the figure, the thin devices up to 100 μm have little duty-dependence of V_b, whereas for the thicker devices V_b is in inverse proportion to the one-third power of duty cycle of the applied pulse voltage. Such duty-dependent and constant-field breakdown in thin devices suggests that the mechanism of threshold switch arises from some electronic process. The strong duty-dependence of V_b is caused by thermal effects in thick OTS devices above 200 μm.

Fig.6-15 shows temperature dependence of V_b for the $Si_3As_8Te_{12}$ point-contact devices of thickness 100 and 500 μm. Both devices have

the same exponential temperature-dependence of V_b. The activation energies are about 0.2 eV over the measured temperature range. The branch in the high temperature region is caused by distortions of the switching pulse waveform, as shown in Fig.6-16. The resemblance between two data in Fig.6-15 may occur merely accidentally. For steady-state breakdown in a thick sample with 1 cm^2 electrode area, the switch takes place when V×I is constant, i.e., $V_b^2 \cdot \sigma(T_o)$ is constant, as shown in Fig.6-17. This is in agreement with the result of Iizima *et al.*[25] For impulse breakdown, the activation energy in the 500 μm thick sample corresponds to one-third of that of the dc resistivity. On the other hand, the activation energy for thin devices is likely to be related to

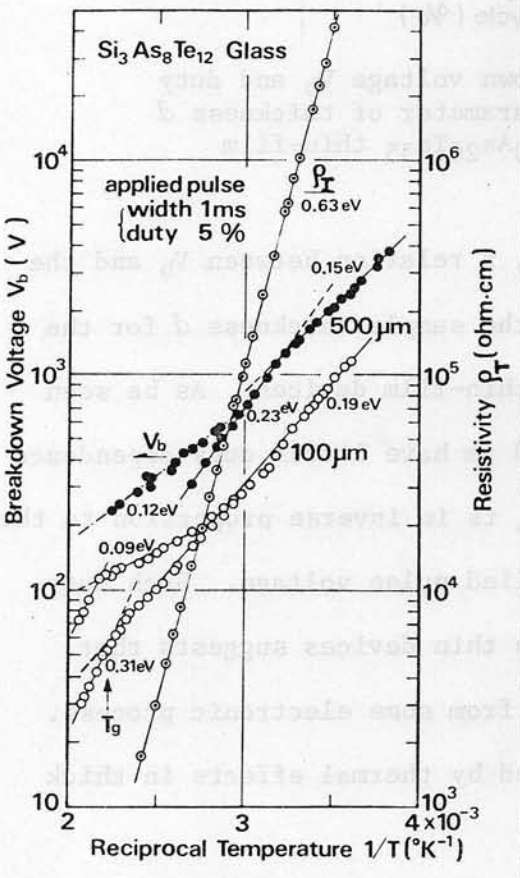

Fig.6-15. Temperature dependence of impulse breakdown voltage V_b for threshold swith of $Si_3As_8Te_{12}$ glass.

($Si_3As_8Te_{12}$ glass, 100μm thick.)

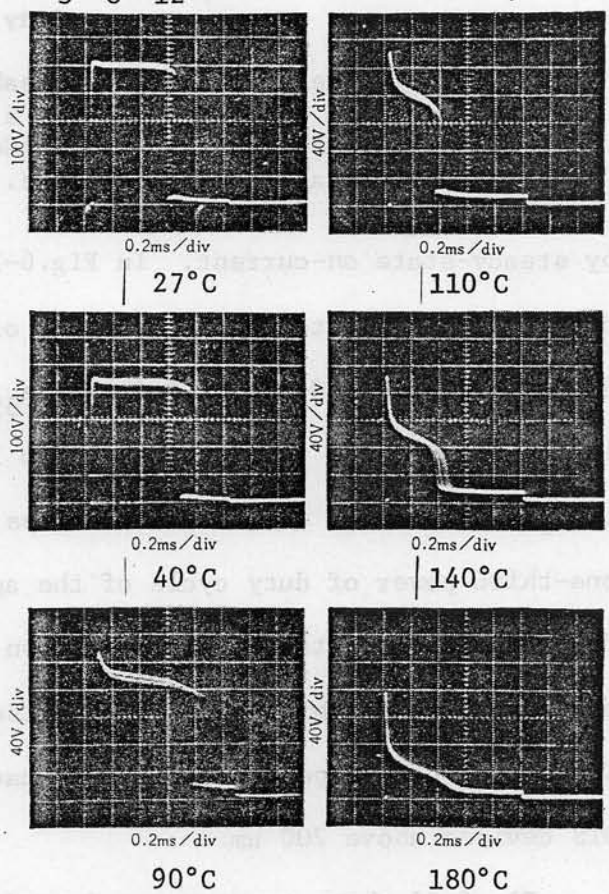

Fig.6-16. Temperature dependence of applied pulse waveform for threshold switch of $Si_3As_8Te_{12}$ glass.

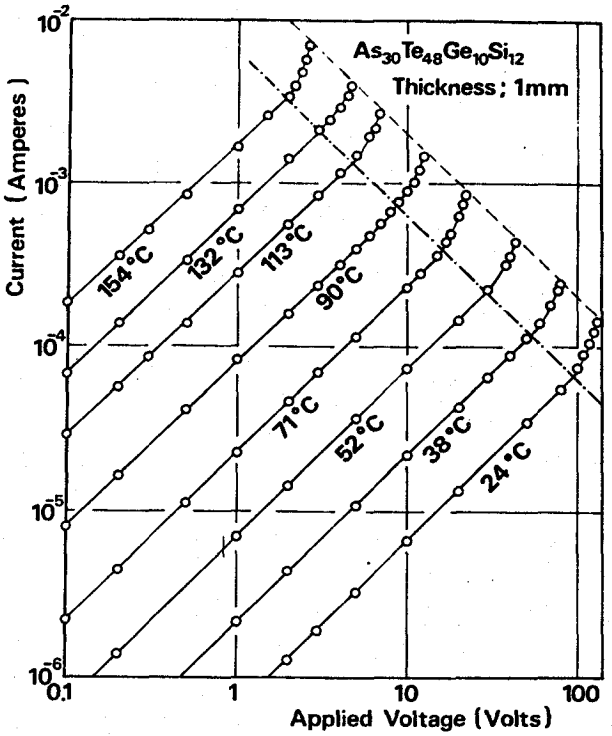

Fig.6-17. Dc V-I characteristics for thick sample with 1 cm^2 electrodes at varying ambient temperatures.

the localized states.

As shown in Table-4, F_b depends on glass composition. Figs.6-18 and 6-19 represent relations between the breakdown field F_b and the inherent dc conductivity σ_{25} at 25 °C for impulse and dc steady-state breakdowns in various Si-As-Te-(Ge) glasses with the identical thicknesses. As seen from the figures, F_b is closely dependent on σ_{25} rather than the composition. Above 200 μm thick, the impulse breakdown is approximated by $F_b \propto \sigma_{25}^{-1/3}$ and the steady-state breakdown is expressed as $F_b \propto \sigma_{25}^{-1/2}$. The data for the thin devices do not follow the above empirical relationships.

The threshold switching characteristic is influenced by many other external parameters like a load resistance, frequency and overvoltage of the applied voltage, and *on*-state current.

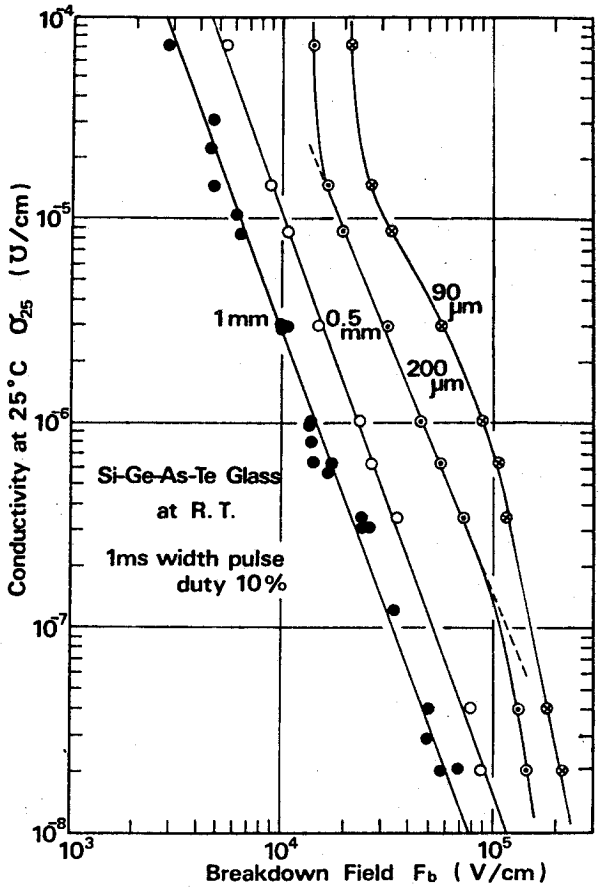

Fig.6-18. Relation between impulse breakdown field F_b and specific conductivity σ_{25} of Si-As-Te-(Ge) glasses at room temperature as a parameter of sample thickness.

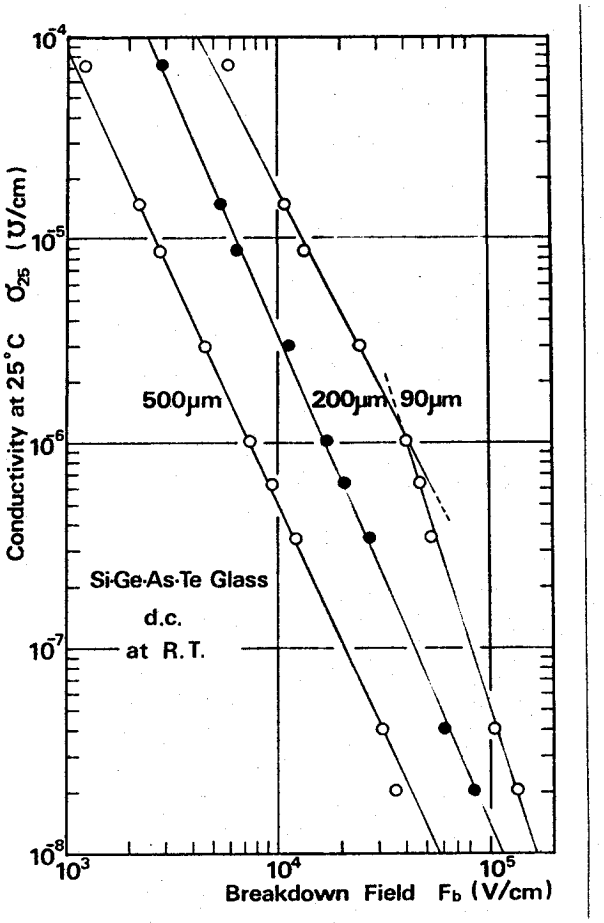

Fig.6-19. Relation between dc steady-state breakdown field F_b and dc conductivity σ_{25} of Si-As-Te-(Ge) glasses at room temperature as a parameter of sample thickness.

6-4. Mechanisms of Electric Breakdown and Threshold Switch

The threshold switching process observed in various amorphous semiconductors is characterized not only by the electric pre-switching breakdown but also by the presence of a positive feedback mechanism in the region of an electrical instability. The process is inseparably tied to the mechanisms of high-field non-Ohmic conduction and breakdown. As pointed out by Mott[26], the non-Ohmic pre-breakdown conduction can be considered as three categories: (1) Bulk effects such as Poole-Frenkel

mechanism or hopping conduction, (2) space-charge effects near the electrode interfaces, and (3) thermal effects. For a few thin amorphous films, Hill succeeded in analyzing the data of non-Ohmic current in terms of a thermally activated internal field-emission from localized states to the conduction band (Poole-Frenkel effect).[27] Otherwise, with traps present, many of injected carriers will be captured by the trapping centers and consequently the space-charge-limited current may take part in the non-Ohmic behavior. It is difficult at present to find indisputable experimental evidences for these processes because of few experiments about the nature of contacts and of localized states. Whether the result is breakdown or switching, however, the essential conditions leading to the instability can arise naturally from the pre-breakdown processes.

As described in the previous section, the breakdown can be phenomenally separated into two regimes by the sample thickness d. Although the aspects of OTS may be more or less puzzled by various parameters like material properties and device geometries, the mechanism can be either interpreted as a thermal effect or an electronic process. In the case of the thermal runaway in terms of Joule's self-heating, the non-linear pre-breakdown regime is governed by the following heat balance equation:

$$C_v \frac{\partial T}{\partial t} = \sigma(T) \cdot F^2 + \vec{\nabla} \cdot (\kappa \vec{\nabla} T) \quad , \qquad \text{.....} \qquad (6\text{-}2)$$

where T is the temperature as a function of position and time t, C_v the specific heat per unit volume, κ the thermal conductivity, $\vec{F}$ the local electric field and $\sigma(T)$ the electrical conductivity of the approximate form of Eq.(3-7). The thermal breakdown theory as a true bulk effect is independent of the detailed conduction mechanism. A general solution

to Eq.(6-2) cannot be found with realistic boundary conditions. According to Chen,[8] Stocker,[6] and Fritzsche *et al.*,[10] however, the solution of Eq.(6-2) for a point-contact can be approximately obtained in two limited cases: (i) For the impulse breakdown which can approximate Eq. (6-2) by neglecting the heat conduction term, i.e., $\vec{\nabla}\cdot(\kappa\vec{\nabla}T) = 0$, the average breakdown field F_b is derived in the form,

$$F_b \propto [C_v \cdot T_o^2/d^2 \cdot E_g \cdot \sigma(T_o)]^{1/3} . \quad \ldots\ldots \quad (6\text{-}3)$$

(ii) The steady-state breakdown by dc or 60 Hz ac voltage allows one to neglect the time derivative term, i.e., $\partial T/\partial t = 0$, and then F_b can be expressed as

$$F_b \propto [\kappa \cdot T_o^2/E_g \cdot \sigma(T_o)]^{1/2}/d . \quad \ldots\ldots \quad (6\text{-}4)$$

Here T_o is the ambient temperature, d the sample thickness, E_g the electrical energy-band gap [$E_{g(el)}$] and $\sigma(T_o)$ the conductivity at T_o. These results of Eqs.(6-3) and (6-4) agree closely with the dependences of F_b on d, σ_{25}, T_o and the duty cycle for the thicker devices above 200 μm as obtained experimentally in Eq.(6-1) in Sec.6-3. Accordingly, it can be evidently identified that the breakdown and switch for the thick devices are invited by the thermal effect of Joule self-heating in the amorphous semiconductor bulk. Fig.6-20 displays an actual surface temperature profile between a pair of point-contacts measured with AGA infrared thermo-vision. The steady-state temperature rise of the *on*-current filament of 1 mA is about 50 deg and that in the pre-switching state is less than 20 deg. These values are coincident with the results of Stocker,[6] but are relatively lower than the estimates by Kaplan *et al.*[11], and Fritzsche *et al.*[10]

On the other hand, the experimental data for the thin-film switching devices do not adequately fit into the above thermal model.

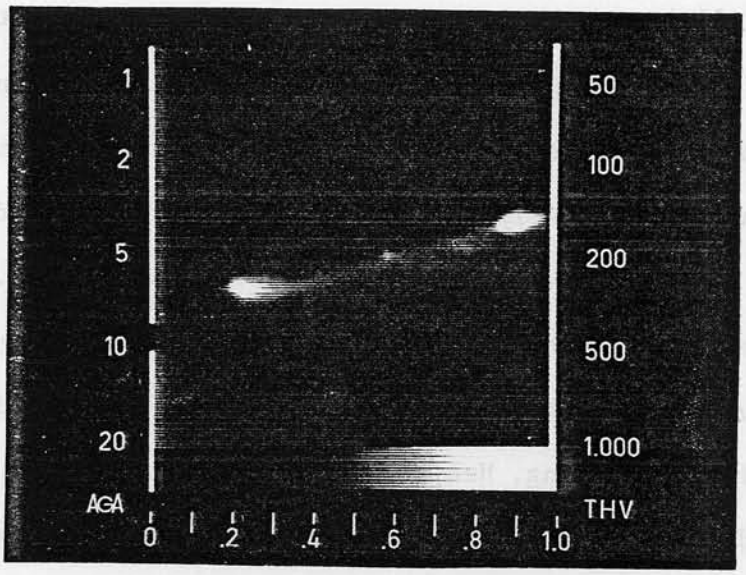

Fig.6-20. Temperature profile between a pair of point-contacts of 0.5 mm gap on a bulk surface measured with AGA infrared thermo-vision. I_{on}=1 mA. Temperature rise is about 50 deg along *on*-current filament on dc operation.

Since F_b is duty-independent and depends only on the dc conductivity, the breakdown and consequent switching effects in chalcogenide films must be associated primarily with electronic processes. The threshold switch very likely is not due to avalanche[13] and Zener[14] breakdowns, because hot-electron effect and interband tunneling probability enough to overcome the recombination rate cannot be expected from the breakdown field of 10^5 V/cm. A number of plausible models for electronic breakdown and positive feedback processes have recently been proposed in taking account of high-field conduction based on the mobility gap and localized states in amorphous semiconductors, as follows:

(1) charge-controlled double injection model,[15]

(2) field-assisted hopping model,[16]

(3) space-charge overlap model,[17]

(4) double injection recombination instability model,[18]

(5) relaxation-case recombinative injection model.[19]

These models all have much in common with the double injection and the space charge. In an amorphous semiconductor with a high density of the localized states, a large fraction of two-types of carriers injected from both contacts is likely to be trapped in the localized states or to recombine with positively and negatively charged states. Through these processes, the space charge is established and limits the current flow in the vicinity of the electrodes. By using crystalline Ge electrodes of different doping, Henisch *et al.*[28] and Stiegler *et al.*[29] have verified that the double injection is the primary cause for the switching operation in chalcogenide glass films. If merely one kind of carriers was injected, no switching process could be triggered even by applied voltages and currents above the threshold level. This fact also indicates that an electronic process is evidently predominant in such a thin-film switching device.

In the model of Fritzsche *et al.*[16] in Fig.6-21(a), since non-equilibrium excess current cannot be enough replenished from the electrodes, the field-induced carriers can produce a positive space-charge

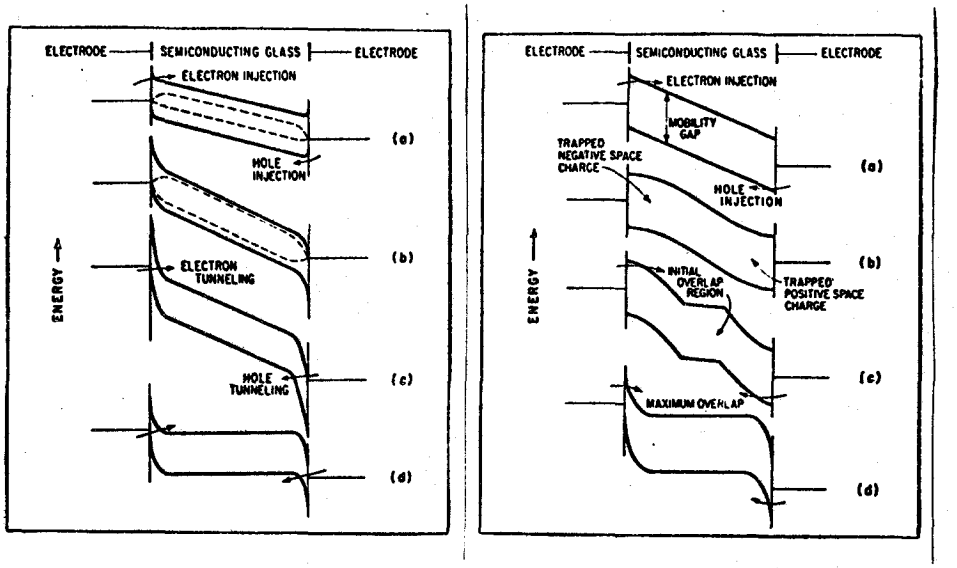

(a) (b)

Fig.6-21. Tentative switching models, (a) The FO model[16] and (b) The HFO model.[17]

near the cathode and a negative space-charge at the anode. At higher voltages trap-limited current proceeds until traps are filled, and then switching takes place rapidly. The HFO model[17] assumes that a negative space-charge builds up near the cathode and positive space-charge near the anode because of trapping the double-injected carriers. The switching process occurs as soon as the two space-charge regions overlap at the threshold voltage, as shown in Fig.6-21(b). Trap-free space-charge-limited current makes the overlapping region inside the film highly conductive. The model of Lucas[18] is based on the idea of *recombination instability*, in which the lifetime and diffusion-length in front of the electrodes increase sharply with recombination centers filled. Further, Schmidlin has speculated a build-up of mobile carrier accumulations near both contacts and a field-enhancement charge-controlled double injection.[15] Recently Roosbroeck[19] has discussed in detail a unique transport and switching mechanisms in the relaxation-case semiconductors, and that the threshold switching is caused by characteristic *recombinative space-charge injection* of minority carriers (electrons) in a narrow recombination front at the anode.

Thus, most of explicit predictions in these tentative switching models resemble one another at glance. It is not clear, however, whether the space-charge is established by negative or positive charges and is associated predominantly with free carriers or with traps. At the present time, it is not possible to reach any firm conclusions about the dynamic mechanisms of the electronic breakdown and the positive feedback in thin-film OTS because of the lack of direct experimental evidences. On the other hand, most models have a similar band profile for the *on*-state, as shown in Fig.6-21. It has been speculated by Mott[26]

and Böer *et al.*[9] that the carriers in the *on* state should be supplied by electron tunneling through the high field barriers at the contacts. Then, the holding voltage V_h observed for metallic electrode devices is approximately equal to or somewhat larger than the band gap of the switching material. The *on*-current flow is always concentrated into a filament of high current density after the current-controlled switch. The filament has a diameter of about a few microns and a current density of the order of 10^5 A/cm^2. In the thin-film amorphous device, an electronic mechanism sustaining of such a surprising high current density, as well as the drastic switching process, is pending so far.

6-5. Stability, Life and Reliability of Thin-Film Switching Devices

The wide range of controllable material properties, the low cost of film deposition processes and the lack of limitation in the substrate size have always been the motivating forces in the search for thin-film amorphous devices. The most important point in the device-fabrication work of amorphous materials is to find out critical conditions for the material properties and external factors such as device shape and electrode material. Indeed, the practical threshold switching devices can be obtained only in the form of amorphous thin-films, in which the principal switching process is induced by an electronic breakdown rather than by thermal effects. The nature of vitreous materials is unlikely to be structurally affected by vacuum film-deposition techniques.

On the basis of the results obtained in the previous section, the earliest attempt was made to fabricate a thin-film crossover device of threshold switch. The first all-film devices were obtained on the microscope slide glass by using a vacuum evaporation method, as demon-

strated in the upper of Fig.6-22. Two important structural parameters that control the switching characteristics were determined: the film thickness of switching material controls the threshold voltage and the contact area establishes the *off*-state resistance. For this thin-film device, the switching material of thickness about 5 μm was evaporated from the Ovonic glass source at a pressure of 8×10^{-6} Torr and at a source temperature of 700 °C. Evaporated Au thin-films 500 μm wide were employed as the crossover electrodes which sandwitch the active material film. This device could not be switched over only 10^3 cycles on applying unipolar pulses.

The strong influence of the choice of amorphous materials and of contacts is exerted on the success in obtaining more stable and reproducible switching devices having a very long operating life. The glass composition relevant to the threshold switch is to have no peak of crystallization, devitrification, decomposition or phase separation on

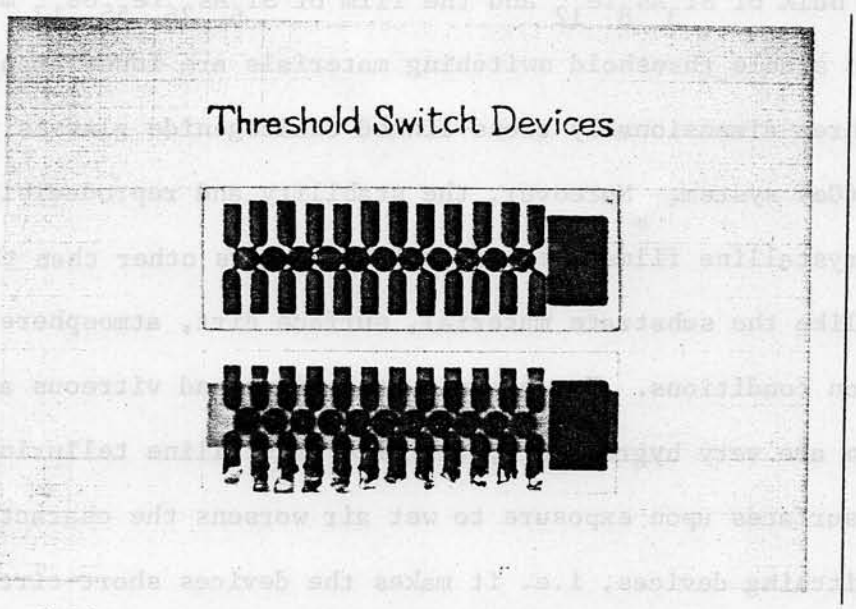

Fig.6-22. Crossover sandwitch-type devices of all-film threshold switch on microscope slide-glass substrate. The underlaid devices are covered with two thin-films of SiO_2 and As_2S_3.

the DSC trace at temperatures up to 500 °C. The alloys containing Si content less than 10 atomic % and Te content above 80 atomic % are inadequate to a stable threshold switch because of their low-temperature crystallization. Glasses with too much As content are eliminated by reason of the As vaporization on switching. On the other hand, evaporated films of Si-As-Te system are very liable to peel and crack, so that germanium was added in the films. The films containing Ge atoms are easy to be deposited very stably and reproducibly on the slide glass. To deposit an amorphous film with the required composition, the source material composition was chosen by experience under the fixed evaporating condition. Considerable work was expended in developing techniques to compensate for the compositional changes resulting from the vacuum evaporation process and caused by the differences in vapor pressure of the individual components of the source material. As the result, the stable switching devices in this thesis work have been realized by using the bulk of $Si_3As_8Te_{12}$ and the film of $Si_6As_{26}Te_{55}Ge_{13}$ mainly. Thus, more stable threshold switching materials are found among nearly ideally three-dimensionally cross-linked chalcogenide glasses in the Si-As-Te-(Ge) system. Moreover, the stability and reproducibility of the non-crystalline films are affected by factors other than the compositions, like the substrate material, surface dirt, atmosphere and the preparation conditions. For example, the films and vitreous alloys in the system are very hygroscopic, and free crystalline tellurium educed on their surfaces upon exposure to wet air worsens the characteristics of the switching devices, i.e. it makes the devices short-circuit between the electrodes. In particular, the as-deposited amorphous films contain many kinds of structural unstableness, as well as are strongly

affected by the surface.

For successful operation of the threshold switches, it is further important to select the electrode metals. Poor reliability and short operating life also result when metal contacts such as Al, Au, Pt, Cu, or other low melting eutectic forming elements are used. Figs.6-23(a), (b) and (c) represent respectively appearances of the upper Al, Au and Mo electrodes destroyed by switching operations. As can be seen from these photos, the destruction of each electrode is enhanced by a consid-

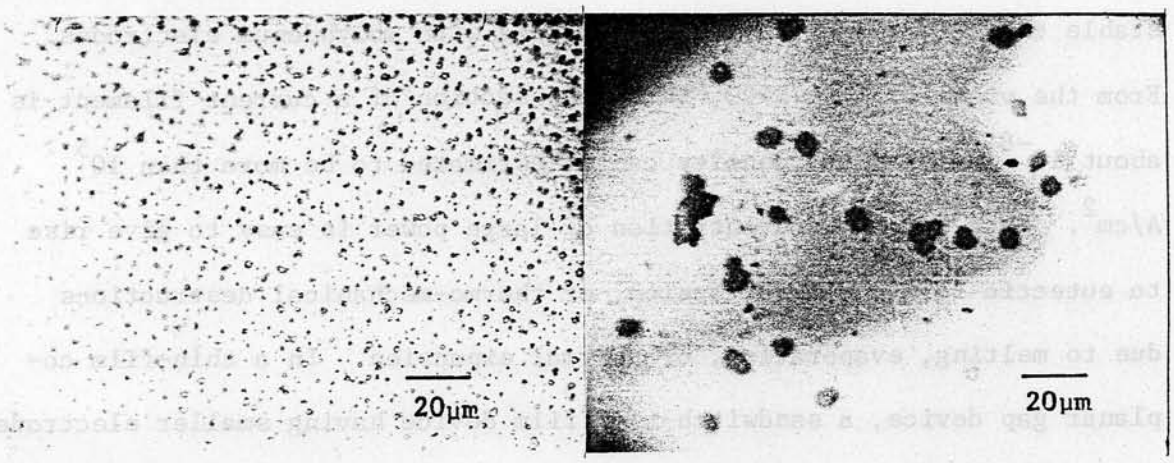

(a) (b)

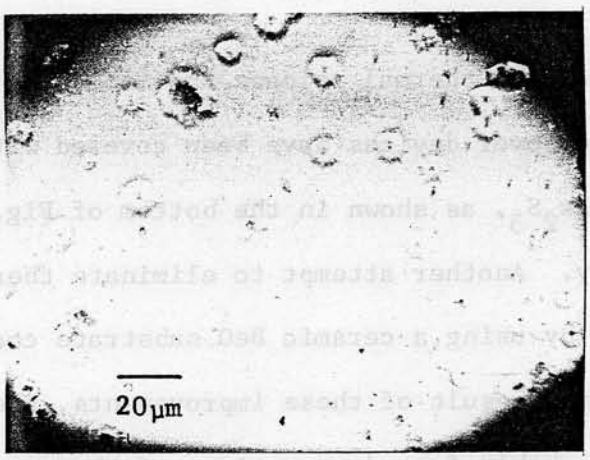

(c)

Fig.6-23. Micro photographs of top electrode of thin-film OTS devices destroyed by impulse switching operations. (a) Thin evaporated Al strip, (b) thin evaporated Au strip and (c) thin evaporated Mo strip. Each electrode metal has partially dissolved and been depressed at current filaments formed on switching.

erable high temperature rise due to a filamentary current and a high electric field at the contact. Especially the upper electrode-strips are badly broken down. The Al and Au strips have partially dissolved in current filaments. The Mo strip has been depressed around filaments. Whenever a switch occurs, the filament seems to jump here and there in the active region. The breakdown voltage becomes higher and at last the device is burnt down. As a result of evaluating the effects of electrode metals (Al, Au, Cr, Cu, Mo, Nb, Pt, Ti, Ta, W), the most stable characteristics have been obtained with molybdenum electrodes. From the views of Figs.6-23, the cross section of a current filament is about 10^{-8} cm^2 and its density can be estimated to be more than 10^5 A/cm^2. Such a local concentration of large power is easy to give rise to eutectic forming, in-diffusion, or thermo-mechanical destructions due to melting, evaporation, or thermal expansion. In a thin-film co-planar gap device, a sandwitch-type film device having smaller electrode area, and even a point-contact bulk device, similar behavior has been observed.

With the aim of the thermal release and isolating the external atmosphere, the crossover devices have been covered with two other thin films of SiO_2 and As_2S_3, as shown in the bottom of Fig.6-22, in the author's laboratory. Another attempt to eliminate thermal effects still more has been made by using a ceramic BeO substrate coated with a very thin SiO_2 film. As a result of these improvements, the devices have been prevented remarkably from destructions of the upper electrode, and kept continuously operating for more than 10^9 cycles (about 1600 hours) for 2-mA *on*-current by using unipolar pulses of width 80 μsec and of duty cycle 33 %. A typical ac 60 Hz switching characteristic of the

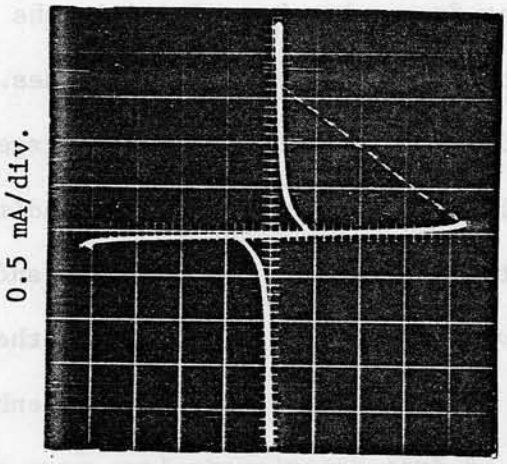

Fig.6-24. Threshold switching characteristic of thin-film crossover device 7.6 μm thick of $Si_6As_{26}Te_{55}Ge_{13}$, coated with SiO_2 and As_2S_3 films. Load resistance: 200 kΩ. Scale: horizontal, 20 V/div. and vertical, 0.5 mA/div.

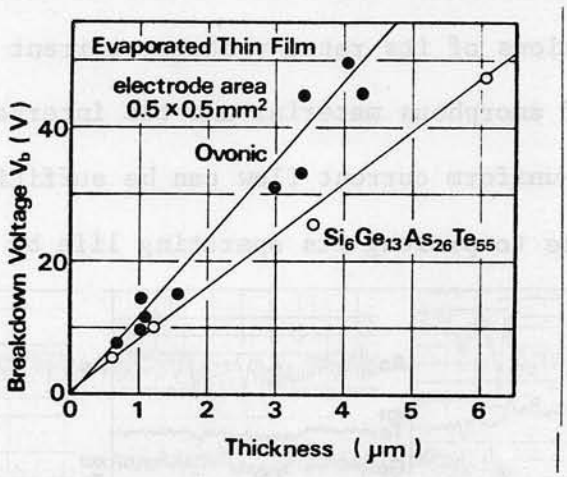

Fig.6-25. Threshold voltage V_{th} as a function of electrode separation (or thickness) for thin-film of $Si_6As_{26}Te_{55}Ge_{13}$ and Ovonic fraction devices.

device is represented in Fig.6-24. The *off* resistance is about 1∿10 MΩ and the *on* resistance is nearly equal to 1 kΩ. As shown in Fig.6-25, The breakdown field F_b is constant and the threshold voltage $V_{th}=V_b$ is controllable for the film thickness of switching material in the wide range from 5 to 100 V. One observes fluctuation in V_{th} of roughly ±10% for the same lot of devices.

Another important factor has been found in the testing procedure or in the operating condition of threshold switches. Switching devices are strongly affected by the sort of applied voltage (amplitude, duty cycle, frequency, polarity), *on* current, load condition or external temperature. Under the conditions of high field and current densities the device suffers even compositional changes in the current filament. On applying voltages of a single polarity, field-enhanced diffusions of electrode metals and of free constituent ions were observed as shown in Fig.6-26. The EPMA observation (Shimadzu, EMX-9734) shows compositional segregation induced by switching of high current density in an OTS bulk device with a pair of point contacts. Provided that the device is operated under conditions of its rated voltage, current and load, the viscoelastic motion of amorphous material and the internal strains produced by the large non-uniform current flow can be sufficiently held in check. It may be possible to prolong its operating life by at least a few

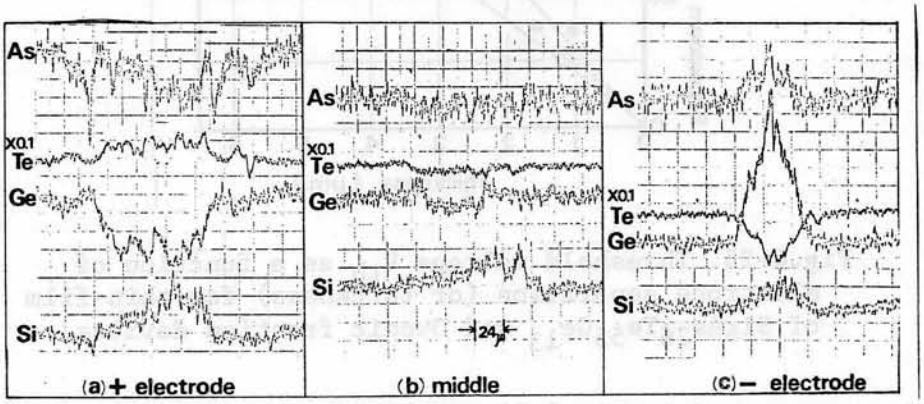

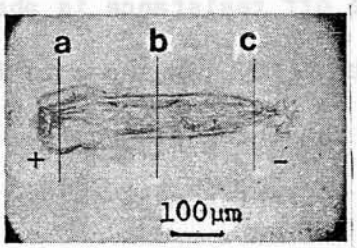

$Si_{12}As_{30}Te_{48}Ge_{10}$ Glass

{Electrode separation:500 μm
Applied voltage: 60 Hz half wave
I_{on}=10 mA
Time: 1 min.

Electron Microprobe X-ray Analyzer
{20 kV, 0.01 μA, 2 μm$^{\phi}$
Scanning speed: 24 μm/min.

Fig.6-26. EPMA observation of compositional segregation by threshold switching in OTS bulk device with a pair of point contacts.

figures beyond 10^9 cycles in the all-film device.

The stable thin-film device of threshold switch can be realized through designing with the above-mentioned factors in mind. Such an amorphous switching device is in the improvement stage for practical application at present. Reliability and reproducibility of the characteristics of thin-film switching devices depend essentially on the film-deposition technologies and the device fabrication processes like sputtering and micro photo-etching.

6-6. Summary

In this chapter, the author has dealt with threshold switching phenomena of the Si-As-Te-(Ge) amorphous semiconductors from a practical interest. Two types of switching devices, a point-contact bulk device and an all-film sandwitch-type device, have been fabricated. A series of systematic experiments has been carried out on the electric breakdown and threshold switching regimes for these devices. Effects of the material properties and the external factors such as device configurations and applied voltage conditions upon the pre-breakdown regime, e.g. the breakdown voltage V_b, have been examined in details. For thick devices above 100 μm the average breakdown field F_b has been observed to decrease with the sample thickness d, dc conductivity σ_{25} and duty cycle of applied pulse voltage, while for thin devices F_b is constant except for σ_{25}. From these results, the author could separate evidently an electronic breakdown from a thermal runaway in the thin devices below 100 μm. For successful operation of the threshold switch under unipolar ac and pulse conditions, the improvements of the thin-film sandwitch device having an active area of 500 μm square have been made

as follows: (1) The adoption of a device structure having a BeO substrate as a heat sink and two coating films of SiO_2 and As_2S_3 in order to eliminate thermal effects and isolate the external atmosphere. (2) The film evaporation of composition $Si_6As_{26}Te_{55}Ge_{13}$ having a nearly ideally cross-linked network structure. (3) The use of evaporated molybdenum electrodes. As a result of these improvements, the all-film device has been kept continuously operating, for example, for more than 10^9 cycles (about 1600 hours) by using 2-mA *on*-current and unipolar pulses of width 80 μsec and of duty cycle 33 %. The *off* resistance is about 1∿10 MΩ and the *on* resistance is less than 1 kΩ. The V_b is controllable for the film thickness of switching material in the wide range from 5 to 100 V. The fluctuation in V_b of roughly ±10 % has been observed for the same lot of devices.

REFERENCES-VI

1) S. R. Ovshinsky and H. Fritzsche, IEEE Trans. on Elect. Devices ED-20, 91 (1973).

2) S. R. Ovshinsky, Phys. Rev. Letters 21, 1450 (1968).

3) K. Tanaka *et al.*, Solid State Commun. 8, 1333 (1970).

4) H. Fritzsche, in *Proc. 5th Conf. on Solid State Devices, Tokyo* (Japan Soc. of Appl. Phys., Tokyo, 1974), p.32.

5) F. M. Collins, J. Non-Cryst. Solids 2, 496 (1970).

6) H. J. Stocker, J. Non-Cryst. Solids 4, 371 (1970), *ibid.* 4, 523 (1970).

7) A. C. Warren, IEEE Trans. on Elect. Devices ED-20, 123 (1973).

8) H. S. Chen *et al.*, Phys. Stat. Sol. A-2, 79 (1970).

9) K. W. Böer *et al.*, J. Non-Cryst. Solids 4, 573 (1970).

10) H. Fritzsche and S. R. Ovshinsky, J. Non-Cryst. Solids 4, 464 (1970).

11) T. Kaplan and D. Adler, J. Non-Cryst. Solids 8-10, 538 (1972).

12) D. M. Kroll and M. H. Cohen, J. Non-Cryst. Solids 8-10, 544 (1972).

13) A. E. Owen and J. M. Robertson, IEEE Trans. on Elect. Devices ED-20, 105 (1973).

14) D. C. Mattis, Phys. Rev. Letters 22, 936 (1969).

15) F. W. Schmidlim, Phys. Rev. B-1, 1583 (1970).

16) H. Fritzsche and S. R. Ovshinsky, J. Non-Cryst. Solids 2, 393 (1970).

17) H. K. Henisch, E. A. Fagen and S. R. Ovshinsky, J. Non-Cryst. Solids 4, 538 (1970).

18) I. Lucas, J. Non-Cryst. Solids 6, 136 (1971).

19) W. van Roosbroeck, Phys. Rev. Letters 28, 1120 (1972).

20) R. G. Neale, J. Non-Cryst. Solids 2, 558 (1970).

21) M. Nunoshita, T. Suzuki, M. Hirano and H. Arai, *Mitsubishi-Denki Giho* 47, 1303 (1973).

22) B. K. Ridley, Proc. Phys. Soc. 82, 954 (1963).

23) H. Fritzsche, *Amorphous and Liquid Semiconductors*, Edited by J. Tauc (Plenum Press, London & New York, 1974), p.334.

24) B. T. Kolomiets *et al.*, Soviet Phys. Semicond. 3, 267 (1969).

25) S. Iizima *et al.*, in *Proc. 2nd Conf. on Solid State Devices, Tokyo* (Japan Soc. Appl. Phys., Tokyo, 1970), p.73.

26) N. F. Mott, Phil. Mag. 24, 911 (1971).

27) R. M. Hill, Phil. Mag. 23, 59 (1971).

28) H. K. Henisch *et al.*, J. Non-Cryst. Solids 8-10, 415 (1972).

29) H. Stiegler and D. R. Haberland, J. Non-Cryst. Solids 11, 147 (1972).

Chapter-VII

CONCLUSIONS

A series of experimental investigations has been carried out on the compositional dependences and the stabilization process of electrical and optical properties of the Si-As-Te-(Ge) amorphous semiconductors. Characteristic parameters of the electronic semiconducting properties such as dc and ac conductivities, electrical and optical energy-band gaps, band-tailing factor have been determined, and systematic changes of these parameters with the glass compositions and the annealing have been observed. Such electronic processes in the Si-As-Te glasses have been clarified from a viewpoint of the glass-network structures by considering a pseudo-gap and localized tail states. A thin-film device for the threshold switch having a considerably high reliability and reproducibility has been fabricated.

In conclusion, the principal results obtained in this thesis work are summarized as follows:

1) A new fabrication procedure by the convenient RF heating has been developed to obtain a large size of semiconducting glass ingots with a good homogeneous quality in a relatively short melting time.
2) The electrical dc conductivity of stable chalcogenide semiconductors in the Si-As-Te system can be controlled very widely (e.g. within the range of $10^{-4} \sim 10^{-11}$ $\Omega^{-1} \cdot cm^{-1}$) by changing the compositions within the wide glass-forming region.
3) From the measurements of dc conductivity and optical absorption, it has been cleared that the electronic properties in these glasses

are essentially analogous to those in 'intrinsic' crystalline semiconductors. The temperature-dependent dc conductivity σ_T follows nicely the formula of $\sigma_T = \sigma_o \cdot \exp\{-E_{g(el)}/2kT\}$, and the pre-exponential σ_o term has been determined to be about $(2.1\pm0.6) \times 10^4$ $(\Omega \cdot cm)^{-1}$ for all Si-As-Te vitreous semiconductors. This value of σ_o is also consistent with the theoretical value in the conventional crystalline semiconductors.

4) The electrical and optical band gaps, $E_{g(el)}$ and $E_{g(op)}$, have been also determined for various glass compositions in the Si-As-Te system. From these data, an empirical relationship between both gaps are expressed as $E_{g(el)} = 1.60\ E_{g(op)} - 0.15$ in eV. Theoretical backgrounds for this relation have been discussed on the basis of the concept of mobility edges.

5) An optical absorption spectrum near the fundamental edge has an exponential tail; $\alpha(\omega)=\alpha_o \cdot \exp(\hbar\omega/E_s)$, which is originated from the localized states due to potential fluctuations in the disordered system. The band-tailing factor E_s is of the order of 0.05 eV and increases linearly with increasing $E_{g(op)}$.

6) A tentative energy-band model has been postulated to explain the electronic semiconducting properties of the Si-As-Te amorphous materials. This model is characterized by the existence of a pseudo-gap between the valence- and conduction-band states and of localized tail states at the mobility edges.

7) In the Si-As-Te glass system, the electronic properties like the electrical and optical gaps, as well as the glass-structural parameters, are strongly dependent on the Si and Te contents, and relatively insensitive to the As content. This fact observed in

their compositional dependences implies that this glass has a three-dimensionally cross-linked network structure based on covalent Si-Te bonds. It can be concluded that the static electronic properties such as extended band states and a band gap are originated by short-range chemical and configurational order preserved around the Si-Te bonds in the disordered system.

8) A relation between localized tail states and random potential fluctuations by the lack of long-range order has been characterized by annealing effects on dc and ac conductivities and optical absorption in the Si-As-Te amorphous semiconductors. During the stabilization process of an as-quenched glass, relaxation of the excess stored deformation energy involving a decrease of a kind of disorderness leads to not only a little increase of the band gap, but also to appreciable reduction and regularization of the localized tail-states at the band edges.

9) In order to find the proper synthetic conditions for a stable amorphous switching operation in the material properties and the device geometries like electrode area and sample thickness, the pre-breakdown regime of the Si-As-Te-(Ge) vitreous semiconductors has been systematically investigated. It has been confirmed that the threshold switch in thin device less than 100 μm thick is governed by electronic breakdown rather than by thermal runaway.

10) By using film deposition techniques, thin-film switching devices have been manufactured in the form of a crossover sandwitch-type structure. The device improvements have been made by using a BeO substrate, two SiO_2 and As_2S_3 coating films, the $Si_6As_{26}Te_{55}Ge_{13}$ switching material-film and molybdenum electrodes. As the results,

the all-film device has a long operating life, for example above 1600 hours (10^9 cycles) for 2-mA *on*-current in applying unipolar pulses of width 80 μsec and of duty 33 %. The *off* resistance is about 1∿10 MΩ and the *on*-resistance is less than 1 kΩ. The V_{th} is controllable for the film thickness of switching material in the wide range from 5 to 100 V. The fluctuation in V_{th} of roughly ±10% has been observed for the same lot of devices.

ACKNOWLEDGEMENTS

This work has been made in the Central Research Laboratory of Mitsubishi Electric Corporation, Amagasaki, Hyogo, co-operated with the Semiconductor Laboratory at the Department of Electrical Engineering in the Faculty of Engineering Science, Osaka University, Toyonaka, Osaka.

The author would like to appreciate his heartfelt thanks to Professor S. Namba and Professor Y. Hamakawa, Osaka University, for their kind advices and critical reading of this thesis. Especially the author would like to acknowledge the continuous guidance and encouragement of Professor Y. Hamakawa as the supervisor of the Semiconductor Laboratory and of Dr. S. Ibuki as the chief of his laboratory of Mitsubishi Electric Corporation throughout this collaboration.

The author is grateful to Professor S. Namba, Professor T. Makimoto, Professor K. Fujisawa, Professor T. Sueta, Professor Y. Hamakawa and Professor Y. Sakurai, Osaka University, for helpful suggestions and their kind guidances of this thesis.

The author wishes to express his gratitude to Dr. S. Ibuki, Dr. J. Hayashi, Dr. H. Komiya, Dr. J. Kai, Mr. S. Uematsu, Dr. T. Nakayama, Mr. H. Arai, Mr. M. Hirano, Mr. T. Suzuki, Dr. Y. Utsumi, Mr. T. Shinnishi and many co-workers in the Central Research Laboratory of Mitsubishi Electric Corporation for their useful discussions, encouragements, or considerable assistances in this thesis work. In particular, the author takes pleasure in acknowledging the important part played by his colleagues, Mr. H. Arai, Mr. M. Hirano and Mr. T. Suzuki.

The author also is indebted to Professor H. Fritzsche of Chicago University, Dr. M. Kikuchi* and Dr. H. Namikawa of Electrotechnical Laboratory and Professor T. Minami of University of Osaka Prefecture

for drawing his attention and stimulating his interest in this problem.

Great thanks are due to Dr. T. Nishino, Dr. M. Okuyama, Mr. T. Taneki, Mr. T. Fujimoto and his many colleagues of Semiconductor Laboratory of Osaka University for their technical assistances in the course of experiments.

Finally the author wishes to thank his parents, wife and some friends, Dr. Y. Akasaka, Dr. Y. Aoyagi and Mr. A. Ishizu, for their encouragements.

---

* Present Address: Central Research Laboratory of Sony Corporation.

論　文　目　録

大阪大学

報告番号	乙第1556号	氏名	布　下　正　宏

主論文

題名 "Electrical and Optical Properties of The Amorphous Si-As-Te Semiconductor System."

(Si-As-Te系非晶質(ガラス)半導体の電気的および光学的性質に関する研究)

参考論文

題名 "Band Gap in Si-As-Te Amorphous Semiconductor."

(Si-As-Te系非晶質半導体のバンドギャップ)

Solid State Commun. 11 (1972) p.213~216.

新居宏壬と共著

題名 "Relation between Band Gap and Density of Si-As-Te Amorphous Semiconductors."

(Si-As-Te系非晶質半導体のバンドギャップと密度との関係)

Solid State Commun. 11 (1972) p.337~341.

新居宏壬と共著

題名 "Electrical and Optical Gaps in Si-As-Te Amorphous System."

(Si-As-Te系非晶質における電気的および光学的ギャップ)

J. Non-Crystalline Solids 12 (1973) p.339∿352.

浜川圭弘 他2名と共著

題名 "Effects of Annealing on Physical Properties in Amorphous Si-As-Te Semiconductors."

(Si-As-Te非晶質半導体の物理的性質に対するアニーリング効果)

Proc. of the 5th Intern. Conf. on Amorphous and Liquid Semiconductors held at Garmisch, vol.2 (1974) p.753∿759.

浜川圭弘 他2名と共著

題名 "Electrical and Optical Properties of Si-As-Te Chalcogenide Glass System."

(Si-As-Te系カルコゲナイドガラスの電気的および光学的性質)

Proc. of the 10th Intern. Conf. on Glass held at Kyoto, vol.7 (1974) p.37∿44.

浜川圭弘 他2名と共著

論　文　目　録

大阪大学

報告番号	乙第1556号	氏名	布　下　正　宏

主論文

題名 "Electrical and Optical Properties of The Amorphous Si-As-Te Semiconductor System."

(Si-As-Te系非晶質(ガラス)半導体の電気的および光学的性質に関する研究)

参考論文

題名 "Band Gap in Si-As-Te Amorphous Semiconductor."

(Si-As-Te系非晶質半導体のバンドギャップ)

Solid State Commun. 11 (1972) p.213~216.

新居宏壬と共著

題名 "Relation between Band Gap and Density of Si-As-Te Amorphous Semiconductors."

(Si-As-Te系非晶質半導体のバンドギャップと密度との関係)

Solid State Commun. 11 (1972) p.337~341.

新居宏壬と共著

題名 "Electrical and Optical Gaps in Si-As-Te Amorphous System."

(Si-As-Te系非晶質における電気的および光学的ギャップ)

J. Non-Crystalline Solids 12 (1973) p.339∿352.

浜川圭弘 他2名と共著

題名 "Effects of Annealing on Physical Properties in Amorphous Si-As-Te Semiconductors."

(Si-As-Te非晶質半導体の物理的性質に対するアニーリング効果)

Proc. of the 5th Intern. Conf. on Amorphous and Liquid Semiconductors held at Garmisch, vol.2 (1974) p.753∿759.

浜川圭弘 他2名と共著

題名 "Electrical and Optical Properties of Si-As-Te Chalcogenide Glass System."

(Si-As-Te系カルコゲナイドガラスの電気的および光学的性質)

Proc. of the 10th Intern. Conf. on Glass held at Kyoto, vol.7 (1974) p.37∿44.

浜川圭弘 他2名と共著